U.S.NRC
United States Nuclear Regulatory Commission
Protecting People and the Environment

NUREG/CR-7224
ORNL/TM-2015/544

Axial Moderator Density Distributions, Control Blade Usage, and Axial Burnup Distributions for Extended BWR Burnup Credit

Office of Nuclear Regulatory Research

AVAILABILITY OF REFERENCE MATERIALS IN NRC PUBLICATIONS

NRC Reference Material

As of November 1999, you may electronically access NUREG-series publications and other NRC records at NRC's Library at www.nrc.gov/reading-rm.html. Publicly released records include, to name a few, NUREG-series publications; *Federal Register* notices; applicant, licensee, and vendor documents and correspondence; NRC correspondence and internal memoranda; bulletins and information notices; inspection and investigative reports; licensee event reports; and Commission papers and their attachments.

NRC publications in the NUREG series, NRC regulations, and Title 10, "Energy," in the *Code of Federal Regulations* may also be purchased from one of these two sources.

1. **The Superintendent of Documents**
   U.S. Government Publishing Office
   Mail Stop IDCC
   Washington, DC 20402-0001
   Internet: bookstore.gpo.gov
   Telephone: (202) 512-1800
   Fax: (202) 512-2104

2. **The National Technical Information Service**
   5301 Shawnee Rd., Alexandria, VA 22312-0002
   www.ntis.gov
   1-800-553-6847 or, locally, (703) 605-6000

A single copy of each NRC draft report for comment is available free, to the extent of supply, upon written request as follows:

Address: **U.S. Nuclear Regulatory Commission**
Office of Administration
Publications Branch
Washington, DC 20555-0001
E-mail: distribution.resource@nrc.gov
Facsimile: (301) 415-2289

Some publications in the NUREG series that are posted at NRC's Web site address www.nrc.gov/reading-rm/doc-collections/nuregs are updated periodically and may differ from the last printed version. Although references to material found on a Web site bear the date the material was accessed, the material available on the date cited may subsequently be removed from the site.

Non-NRC Reference Material

Documents available from public and special technical libraries include all open literature items, such as books, journal articles, transactions, *Federal Register* notices, Federal and State legislation, and congressional reports. Such documents as theses, dissertations, foreign reports and translations, and non-NRC conference proceedings may be purchased from their sponsoring organization.

Copies of industry codes and standards used in a substantive manner in the NRC regulatory process are maintained at—

The NRC Technical Library
Two White Flint North
11545 Rockville Pike
Rockville, MD 20852-2738

These standards are available in the library for reference use by the public. Codes and standards are usually copyrighted and may be purchased from the originating organization or, if they are American National Standards, from—

American National Standards Institute
11 West 42nd Street
New York, NY 10036-8002
www.ansi.org
(212) 642-4900

Legally binding regulatory requirements are stated only in laws; NRC regulations; licenses, including technical specifications; or orders, not in NUREG-series publications. The views expressed in contractorprepared publications in this series are not necessarily those of the NRC.

The NUREG series comprises (1) technical and administrative reports and books prepared by the staff (NUREG–XXXX) or agency contractors (NUREG/CR–XXXX), (2) proceedings of conferences (NUREG/CP–XXXX), (3) reports resulting from international agreements (NUREG/IA–XXXX), (4) brochures (NUREG/BR–XXXX), and (5) compilations of legal decisions and orders of the Commission and Atomic and Safety Licensing Boards and of Directors' decisions under Section 2.206 of NRC's regulations (NUREG–0750).

U.S.NRC
United States Nuclear Regulatory Commission
Protecting People and the Environment

NUREG/CR-7224
ORNL/TM-2015/544

Axial Moderator Density Distributions, Control Blade Usage, and Axial Burnup Distributions for Extended BWR Burnup Credit

Manuscript Completed: April 2016
Date Published: August 2016

Prepared by: William (B.J.) Marshall, Brian J. Ade,
Stephen Bowman, Jesus S. Martinez-Gonzalez*

Oak Ridge national Laboratory
Managed by UT-Battelle, LLC
Oak Ridge, TN 37831-6170

*Universidad Politecnica de Madrid
c/ José Gutiérrez Abascal, 2-28006 Madrid Spain

Mourad Aissa, NRC Project Manager

NRC Job Code Number V6452

Office of Nuclear Regulatory Research

ABSTRACT

Applications for certificates of compliance for spent nuclear fuel (SNF) dry storage and transportation systems must include criticality safety analyses demonstrating that these systems are subcritical. This requirement also applies to applications for (specific) licenses for 10 Code of Federal Regulations (CFR) Part 72 SNF storage facilities. As part of the licensing process, the US Nuclear Regulatory Commission (NRC) staff reviews analyses of pressurized water reactor (PWR) SNF that credit the reduction in assembly reactivity caused by depletion of fissile nuclides and buildup of neutron-absorbing nuclides during power operation. These reviews are conducted according to the guidance in the *Division of Spent Fuel Storage and Transportation Interim Staff Guidance* (ISG) 8, Revision 3. This credit for reactivity reduction during depletion is commonly referred to as *burnup credit* (BUC). However, BUC for boiling water reactor (BWR) SNF is not addressed in ISG-8.

NUREG/CR-7194, *Technical Basis for Peak Reactivity Burnup Credit for BWR Spent Nuclear Fuel in Storage and Transportation Systems* (April 2015), provides a technical basis for peak reactivity BWR BUC methods in SNF dry storage and transportation systems. Members of the nuclear industry have expressed interest in extending BWR BUC beyond these peak reactivity methods. This report documents the studies performed to assess the impacts of (1) axial moderator density distributions, (2) control blade usage, and (3) axial burnup profiles on extended BWR BUC. Each of these parameters was identified as high importance in NUREG/CR-7158, *Review and Prioritization of Technical Issues Related to Burnup Credit for BWR Fuel.* This report evaluates the impact of each of these phenomena, with the objective of identifying limiting conditions and assumptions in BWR BUC analyses.

The data used in this report are BWR core follow data from a recent cycle that contained four different modern BWR fuel assembly design types: GE14, GNF2, SVEA-96 Optima 2, and ATRIUM-10. The data from the nodal simulator has 25 axial nodes and includes more than 240 time steps for the 690-day cycle. Variables such as the moderator density, power level, burnup, and control blade positions can be extracted from the simulated data. The studies documented herein draw on this data set because it contains sufficient detail to model axial moderator density profiles (and other variables that need to be analyzed, such as control blade usage and axial burnup profiles) and because the data also use modern fuel assemblies in a modern BWR cycle.

Axial moderator densities in BWRs can vary by 80% or more within a fuel assembly at a single location at any time during core operations. The axial moderator density distributions shift during an operating cycle and from one cycle to the next as assembly power varies with depletion, control blade use, and other core operating parameters. Two studies were performed related to axial moderator density distributions: (1) a study investigating the frequency with which the moderator density must be updated during the reactor cycle depletion calculations to obtain accurate results (termed *temporal fidelity study* throughout this document) and (2) a study of the effect of the axial moderator density distribution on storage and transportation system reactivity. The second study includes an assessment of limiting axial moderator density profiles and an investigation of axial profile parameterization that could identify limiting profiles without requiring extensive depletion and subsequent k_{eff} calculations.

Control blade use is entirely different in BWR plants than in PWR plants. PWRs are typically operated with all rods out of the core during power operations, and reactivity control is maintained with adjustments to soluble boron concentration. BWRs rely on control blade

insertion to maintain power distribution and reactivity control throughout the cycle. The control blades are inserted to different distances into the core for different durations at different times during the cycle. Use of a control blade in a BWR hardens the neutron spectrum, resulting in increased ^{239}Pu production. Based on increased plutonium with control blade usage, increased control blade usage is expected to result in increased cask reactivity. Due to the top-peaked axial fission distribution in typical SNF storage and transportation casks, the operating conditions experienced in the top portion of the fuel assembly have a disproportionately large effect on cask reactivity. A combination of hypothetical and realistic profiles are used in this study to establish sensitivity to the blade insertion distance, duration, and time in assembly life and to assess the potential magnitude of these effects.

The effect of axial burnup profiles on BWR SNF is expected to be similar to that seen for PWR SNF: that is, low burnup near the top end of the fuel assembly is expected to cause an increase in discharged fuel reactivity when compared to a uniform profile assumption. Conversely, the axial burnup profiles that result from BWR operation are expected to be different from those resulting from PWR operations because of the differences in axial moderator density and control blade effects between PWR and BWR operations. A set of 624 BWR axial burnup profiles was used to generate a range of cask k_{eff} values at burnups of 30, 40, and 50 GWd/MTU, including both the actinide-only and the actinide-plus-fission-product isotope sets. This report presents the analysis of the calculation results, including the range of k_{eff} values which result from the profiles considered, the magnitude of the end effect associated with the profiles, potential indicators for relative reactivity of axial burnup profiles, and a brief examination of the effect of the discharge burnup of the assembly from which each profile is taken on cask k_{eff}. This analysis is performed for models that neglect the presence of natural enrichment blankets and for models that include these blanket regions.

The studies in this report lead to many important conclusions. This report provides specific recommendations based on the analyses described to help identify limiting cases or conditions for modeling the impact of axial moderator density distributions, control blade usage, and axial burnup profiles on BWR BUC in storage and transportation casks. Because the detailed data used in these studies were only readily available from one source and only covered a single cycle of operations from a single plant, these recommendations should be regarded as instructive but preliminary in nature. Future work can be performed to demonstrate wider applicability of the conclusions drawn here. Future work will also include the impact of correlated operating parameters such as the impact of control blade insertion on moderator density distribution and fuel temperature.

CONTENTS

LIST OF FIGURES

LIST OF TABLES

1 INTRODUCTION

Applicants for certificates of compliance for spent nuclear fuel (SNF) transportation and dry storage systems perform analyses to demonstrate that these systems are adequately subcritical according to the requirements of Title 10 of the Code of Federal Regulations (CFR) Parts 71 and 72 [1]. For pressurized water reactor (PWR) SNF, these analyses may credit the reduction in assembly reactivity caused by depletion of fissile nuclides and buildup of neutron-absorbing nuclides during power operation. This credit for reactivity reduction during depletion is commonly referred to as *burnup credit* (BUC). US Nuclear Regulatory Commission (NRC) staff review BUC analyses according to the guidance in the *Division of Spent Fuel Storage and Transportation Interim Staff Guidance* (ISG) 8, Revision 3 [2], "Burnup Credit in the Criticality Safety Analyses of PWR Spent Fuel in Transportation and Storage Casks."

ISG-8 does not address BUC for boiling water reactor (BWR) SNF. However, NUREG/CR-7194, *Technical Basis for Peak Reactivity Burnup Credit for BWR Spent Nuclear Fuel in Storage and Transportation Systems* (April 2015) [3], does provide a technical basis for peak reactivity BWR BUC methods. Peak reactivity occurs when the effective multiplication factor (k_{eff}) for an assembly or 2-dimensional (2D) slice reaches its highest value at some burnup beyond beginning of life (BOL). This common feature of BWR assemblies is caused by the burnable absorber depleting at a more rapid rate than the fuel. Members of the nuclear industry have expressed interest in extending BWR BUC beyond these peak reactivity methods to higher burnups. This report documents the studies performed to assess the impacts of axial moderator density distributions, control blade usage, and axial burnup profiles on extended BWR BUC. In this document, *extended BWR BUC* is defined as credit for the reduction in reactivity at burnups greater than the peak reactivity burnup. The impact of each of these phenomena is evaluated to identify limiting conditions and assumptions for use in extended BWR BUC analyses. Unless otherwise noted in the text, a limiting parameter is defined as that which leads to higher reactivity when the SNF is loaded into a storage and transportation system, commonly referred to as a cask.

Axial moderator densities in BWRs can vary by 80% or more within a fuel assembly at a single location at any time during core operations. This is in stark contrast to axial moderator densities in PWRs, which experience water density variations of approximately 10% from core inlet to outlet. Therefore, there is no directly applicable PWR BUC methodology for treating moderator density variations of the magnitude experienced in BWR operations. The axial distributions generated in a BWR also shift within a cycle and from one cycle to the next as assembly power varies with depletion, control blade use, and other core operating parameters. The studies presented in Section 4 of this report are designed to address the key aspects of modeling these axial moderator density distributions.

As with axial moderator density distributions, control blade use is entirely different in BWR plants from control rod use in PWRs. PWRs are typically operated with all rods out of the core during power operations, and reactivity control is maintained with adjustments to soluble boron concentration. BWRs cannot use soluble poisons because boiling would cause the poison to be deposited on fuel rod surfaces within the core. Instead, BWRs rely on control blade insertion to maintain power distribution and reactivity control throughout the cycle. Control blades are inserted at different distances into the core for varying durations and at various times during the cycle. Section 5 presents studies of the sensitivity of BWR SNF reactivity to control blade use. A combination of hypothetical and realistic profiles is used to establish the sensitivity of cask k_{eff} to the blade insertion distance, duration, and time in assembly life.

The effect of axial burnup profiles on BWR SNF is expected to be similar to that seen for PWR SNF: that is, low burnup near the top end of the fuel assembly is expected to cause an increase in discharged fuel reactivity compared with a uniform profile assumption. Conversely, the axial burnup profiles resulting from BWR operation are expected to be different from those resulting from PWR operations because of the differences in axial moderator density and control blade effects between PWR and BWR operations. The studies presented in Section 6 use a similar approach to established methodologies in PWR BUC to assess the impact of BWR axial burnup profiles on discharged SNF reactivity.

Before the three studies discussed above, Section 2 describes the codes, methods, and models employed in the depletion and criticality safety analyses performed in the studies. Section 3 provides a discussion of the available data sets that were considered for use in these studies and the data set that was selected. Details of the studies are presented in Sections 4–6: axial moderator density distributions are covered in Section 4, control blade use is described in Section 5, and axial burnup profiles are presented in Section 6. Final conclusions are in Section 7.

2 CODES, METHODS, AND MODELS

2.1 Codes and Methods

BUC analyses require the use of a series of codes and models to simulate fuel depletion in the core and SNF reactivity in the storage and transportation system. The SCALE code system [4] was used for all calculations in this work.

2.1.1 TRITON

TRITON is a multipurpose SCALE control module for transport, depletion, and sensitivity and uncertainty analysis [5]. TRITON can be used to provide automated, problem-dependent, cross section processing followed by multigroup transport calculations for one-, two-, or three-dimensional (1D, 2D, or 3D) configurations. This functionality can be used in tandem with the ORIGEN depletion and decay module to predict time-dependent isotopic concentrations, source terms, and decay heat; and it can be used to generate few-group homogenized cross sections for nodal core calculations. In this work, TRITON automated resonance self-shielding (BONAMI /CENTRM/PMC), 2D neutron transport (NEWT), and fuel depletion calculations (ORIGEN) in a series of coupled transport-depletion calculations (depletion steps) to simulate the full depletion history. Following the depletion calculations, ORIGEN was used again to decay the SNF isotopic compositions to simulate the cooling time experienced in a spent fuel pool before loading into the storage and transportation system.

TRITON performed 2D lattice depletion calculations over a range of varying operating conditions. The transport model included a set of 94 nuclides corresponding to the “addnux=2” option (default in TRITON), while more than 2,000 nuclides were tracked during the ORIGEN depletion and decay calculations. The gadolinium-bearing fuel pins were modeled with seven equal-area radial rings to accurately capture the radial dependence of the gadolinium depletion. This modeling approach provides adequate solution accuracy in a reasonable computational time [6]. The 238-group ENDF/B-VII.0 neutron cross section library was used for all calculations. After the TRITON depletion calculations were complete, the output files generated during these calculations were post-processed to generate depleted and decayed fuel composition files for use in subsequent criticality calculations for the storage system. Figure 2.1 is a flow chart showing the steps used in a typical TRITON depletion calculation followed by KENO calculations. In this figure, the library management code COUPLE facilitates the update of the cross section and flux data that ORIGEN requires for depletion calculations. The update is based on the NEWT transport solution.

The TRITON calculations documented in this report were performed with SCALE 6.2 Beta4, which was configured under the SCALE quality assurance plan in March 2015. This version of SCALE was used because deficiencies in the SCALE 6.1 implementation of the *timetable* option in TRITON precluded the simulations needed for the current work. In addition, the NEWT transport module runs significantly faster in SCALE 6.2, reducing the computational burden of the calculations performed.

The *timetable* block is used extensively in TRITON calculations. It was provided to modify properties of regions in the model during depletion, and it is commonly used to vary the soluble boron concentration in PWR cores. In this work, the *timetable* block adjusted the moderator densities in each node during depletion. The input includes changes in the number densities to be made and the times at which the changes are to be made.

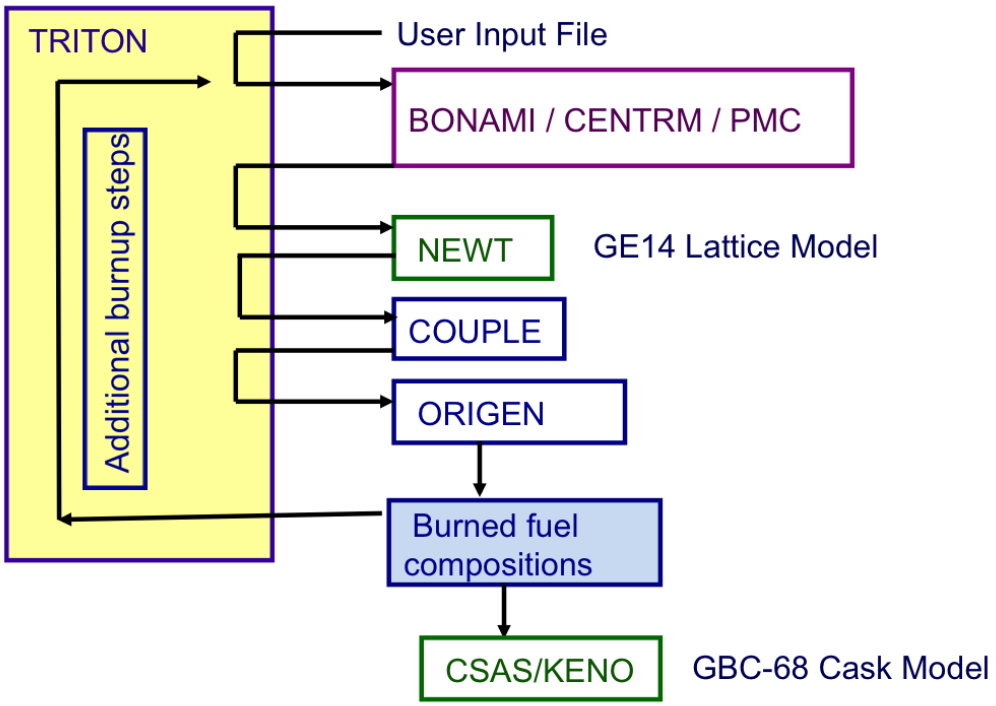

Figure 2.1 SCALE sequences, modules, and codes used for KENO calculations based on explicit TRITON depletion calculations in this report

2.1.2 KENO

The Criticality Safety Analysis Sequence (CSAS)/KENO performed reactivity calculations for the GBC-68 computational benchmark model described later in this section. The sequence provides automated problem-dependent cross section processing followed by 3D multigroup Monte Carlo neutron transport calculations to solve the k_{eff} eigenvalue problem. All calculations were performed using the 238-group neutron cross section library based on ENDF/B-VII.0 data. All KENO calculations performed in this report used SCALE 6.1.3 [4].

Two different sets of nuclides can be used for fuel modeling in the CSAS models: (1) major actinides only (AO) and (2) major and minor actinides and major fission products (AFP). The nuclides used in the AO and AFP nuclide sets are taken from NUREG/CR-7109 [7] and are the same as those typically used when calculating PWR BUC. The same isotope sets are appropriate for use in BWR BUC because the same nuclides result from fission in both types of light water reactors. Table 2.1 provides the BUC nuclides considered in the AO and AFP sets. ^{155}Gd is included in the AFP set, but ^{157}Gd is not.

Table 2.1 Isotopes included in the AO and AFP isotope sets

10 AO isotopes									
^{234}U	^{235}U	^{238}U	^{238}Pu	^{239}Pu	^{240}Pu	^{241}Pu	^{242}Pu	^{241}Am	^{16}O
29 major and minor actinides and major fission products (AFPs)									
^{234}U	^{235}U	^{236}U	^{238}U	^{237}Np	^{238}Pu	^{239}Pu	^{240}Pu	^{241}Pu	^{242}Pu
^{241}Am	^{243}Am	^{95}Mo	^{99}Tc	^{101}Ru	^{103}Rh	^{109}Ag	^{133}Cs	^{147}Sm	^{149}Sm
^{150}Sm	^{151}Sm	^{152}Sm	^{143}Nd	^{145}Nd	^{151}Eu	^{153}Eu	^{155}Gd	^{16}O	

2.1.3 STARBUCS

The STARBUCS sequence provides an automated link between ORIGEN-ARP depletion calculations and CSAS criticality safety calculations. STARBUCS creates depleted fuel compositions based on pregenerated ORIGEN libraries, a fresh fuel description, and an input irradiation history. The sequence performs a depletion and decay calculation for each axial node in the cask model using the ORIGEN-ARP methodology and generates a material composition that can be directly entered into KENO. All STARBUCS calculations performed in this report use SCALE 6.1.3 [4].

The ORIGEN-ARP methodology performs ORIGEN depletion calculations using cross section libraries pregenerated for specific configurations as a function of burnup, and for discrete values of parameters characterizing these configurations (e.g., enrichment, moderator density). The pregenerated cross sections are interpolated using the ARP code over a range of varying fuel assembly properties, including burnup and moderator density. The interpolation scheme retains the accuracy of the explicit TRITON calculations used to pregenerate the cross section libraries. Figure 2.2 provides a flow chart showing the process of generating KENO models using STARBUCS.

A limitation of STARBUCS is that it can only use a single ORIGEN library in a calculation. Since the GE14 assembly design type examined in this work is modeled with two lattices—full and vanished—two STARBUCS calculations are needed to determine depleted compositions for the entire assembly. The compositions from the individual depletion calculations are combined to make a single set of compositions representing the depleted and decayed fuel compositions in each KENO calculation.

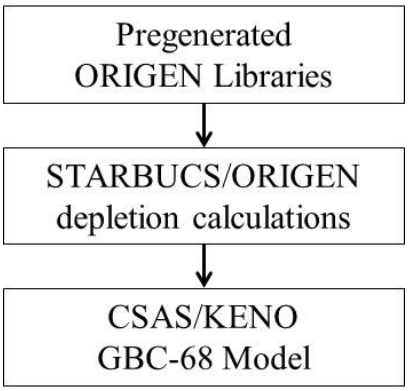

Figure 2.2 STARBUCS process to generate KENO models

2.2 Models

2.2.1 GBC-68

The GBC-68 computational benchmark model was developed in Reference [8] as a generic BUC cask for modeling BWR SNF. The KENO model of the fuel loaded in the cask explicitly represents each fuel rod, including its gap and cladding. Part-length rods are truncated at the appropriate elevation so that both the full lattice (referred to as *full* or *dominant*) and the vanished lattice are included explicitly in the KENO model. Section 2.2.2 includes further discussion of lattice modeling. The fuel assembly channel model is simplified in KENO, represented with constant thickness and squared corners. All fuel assemblies are assumed to contain fuel with identical compositions and irradiation histories. KENO calculations performed with depleted fuel compositions generated by TRITON assume a single average composition for nongadolinium fuel and seven unique compositions for the rings modeling the gadolinium pins in each axial node. KENO calculations performed with depleted fuel compositions calculated in STARBUCS assume a single average composition for all fuel in all pins within an axial node. The cross sections generated for the ORIGEN-ARP depletion represent the entire node, effectively smearing residual gadolinium burnable absorber into all fuel pins. The impact of this approximation is small since there is an insignificant amount of such residual burnable absorber at the burnups examined in these studies. All KENO models contain 25 axial nodes, each 6 inches in length (15.24 cm). This report references the nodes by numbering them from 1 to 25 from top to bottom within the assembly. Figure 2.3 shows a radial view of the GBC-68 half-cask model depicting the cask body, basket, and fuel assemblies. Figure 2.4 shows an axial view of the model with each unique axial fuel composition shown in a different color.

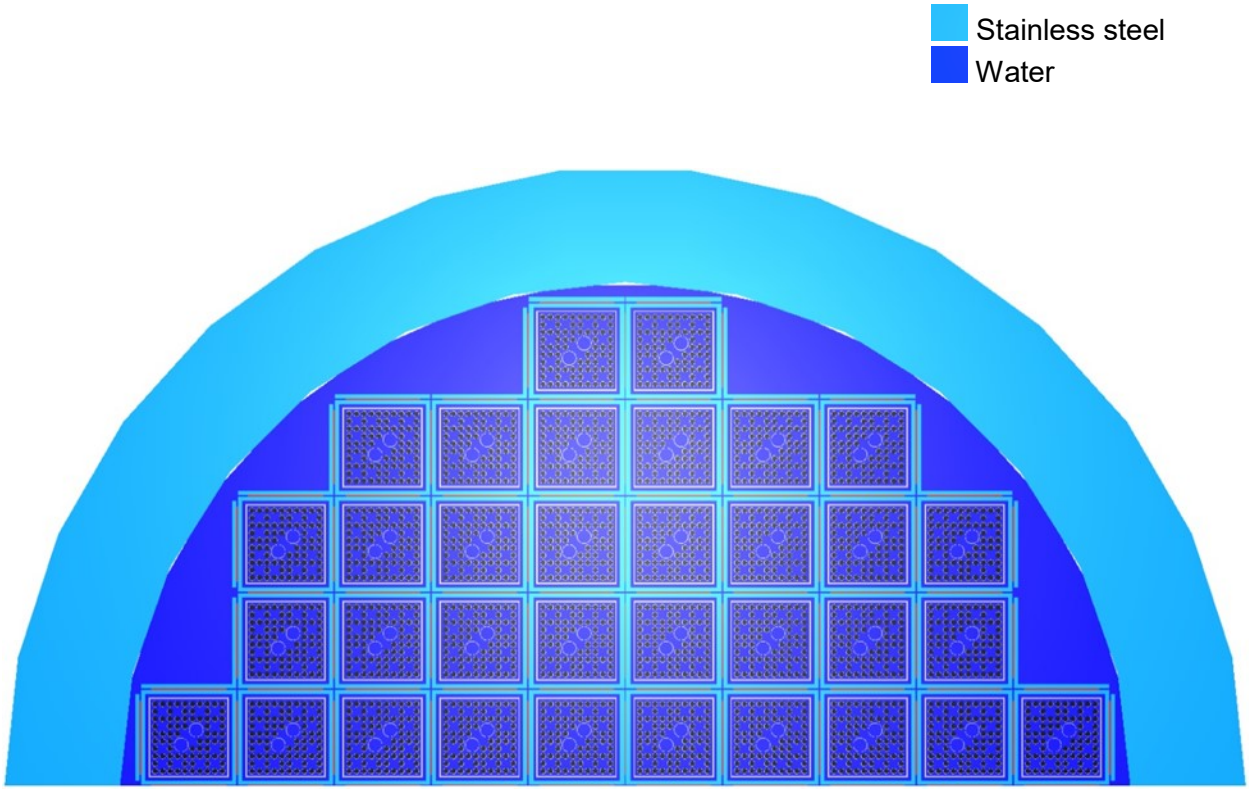

Figure 2.3 Radial view of the GBC-68 cask model in KENO in the VAN lattice

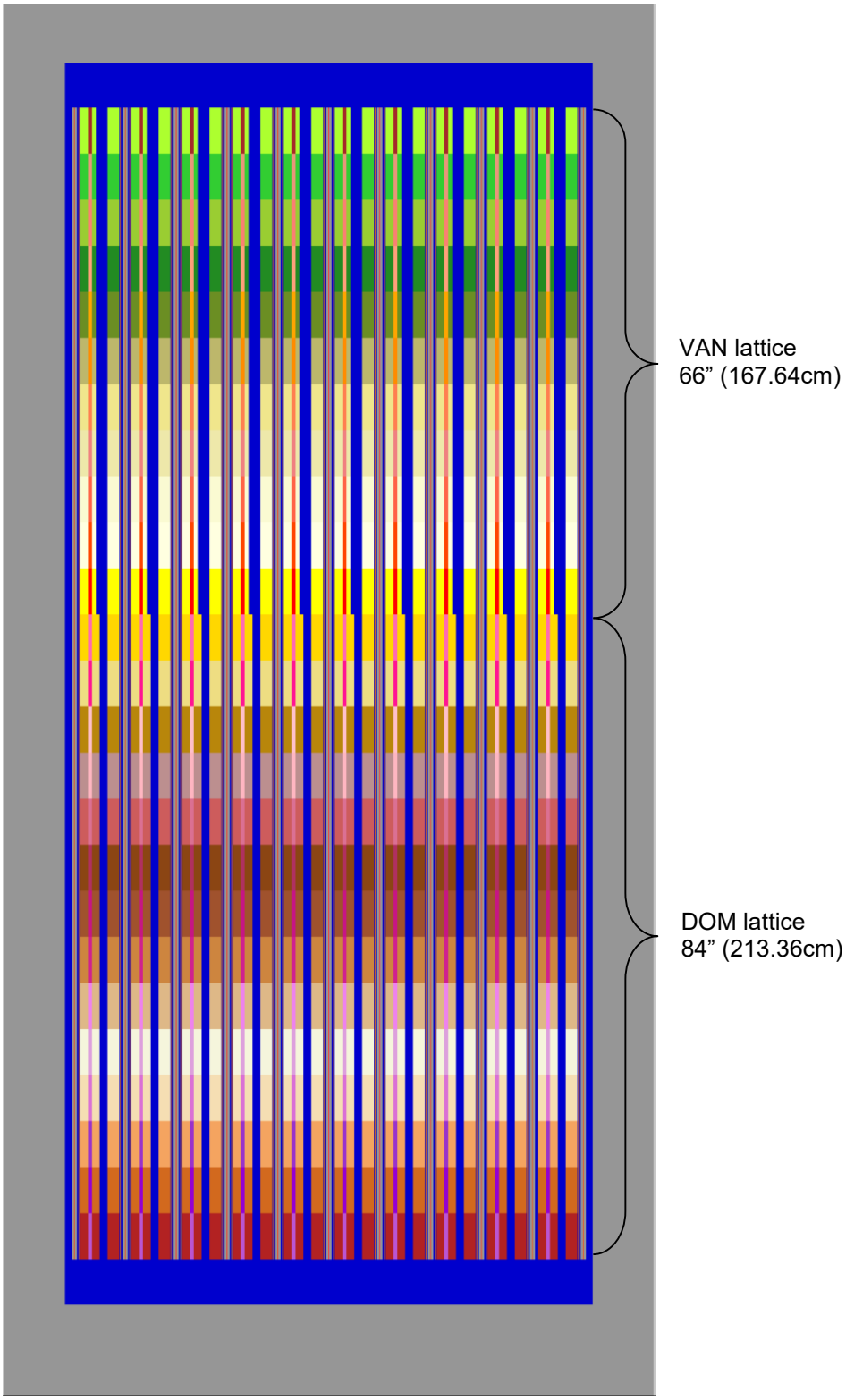

Figure 2.4 Axial view of GBC-68 cask KENO model

2.2.2 GE14

GE14 is the only fuel assembly design type used in these studies. This assembly has a 10 × 10 array of fuel pins and contains two large central water rods, each of which displaces four fuel rods. The GE14 fuel assembly can contain many axial levels with varying fuel enrichment and gadolinium loading. Owing to the presence of part-length fuel rods, which terminate at approximately half the total height of the fuel assembly, the GE14 fuel assembly contains two primary axial zones (or levels). These two axial regions are the dominant (DOM or full) and vanished (VAN) lattices. A 2D slice through one of these axial zones is referred to as a *lattice*. The full lattice has a fuel rod occupying every position in the fuel pin array. The vanished lattice is located axially above the part-length rods, so these rods are in effect *vanished* from the lattice. TRITON representations of the DOM and VAN lattices are shown in Figure 2.5. All gadolinium-bearing rods contain the same absorber loading in both the DOM and VAN lattices. Two-dimensional representations of the two lattices in the KENO model of GBC-68 for use with STARBUCS-generated depleted compositions are shown in Figure 2.6. No axial enrichment zoning is modeled for any calculations in this report aside from the investigation of natural enrichment axial blankets in Section 6.3.

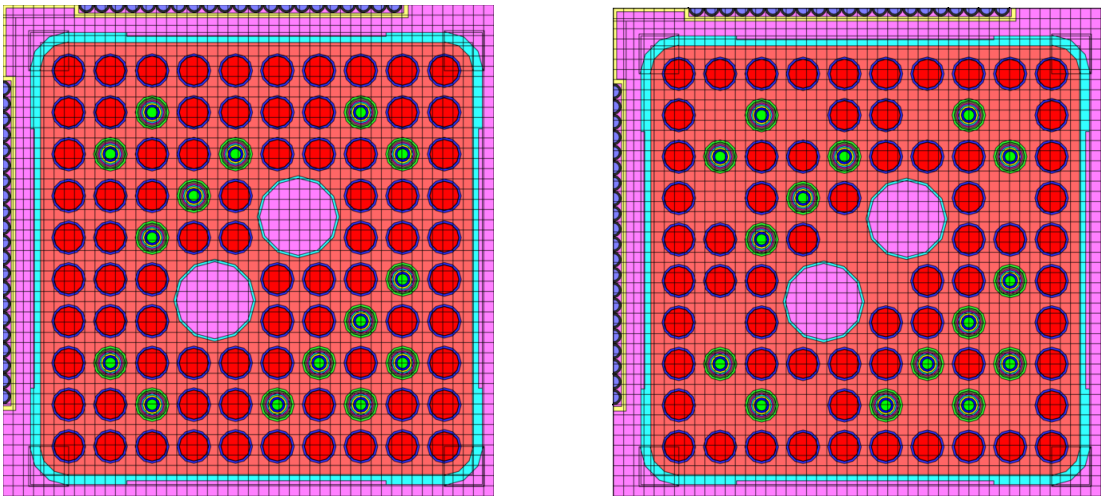

(a) (b)

Figure 2.5 TRITON model of the (a) DOM and (b) VAN lattice

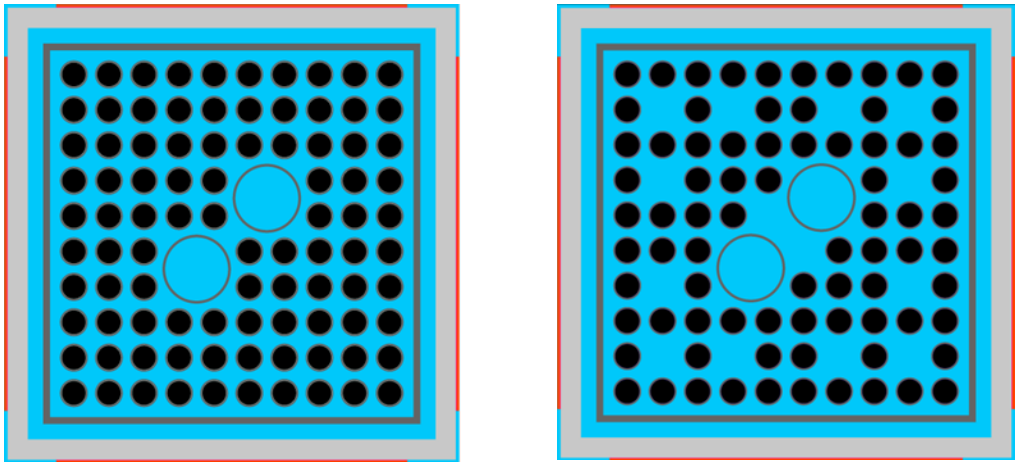

(a) (b)

Figure 2.6 (a) DOM lattice and (b) VAN lattice, both in storage cell in GBC-68

The GE14 fuel assembly was chosen for the studies herein, as it is the most common fuel assembly type used in US BWRs, contains advanced geometry features commonly seen in modern BWR fuel assemblies (e.g., water rods, part-length rods), is commonly loaded with pins enriched to near 5.0 wt % ^{235}U, and typically contains many gadolinium-bearing fuel pins. Results from studying various characteristics in a modern, highly heterogeneous fuel lattice such as the GE14 can be extended to other highly heterogeneous fuel configurations. A previous study [9] has shown that the GE14 assembly design is more reactive than smaller GE lattices (7 × 7, 8 × 8, and 9 × 9) for most burnups. Other lattice sizes may be more reactive at high burnup [9], but moderator density distribution, control blade history, and axial burnup profile effects are expected to be largely independent of assembly lattice size. Off-nominal temperature/density conditions for the moderator inside the cask model have not been considered. Differing fuel-to-water ratios among the different lattices may cause different responses to these off-nominal conditions and should also be examined.

The fuel assembly design used in these studies is based on an actual assembly from the detailed core follow data described in Section 3. All TRITON depletion calculations used 4.5 wt % ^{235}U in all pins and 15 gadolinium-bearing rods with 7 wt % Gd_2O_3. This single assembly design is used throughout the calculations to assess the effect of the different axial moderator density distributions, control blade histories, and axial burnup profiles independent of any effects potentially caused by differing fuel or absorber loadings. Additional enrichments, gadolinium loadings, or gadolinium-bearing pin patterns are not considered in this report. The sensitivities examined in this report are not expected to have a significant impact on any of these parameters. Each of the parameters being studied is varied singly to isolate its effect on discharged fuel reactivity. All other parameters, including specific power, fuel temperature, and moderator temperatures, are unchanged throughout these studies. The axial moderator density profile used in the control blade studies is shown in Figure 2.7a. The axial burnup profile used in studies of the axial moderator density profile and control blade use can be found in Figure 2.7b. The characteristics of higher reactivity fuel assemblies with regard to the axial moderator density distribution and burnup profile are presented in Sections 4 and 6, respectively.

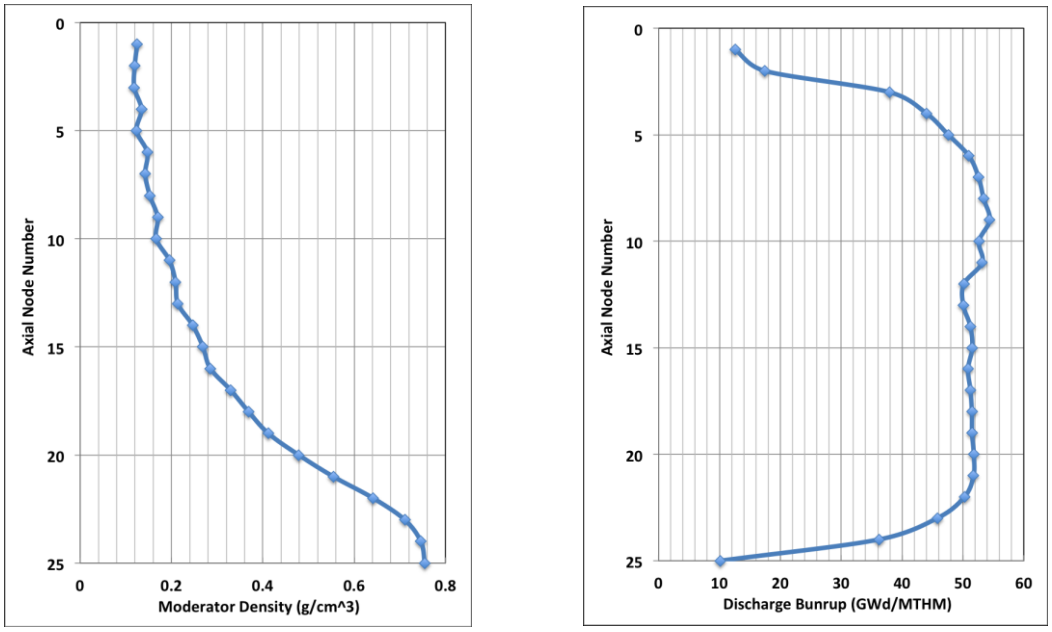

(a) (b)

Figure 2.7 (a) Axial moderator density profile and (b) axial burnup profile

3 POTENTIAL BWR DATA SOURCES

This section includes brief descriptions of the data sources available for axial moderator density distributions, control blade usage, and axial burnup profiles, along with an assessment of the data for their application to the planned studies. The area of study requiring the greatest amount of detailed data is the axial moderator density distribution study because of the need to examine modeling assumptions related to the frequency with which the node-wise moderator density must be changed in the simulation. Most of the data are judged to be insufficient for the planned studies, and information regarding these data sets is provided in Sections 3.2–3.6. The most common shortcomings are the lack of detailed operating data as a function of time (i.e., multiple state points per cycle), lack of recent or current data (most available data are from older fuel assembly design types), and the limited number of locations within the core having data. The description of the core follow data used for the studies documented in this report is provided in Section 3.1; the data sets described in the subsequent subsections are not used in this work.

3.1 Core Follow Data

Through another joint NRC and Oak Ridge National Laboratory (ORNL) project, the ORNL BWR BUC project gained access to proprietary operating data for a BWR core's single cycle. The data include inlet and outlet conditions and traveling in-core probe (TIP) data. These data include CASMO-SIMULATE [10] core follow data for every fuel assembly in the reactor. The data were obtained from a recent cycle that contained four different modern BWR fuel assembly design types: GE14, GNF2, SVEA-96 Optima 2, and ATRIUM-10. Each fuel assembly has been modeled with 25 different axial nodes, and the 690-day cycle was simulated using more than 240 time steps. The size of the time steps varies slightly, but all steps are less than 5 effective full power days in length. State variables such as the moderator density, power level, exposure, and control state can be extracted from the simulated data [10]. This data set was ideal for the studies documented herein because the simulated data contain sufficient detail to model axial moderator density profiles, control blade usage, and axial burnup profiles. The data are from a cycle that features modern fuel assemblies in a modern BWR cycle.

3.2 EPRI Reports on Peach Bottom and Hatch

The Electric Power Research Institute (EPRI) report for Peach Bottom [11] contains operating data (average inlet and outlet conditions) and TIP measurements for cycles 1 and 2 for Peach Bottom Unit 2. Very similar data exist for cycles 1–3 of Hatch Unit 1 [12, 13]. When these cycles operated, the reactors used 7 × 7 and 8 × 8 fuel assembles with very little gadolinium and few liquid water features (i.e., water rods). Thermal-hydraulic (T-H) data are limited to inlet and outlet conditions. The older design of these assemblies and the availability of only inlet and outlet T-H conditions make these sources inadequate for analyzing axial void profiles.

3.3 Grand Gulf Data

ORNL supported the NRC in 2006 for MELCOR analysis of the Grand Gulf Nuclear Station [14]. The data available for that analysis included reactor cycles 3, 4, 5, 11, 12, and 13 and configurations with 8 × 8, 9 × 9, and 10 × 10 fuel arrays. The fuel data provided by GE and Areva covered a diversity of assembly designs and axial moderator density profiles by assembly type. However, only average axial data were available, and the data are proprietary.

3.4 Swedish Interim Storage Facility Data

Data are available for a series of calorimetric measurements performed at the central interim storage facility for SNF (Clab) operated by the Swedish Nuclear Fuel and Waste Management Company (SKB) [15]. A variety of assembly types, including 8 × 8, 9 × 9, and 10 × 10 arrays, were among the 25 assemblies from eight Swedish reactors measured. Both GE and SVEA assembly designs were included, so this is another data set that can be compared across different design types. The axial moderator density profiles provided are lifetime average values by node and therefore cannot be used to support a temporal fidelity study. The data are not adequate for an axial distribution study because they have fairly low precision and generally represent older operating histories. The fuel assemblies included in this data set were irradiated between 1974 and 1996.

3.5 Commercial Reactor Critical Data

The commercial reactor critical data support validation efforts conducted as part of the Yucca Mountain Project. Several of these reports provide detailed information on early cycles of operation for Grand Gulf Unit 1 [16], LaSalle Unit 1 [17], and Quad Cities Unit 2 [18]. These reports contain detailed information about axial burnup profiles and moderator density profiles for each assembly in a specific operating cycle and for all prior cycles that those assemblies experienced. The data are generally only reported for 2–3 state points per cycle and are therefore not useful for a temporal fidelity study. All the cycles considered contain older fuel types and operational strategies. More recent operations are likely to be characterized by higher specific power for assemblies, extensive use of gadolinium burnable absorbers, and high void fractions.

3.6 Radiochemical Assay Data

Data are available for a large number of radiochemical assay (RCA) samples from a variety of programs conducted over the years. Two examples include data from Forsmark Unit 3 [19] and Limerick [20]. Very detailed information is contained in these reports for the conditions near the location or locations at which RCA samples have been taken. Unfortunately, this data coverage does not extend to the entire core, so it does not provide insight into the full range of operating conditions, burnup profiles, or axial moderator density profiles present in a core.

4 AXIAL MODERATOR DENSITY DISTRIBUTIONS

Because of the boiling of the coolant in a BWR, the moderator density (or void fraction) changes significantly as a function of axial position in the reactor. For each fuel assembly in the reactor, the power generated by the assembly has a significant impact on the moderator density change from the bottom to the top of the fuel assembly. Many different factors contribute to the power produced by a fuel assembly, including assembly design, burnup, control blade position, neighboring fuel assemblies, and assembly position within the core. The effects of these factors can be clearly observed in the moderator density profile data.

This section documents studies of two different aspects of axial moderator density distributions. The first is a study investigating the frequency with which the moderator density must be updated during depletion calculations to obtain accurate results. This study is termed *temporal fidelity study* throughout this document. The second study directly examines the effect of the axial moderator density distribution on storage and transportation system reactivity. This second study includes both an assessment of limiting axial moderator density profiles and an investigation of axial profile parameterization. In this context, *parameterization* is the determination of a single quantitative value to describe an axial moderator profile. The parameterization would potentially serve in identifying limiting profiles without performing depletion and subsequent k_{eff} calculations. The second study is referred to as the *axial moderator density study* throughout this document.

The primary goal of the studies presented in this section is to analyze the effects of the moderator density (alternatively, void fraction) axial profile on cask reactivity. To understand these effects, a number of different axial profiles must be generated for testing. BWR design and operation data typically consider void fraction instead of moderator density. Therefore, discussions in this section focus on void fractions for consistency with industry practice. The void fractions are converted to moderator density for use in SCALE input files.

4.1 Void Fraction Variability within the Core

The variability of the void fraction is very large over the entire reactor. Figure 4.1 shows plots of the cycle-average axial void profiles for all 624 fuel assemblies in the detailed core follow data set. Nodes are numbered 1–25 progressing from the top to the bottom of the core. The color of each line indicates the radial distance of the fuel assembly from the centerline of the core, ranging from dark blue for assemblies near the center of the core to dark red for the assemblies farther from it. In general, high void fraction assemblies exist near the center of the core, while low void fraction assemblies are typically near the radial periphery of the core. In Figure 4.1, a bold black line plots the core-average void profile. For a single axial node, the void fraction can change by as much as 65% across the core, illustrating the highly variable nature of the void fraction in modern BWRs. Figure 4.1 indicates depressions in the void fraction for certain axial levels due to the effect of the spacer grids in the fuel assemblies.

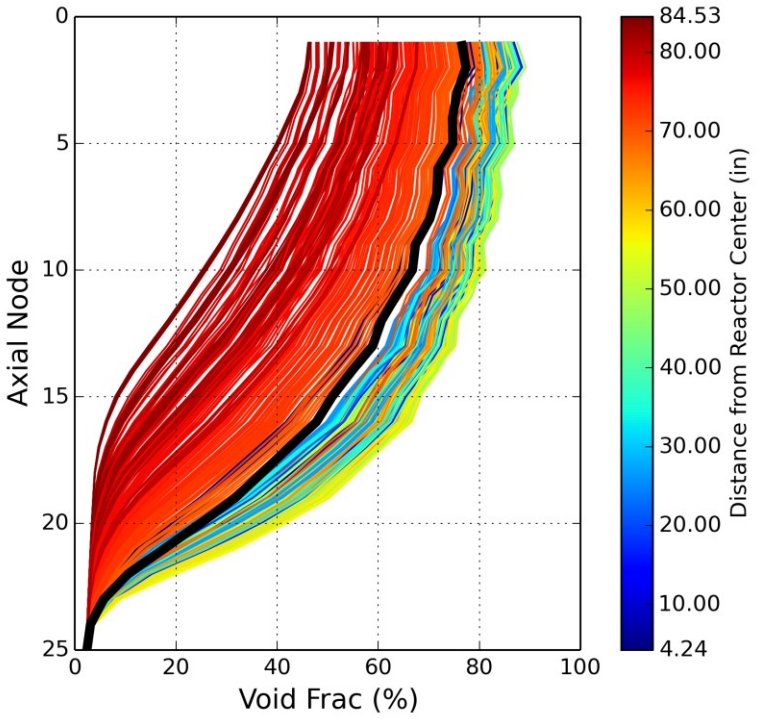

Figure 4.1 Cycle-average axial void fraction profiles for each fuel assembly in the reactor

4.2 Void Fraction Variability for a Single Assembly

The axial void profile data have been divided into first-, second-, and later-cycle fuel assemblies. This classification has been derived because the available operating data did not include information on the number of cycles for which a fuel assembly has been present in the core. First-cycle fuel assemblies are readily identified because the beginning of cycle (BOC) exposure is 0.0 GWd/MTU, but it is not clear which fuel assemblies are second-, third-, or higher cycle fuel assemblies. The BOC exposure of the axial center node (node 13) was used to make a determination for the remaining fuel assemblies. If the BOC node 13 exposure is greater than zero but less than 30 GWd/MTU, then the fuel assembly is a second-cycle fuel assembly. If the BOC node 13 exposure is greater than or equal to 30 GWd/MTU, then the fuel assembly is assumed to be a later cycle fuel assembly.

The void fraction profile varies significantly over time for a single assembly within a single cycle, as well as over the life of the fuel assembly. Figure 4.2 plots the axial void profile for a first-, second-, and later cycle fuel assembly in the core. The color scheme shows the cycle depletion step number of the core follow data. Therefore, blue colors are early in the cycle, and red colors are late in the cycle. Because only a single cycle of data exists, each of the three axial profiles in Figure 4.2 is from a different assembly. However, the axial shapes of the void profiles are largely similar among first-, second-, and later-cycle fuel assemblies. The effect of the gadolinium absorber is apparent in the first-cycle fuel assembly (left plot in Figure 4.2). The blue lines, which represent time (depletion) steps near the beginning of the cycle, are nearly hidden by the later steps. The change in the axial void profile directly correlates with the reactivity of the fuel assembly due to depletion of the gadolinium absorber. As gadolinium is consumed, the void fraction increases due to higher relative power in that fuel assembly. Late in the cycle, the fuel

depletion leads to lower power in the assembly, and the void fraction then begins to decrease. In the second-cycle fuel assembly (middle plot in Figure 4.2), the exit void fraction begins at a relatively high value, above 80%, and then decreases fairly consistently throughout the cycle. For the later-cycle fuel assembly (right plot in Figure 4.2), relatively little fissile material is left in the assembly, so the axial void profile decreases from the beginning to the end of the cycle as the assembly produces progressively less power as the cycle proceeds. Note that the void fraction values are larger in the first two cycles (greater than 80% at the top of the assembly), while the values are much smaller for the later cycle (only 60% at the top of the assembly).

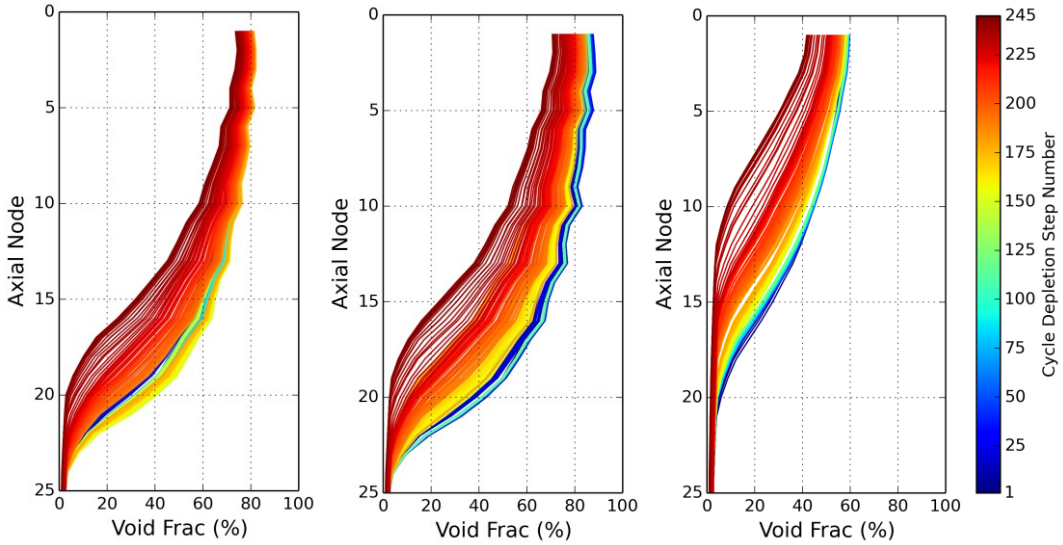

Figure 4.2 Axial void profiles for selected first- (left), second- (middle), and higher cycle (right) fuel assemblies

4.3 Selection of Limiting Profiles

In this report, the profiles expected to be the most limiting were applied to a single assembly design to perform a study that isolates the effect of the axial void profile. However, some axial void profiles may be unique to certain fuel assemblies. To determine whether this is the case, all axial void profiles in the core were averaged over the cycle and then plotted to visually inspect the uniqueness of certain profiles to certain fuel assembly types. Each figure in this section represents the cycle-average void profile for that particular assembly type. Within each assembly type, different designs contain enrichment and gadolinium rods that vary in position and poison content. The impact on axial void distribution of variations in fuel assembly design for the same fuel assembly type have not been studied in this work.

Figure 4.3 plots the cycle-average void profile for each assembly by assembly type. In these figures, the color of the line denotes how many cycles of irradiation a certain fuel assembly has accrued (first cycle is red, second cycle is blue, and later cycle is green). The SVEA-96 Optima 2 (SVEA-96) fuel is the only fuel assembly type that contains fuel for all categories; therefore, the variability of the average void profile is significant. For the GE14 fuel assemblies, there is significant separation between second- and later cycle fuel assemblies, but there is a more continuous distribution of void profiles for the SVEA-96 fuel assemblies. The reason for this behavior is that there are significantly more SVEA-96 fuel assemblies used in this cycle than

any other type. Data from additional plants and cycles could further elucidate potential axial void profile variation and its causes.

Figure 4.4 plots the cycle-average axial void profiles for each assembly, but each plot now corresponds to first- (Figure 4.4a), second- (Figure 4.4b), and later cycle (Figure 4.4c) fuel assemblies. In this figure, the color of the line denotes fuel assembly type: SVEA-96 is plotted using purple, GNF2 is plotted using blue, GE14 is plotted using green, and ATRIUM is plotted using red. SVEA-96 and GNF2 are the only fuel assembly types containing fresh fuel (Figure 4.4a). The axial void profiles in Figure 4.4a for the SVEA-96 and GNF2 fuel types result in nearly identical void profiles for the fresh fuel; the axial void profiles for the GNF2 fuel span the axial void profiles for the SVEA-96 fuel. In Figure 4.4b (second-cycle fuel), only SVEA-96 and GE14 fuel exist, and the GE14 fuel results in axial void profiles with higher average void fraction values (further right) than the SVEA-96 fuel. However, there is still significant overlap between the two fuel assembly types. Because there are significantly more SVEA-96 fuel assemblies than GE14 fuel assemblies in the core, more data are available for SVEA-96 fuel assemblies than for GE14 fuel assemblies. In Figure 4.4c (later-cycle fuel), the axial void profiles for the GE14, ATRIUM, and SVEA-96 fuel assemblies overlap each other. Several SVEA-96 fuel assemblies have higher average void fractions than the others, but this may be due to the choice of exposure boundaries used to define first-, second-, and later cycle fuel assemblies, or it may be related to the location of these fuel assemblies in the core.

These results indicate that the void profile is more sensitive to exposure and core position than to fuel assembly type. The studies herein apply the most limiting profiles to the GE14 fuel assembly design to isolate the impact of the void profile on cask reactivity.

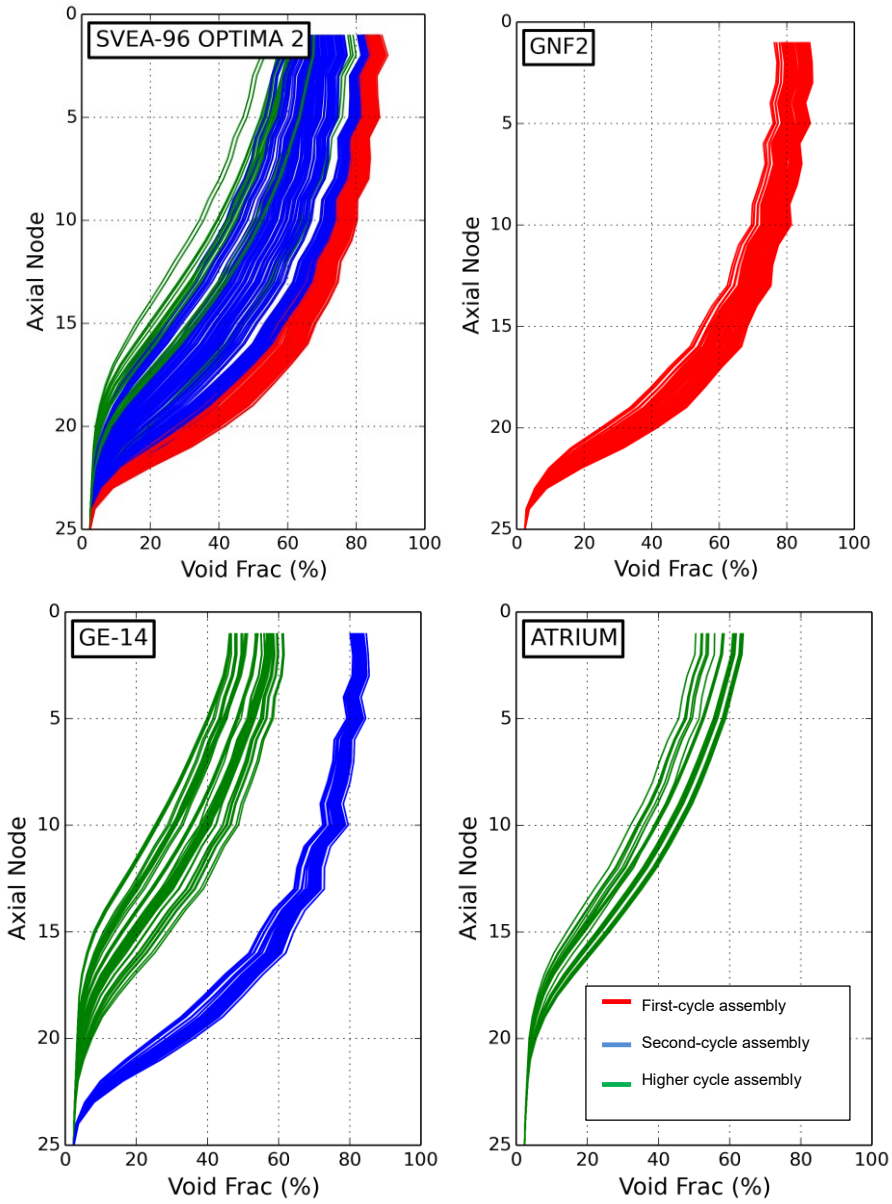

Figure 4.3 Cycle average axial void profiles for SVEA-96 Optima 2 (upper left), GNF2 (upper right), GE14 (lower left), and ATRIUM (lower right) assemblies

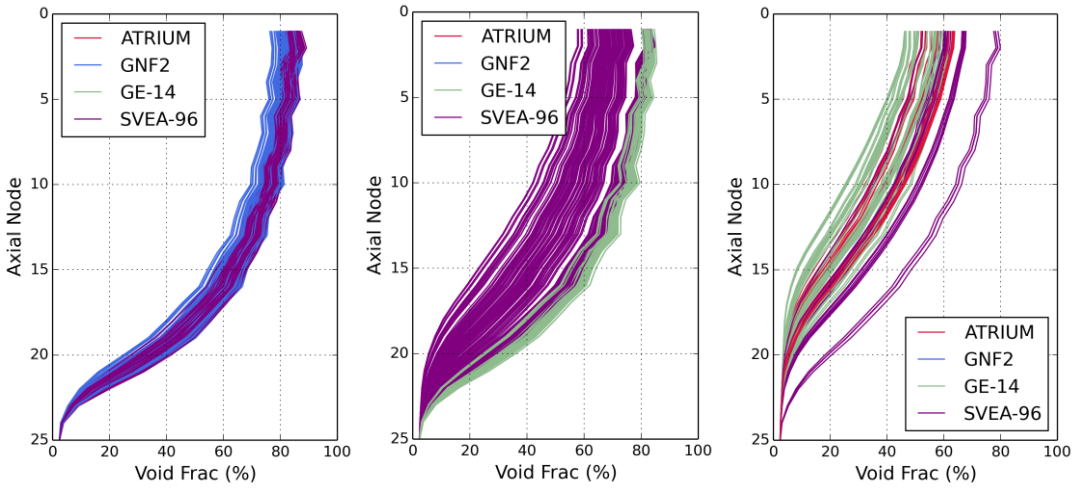

Figure 4.4 Cycle average void profiles for (a) first-, (b) second-, and (c) third- or higher cycle fuel assemblies

4.4 Profiles Used

The requirements of the temporal fidelity study and the axial moderator density study are different, and they drive the selection of different types of axial moderator profiles. The goal of the temporal fidelity study is to determine how frequently the moderator density distribution must be updated during depletion calculations. The best data for this study contain highly variable moderator density distributions. The axial moderator density study is expected to be dominated by profiles with high void fractions in the top portions of the assembly for an extended period of operation. These profiles have inherently low variability and are therefore likely to be excluded from the temporal fidelity study despite being of significant interest in conservative cask reactivity determinations. The following subsections discuss the selection process for the profiles used in each of the studies.

4.4.1 Profiles Used in the Temporal Fidelity Study

To perform depletion calculations that result in conservative reactivity determinations for SNF in casks, one must determine how fine a time scale must be used to capture the time-varying effects of key variables. Sections 4.1 and 4.2 presented the significant variability of the coolant void fraction both throughout the core (variability in space) and within each fuel assembly (variability as a function of time or burnup). With such significant variability in void fraction, the question of how large an impact this variability ultimately has on SNF cask criticality must be answered. A temporal fidelity study has been performed to answer this question.

To begin this study, the fission distribution in a fuel cask filled with depleted BWR fuel assemblies was estimated as seen in Figure 4.5. The figure clearly shows that the majority of fissions in a flooded BWR fuel storage cask occur near the top of the cask; this effect is known as the *end effect*, which is well documented for PWR fuel [21]. These results were generated as part of earlier work for the NRC [22] that examined the effect of fuel reconfiguration on storage and transportation systems. This plot was generated as part of this study to identify the most important axial regions of a spent BWR assembly for cask reactivity. The fuel represented in

Figure 4.5 is based on the GE14 design, also being used in the present studies, and has been depleted to 35 GWd/MTU. Figure 4.5 indicates that the fuel assembly reactivity in the cask is dominated by the upper portion of the fuel assembly. As discussed in Section 5.2.2, deviations from this axial profile could be caused by significant periods of depletion with control blades inserted between 50% and 75% of the core height. There are no realistic control blade exposures that exhibit that type of behavior and, as discussed in Section 5.2.3, all the realistic control blade histories included in this report result in top peak distributions similar to the one shown in Figure 4.5.

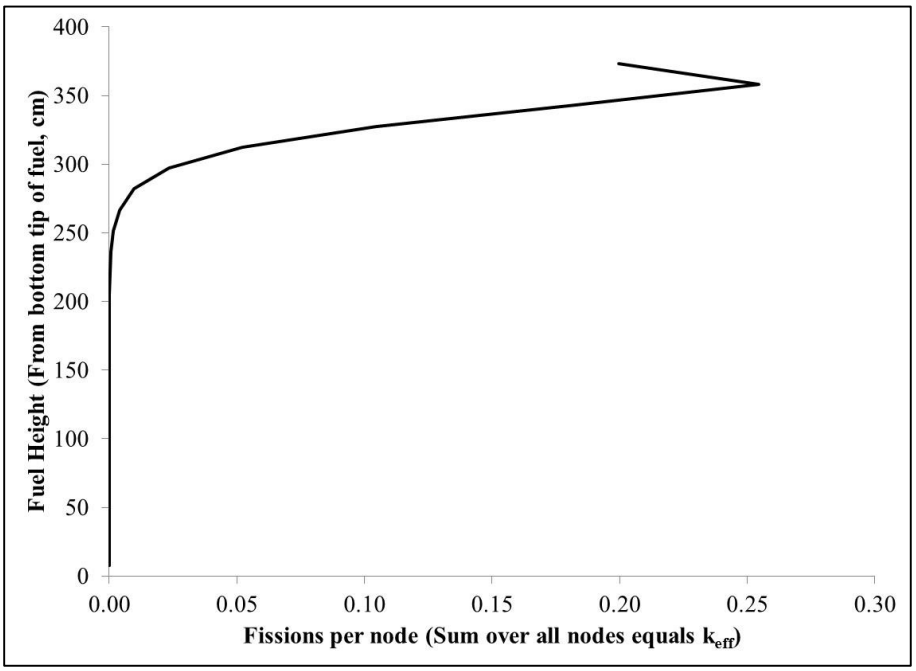

Figure 4.5 Axial fission distribution for BWR SNF in GBC-68

Because the upper portion of the fuel assembly has such a significant impact on cask criticality, axial profiles that have a significant change in the exit void fraction over the cycle were chosen for the temporal fidelity study. A search algorithm was used on the operating data to determine which fuel assemblies underwent the maximum change over the cycle. In general, the later-cycle fuel assemblies have more significant axial void fraction variability over a single cycle than the first- or second-cycle fuel assemblies, but they also tend to exhibit lower cycle-average void fractions than the first- or second-cycle fuel assemblies. Because of these complexities, axial void profiles from two different assemblies were chosen for the temporal fidelity study. The axial void profile from the fuel assembly with the most variability (MV) but with a relatively low average void fraction was selected. The variance of the void fraction over core height is calculated for each assembly at each time step. The variance of the set of variance values is then calculated for each assembly over the cycle, and the largest value identifies the MV assembly. In other words, the MV profile represents the assembly with the greatest change in axial void profile over the cycle. Another axial void profile from a fuel assembly with relatively high variability and high average (HA) void fraction was also chosen for the temporal fidelity study because the high integral void fraction case is likely to result in more conservative discharged fuel k_{eff} values. The two selected axial void fraction profiles are presented in Figure 4.6, with the high exit variability case (MV) on the left plot and the high integral void fraction case (HA) on the right plot. As before, the figures show the void fraction over the

assembly height, with early cycle steps in blue shifting to late cycle steps in red. Testing the profiles that are highly variable over a cycle ensures that the resulting temporal fidelity required for modeling will be sufficient for all other fuel assemblies with lower void fraction variability. The results of the study will demonstrate what temporal fidelity is required for void fraction modeling.

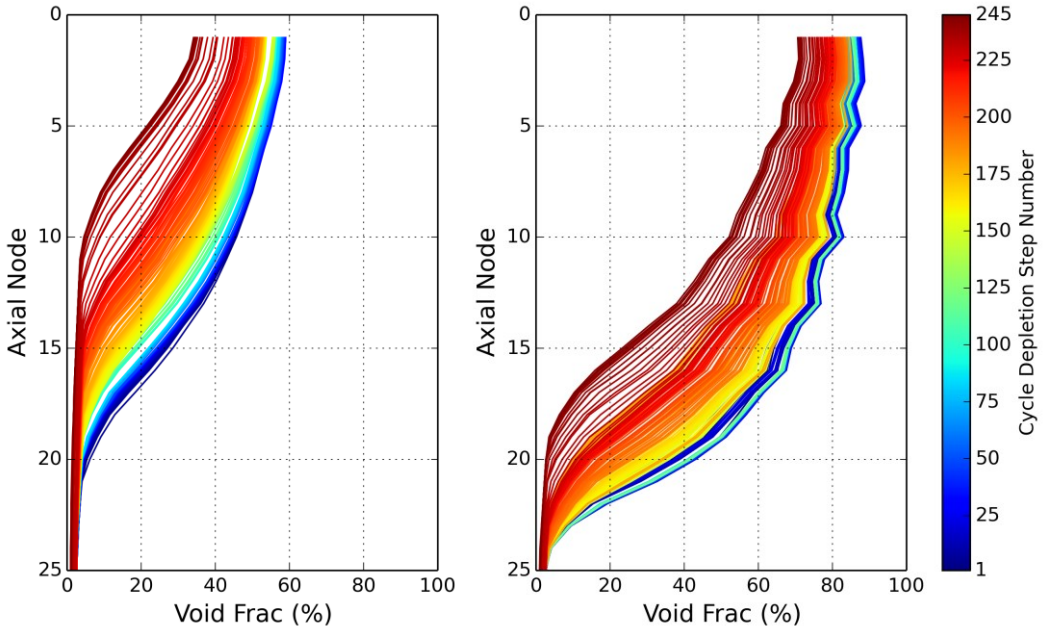

Figure 4.6 Selected axial void profiles used for the temporal fidelity study with the maximum exit void fraction variance case (MV) on the left and the high variance and high integral void fraction case (HA) on the right

4.4.2 Profiles Used in Axial Moderator Density Profile Study

The cycle average moderator density profiles for all 624 assemblies in the detailed core follow data are available for use in the axial moderator density distribution effect study. These data are presented in Figure 4.1. Figure 4.5 shows that the upper portion of a fuel assembly determines its reactivity in the storage and transportation cask, so the upper portion will drive determination of the limiting void profiles. The main goals of this study are (1) to confirm these logical inferences and (2) to clarify, if possible, the length of the upper portion of the assembly that is relevant to reactivity determinations. It is unlikely that a completely defensible formulation can be developed to proscriptively provide the limiting profile in all cases; however, a process through which limiting candidates can be identified and screened to determine limiting conditions will be proposed.

4.5 Results

This section provides the results of the temporal fidelity study and the axial moderator density profile study. The temporal fidelity study results include both TRITON and KENO results, while the axial moderator density profile study is focused on KENO results derived from STARBUCS depletion calculations.

4.5.1 Temporal Fidelity Study

To determine the temporal fidelity required for updating moderator density during depletion, 2D TRITON depletion models were generated for each axial level of the fuel assembly (25 in total). Each model used 23 depletion steps per cycle and was depleted for three cycles (69 total depletion steps) and a zero-power (decay) period of 30 days between consecutive cycles. Each depletion step was 30 days in length, so a full cycle lasted 690 days and reached a burnup of approximately 15.5 GWd/MTU. The power in each TRITON model was adjusted to result in a discharge burnup profile that corresponds to the fuel assembly whose void profile is shown in the left of Figure 4.6 (MV). A 2D representation of the TRITON model used in the temporal fidelity study is presented in Figure 4.7 and the axial burnup profile used is shown in Figure 2.7(b). The fuel lattice shown in Figure 4.7 is the full lattice; however, the vanished lattice was also modeled to represent regions above the part-length rods. As discussed in Section 2.2, no axial enrichment zoning is modeled in this study. Because only a single cycle of operating data exists, the axial profile was not varied between the three cycles; the same axial moderator density profile was modeled for all three consecutive cycles. Although this is not an accurate physical description, it is conservative, as any moderator profile that is limiting would be further limiting if the assembly were to experience that axial moderator density profile for three consecutive cycles. Furthermore, the axial burnup and temperature profiles are held constant to isolate the effect of axial moderator profile modeling in this study.

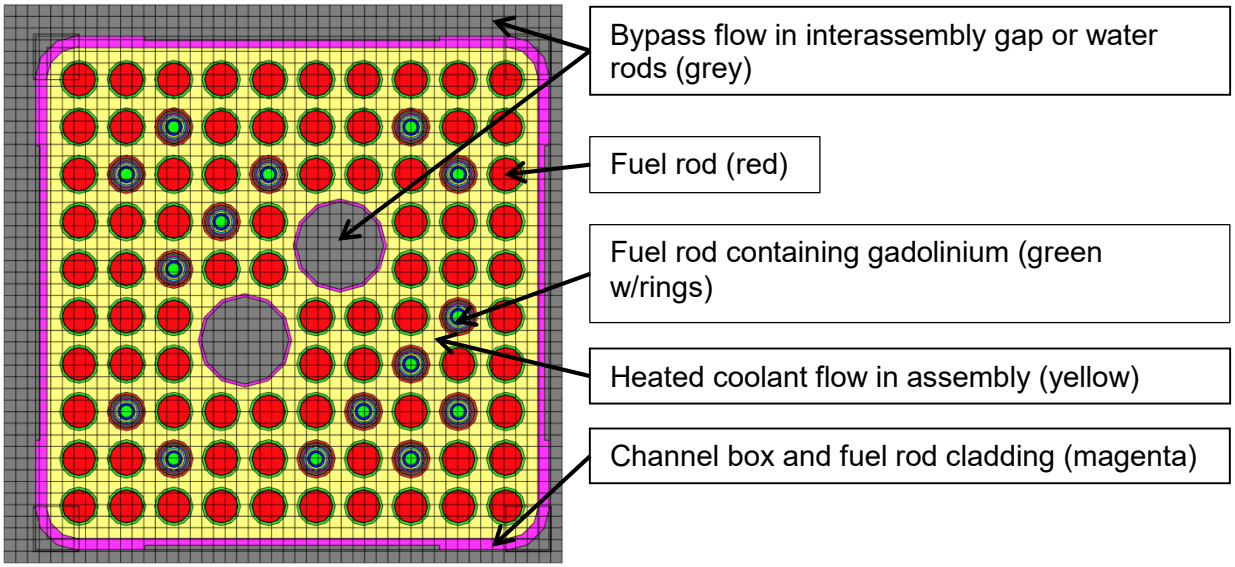

Figure 4.7 TRITON model used for the temporal fidelity study

The operating data were used to generate a TRITON timetable for each node in which the moderator density is modified as a function of time. Because the operating data exist on a much finer timescale than is reasonable for TRITON depletion calculation run times, the moderator density must be time-averaged over each depletion step. This averaging process was performed for a variety of different intervals (1, 2, 4, 7, 13, or 23) per cycle. For example, in the 23-step case, the moderator density was modified for every depletion step; and in the 1-step case, the moderator density was held constant at the cycle-average value. For this study, the depletion steps (23 steps per cycle, 69 total steps) were held constant for all moderator density averaging schemes. The 1-, 2-, and 23-step schemes for the MV and HA cases are presented

in Figure 4.8 for node 3; all other temporal fidelity step schemes have been omitted to enhance clarity of the figure.

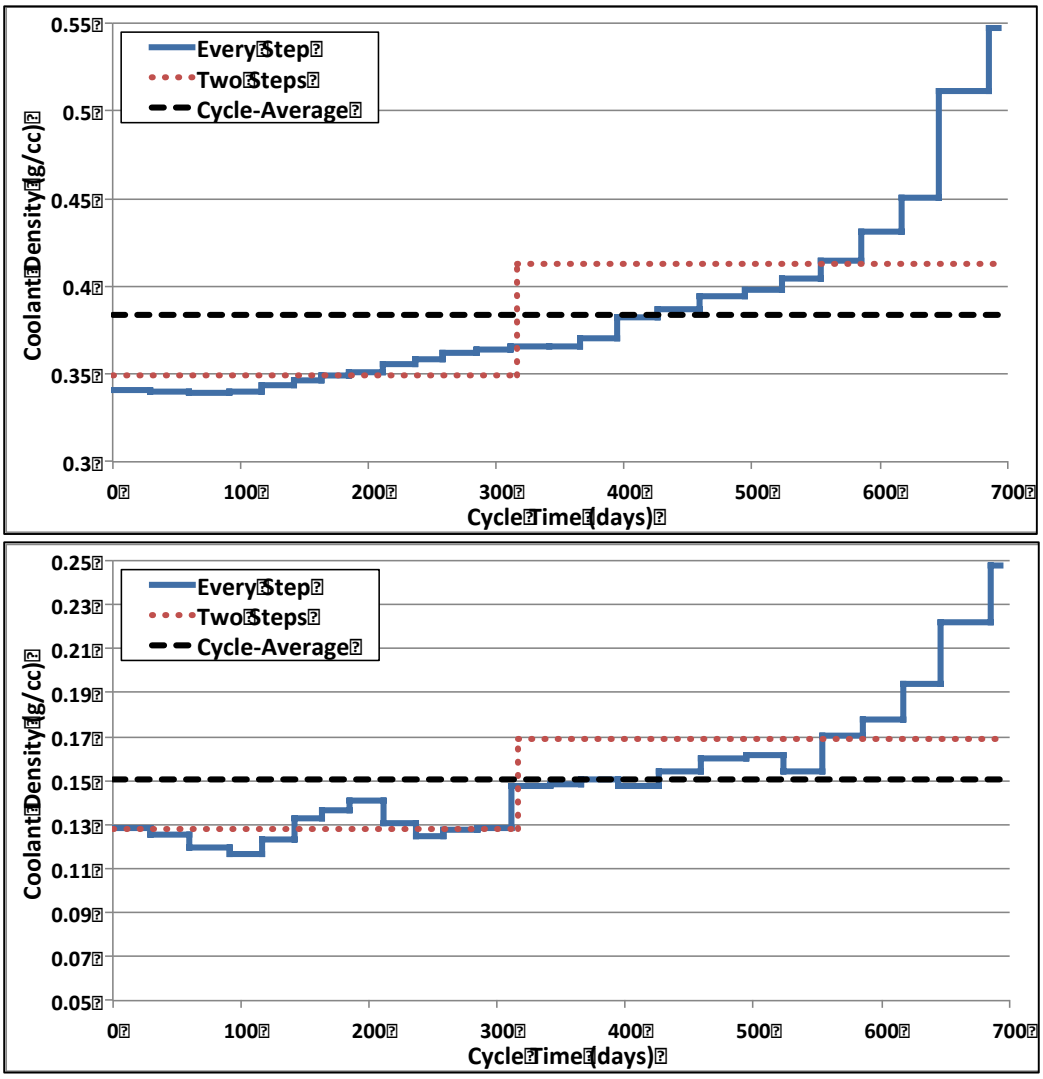

Figure 4.8 Cycle average (one step), two step, and every step (23 steps) moderator density temporal fidelity schemes for MV (top) and HA (bottom)

The key comparison of these temporal fidelity studies is the full-detail (23 steps per cycle) and the cycle-average cases. An adequate number of depletion steps should be performed in order to accurately predict isotopic compositions regardless of the temporal fidelity of the moderator density. The depletion step size used in this study was less than 0.7 GWd/MTU. The most accurate treatment possible is to modify the moderator density with every depletion step. However, if a cycle-average void fraction approach results in a relatively small bias, then a more simplified approach—such as the approach used in STARBUCS/ORIGEN-ARP—is possible. The moderator density cannot be modified as a function of time in STARBUCS, so this type of approach can only be used if a cycle-average moderator density profile provides sufficient accuracy. A cycle-average approach would also be advantageous because a licensee would not need extensive operating history data, which would probably be difficult to obtain.

In Figure 4.9, the ^{239}Pu atom density is plotted as a function of node-average burnup for the 23-step and the cycle-average moderator density schemes for the third axial node from the top of the core in the MV case. This node extends from approximately 320 cm to 335 cm above the bottom of the fuel, and it is selected because it is the node that exhibits the maximum fission density in Figure 4.5. Figure 4.9 shows that ^{239}Pu number densities generated with the cycle-average void fraction compare quite well when compared to the 23-step reference case, with differences in isotopic content of +/- 1% above 10 GWd/MTU burnup. The difference at the discharge burnup of ~40 GWd/MTU is approximately 0.4%. The line plotting the difference in ^{239}Pu between the two cases (cycle average minus 23-step divided by 23-step) shows a distinct trend. At the start and end of each cycle, the ^{239}Pu atom densities are very close because the integral void history is the same for both cases through these points. In other words, the area under each of the curves plotted in Figure 4.8 is equal when integrated to these points. At burnup points that lie between the beginning and end of each cycle, the void history is not equal, leading to a bias. The small differences in the ^{239}Pu number density at the end of cycle (EOC) points are the result of the differences between detailed and average moderator density treatment. These results suggest that if the average void fraction is modeled for each node in the assembly, then the prediction of the end of life (EOL) ^{239}Pu number densities will be sufficiently accurate. The true measure of whether the cycle-average void fraction approach provides sufficient accuracy will be determined by the spent fuel cask criticality calculations, which take into account all isotopes along with ^{239}Pu. The assessment of ^{239}Pu is included only to provide some background regarding the physics of the different temporal void fraction modeling approaches.

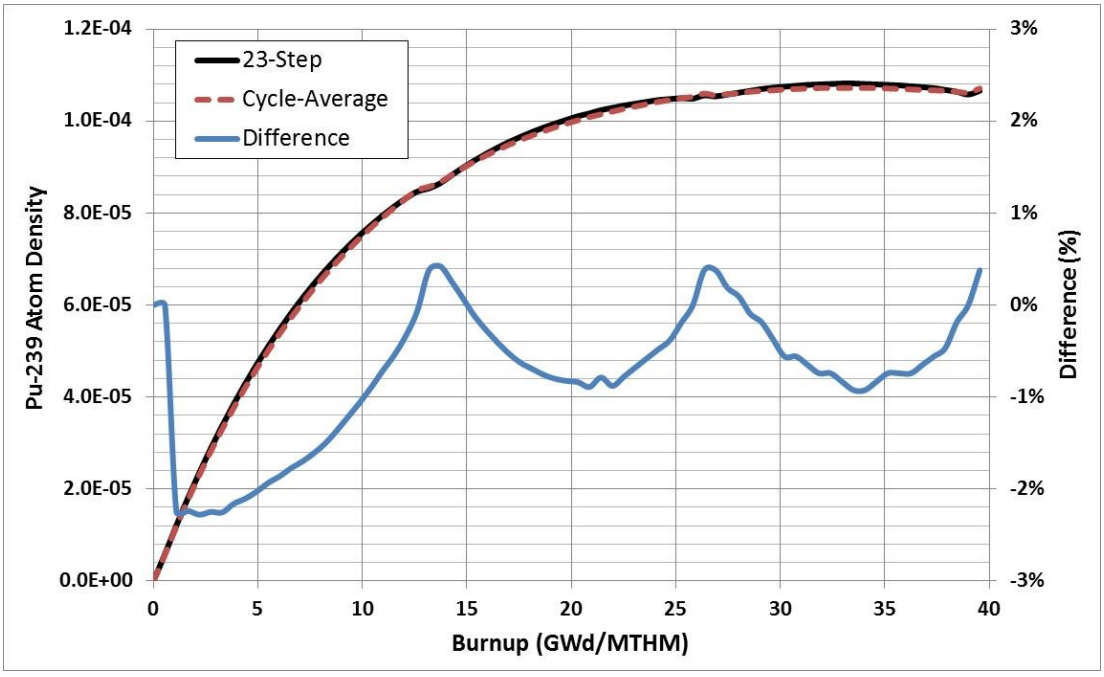

Figure 4.9 ^{239} Pu atom density as a function of burnup for the MV case
The percent difference between the 23-step and cycle-average cases is plotted on the secondary axis

The depleted isotopic compositions which result from the TRITON depletion calculations are used in KENO calculations to determine the k_{eff} value for the GBC-68 cask model loaded with fuel depleted with the different profiles and modeling approaches. The KENO calculations are

performed for both the HA and MV profiles for both the detailed 23-step and the average 1-step moderator density averaging scheme depletion calculations for both the AO and AFP isotope sets.

Figure 4.10 shows the MV profile results for the AO isotope set, and Figure 4.11 shows them for the AFP isotope set. The results are shown as a function of assembly average burnup. The k_{eff} values that correspond to the use of the average moderator density in the depletion calculations are shown with a solid blue line. The k_{eff} values that correspond to the use of detailed moderator density data in the depletion calculations are shown with a dashed red line. These lines are read on the primary vertical axis and show close agreement throughout the full burnup range considered. The difference between the two k_{eff} values (k_{eff} for the cycle average void fraction minus k_{eff} for the detailed void history) is shown with the dotted green line, which is read on the secondary vertical axis. The uncertainty in each KENO-calculated k_{eff} is approximately 0.00010 Δk_{eff}, so the uncertainty in the difference between the two values is about 0.00014 Δk_{eff}. Any difference less than 0.00028 Δk_{eff} represents less than two standard deviations and therefore cannot be considered statistically significant at a 95% confidence level. The difference between the k_{eff} values is small, and the detailed moderator density treatment is usually slightly more reactive than the average moderator density treatment. The shape of the difference as a function of burnup for the AO isotope set shown in Figure 4.10 closely follows the difference in ^{239}Pu number densities shown in Figure 4.9. The differences for the AFP isotope set shown in Figure 4.11 are generally smaller than the differences seen for the AO isotope set. The largest difference between the two sets of results is approximately 0.0013 Δk_{eff} for the AFP isotope set at 25.3 GWd/MTU burnup, where the detailed moderator density treatment is more reactive. The average moderator density treatment is never more than 0.0005 Δk_{eff} more reactive than the detailed treatment. The average moderator density treatment tends to be slightly less reactive than the detailed treatment, but there are some exceptions to this tendency.

The results for the HA profile are shown for the AO isotope set in Figure 4.12 and for the AFP isotope set in Figure 4.13. These results are shown as a function of assembly average burnup. The results for the HA assembly are similar to those for the MV assembly, though the differences between the average and detailed depletion calculations may be slightly smaller in the HA profile. As shown in Figure 4.6, the HA profile has less variability than the MV profile, so smaller differences would be expected. It is difficult to definitively assert that the difference between the average and detailed treatments is smaller for the HA profile given the small size of the differences resulting from both treatments for both profiles. The largest differences between the two sets of results again occurs at a burnup of 25 GWd/MTU in the AFP isotope set, though for the HA profile the difference is only 0.0007 Δk_{eff}, where the detailed moderator profile result is more reactive. The average moderator density results are generally slightly less reactive for the HA profile, just as they were for the MV profile.

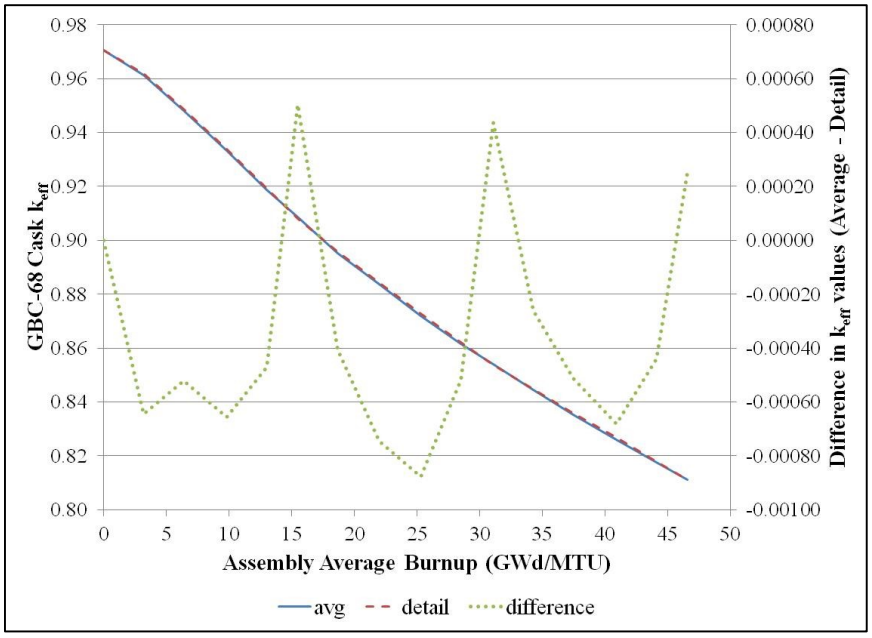

Figure 4.10 GBC-68 results for the MV moderator profile, AO isotope set

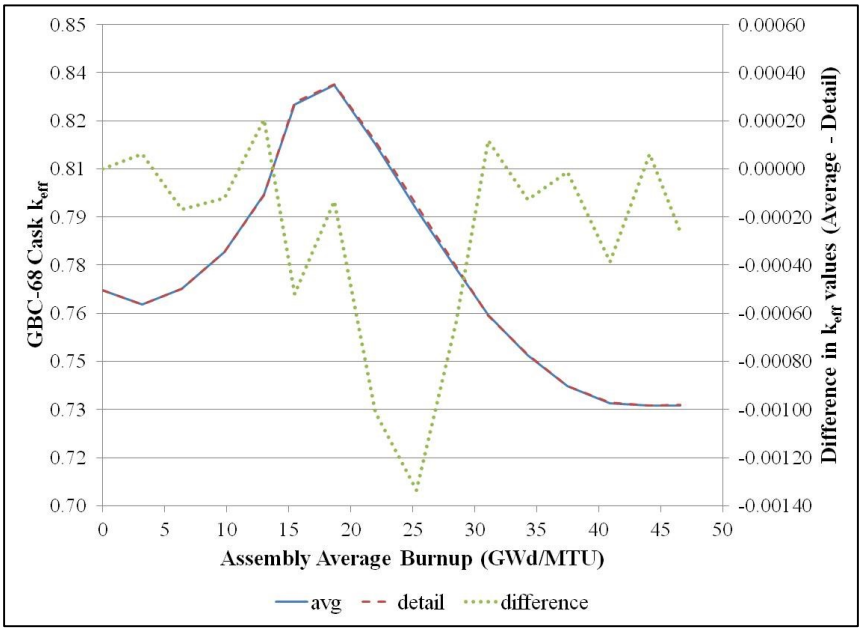

Figure 4.11 GBC-68 results for the MV moderator profile, AFP isotope set

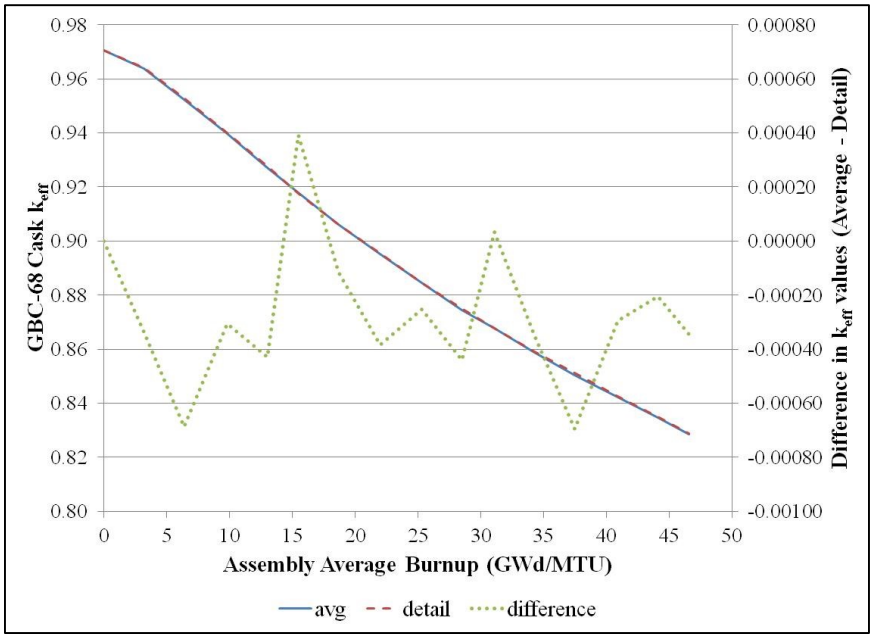

Figure 4.12 GBC-68 results for the HA moderator profile, AO isotope set

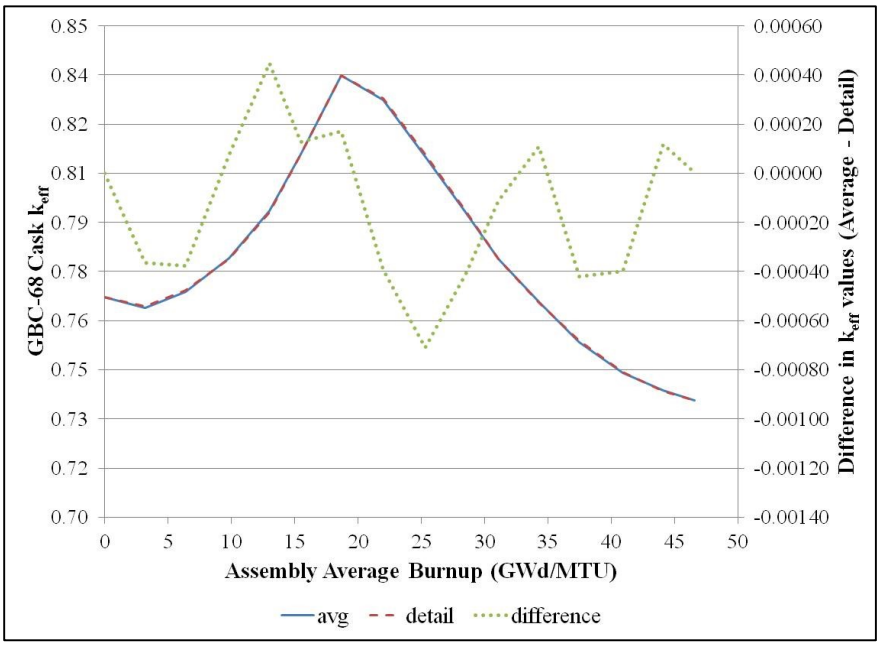

Figure 4.13 GBC-68 results for the HA moderator profile, AFP isotope set

The temporal fidelity study focuses primarily on cycle average behaviors because only a single cycle of detailed data is available in the core follow data set. The effect of multiple cycles of operation can be approximated by considering a series of three different assemblies in different cycles of operation within the single cycle data set used. Three assemblies—a first cycle, second cycle, and later cycle—were selected to create a composite profile to test the use of lifetime average behavior instead of cycle average behavior. Depletion calculations were performed using TRITON for the detailed void history model, cycle average void values, and a

lifetime average value. In the detailed model, the moderator density was updated in each node with each depletion step. The cycle average model updated the moderator density in each node once per cycle. The lifetime average model did not vary the moderator density during depletion. The results of these calculations are provided in Table 4.1 for the AO and AFP isotope sets. These results indicate that, as expected, a set of cycle average values reproduces the detailed depletion history with little deviation. The lifetime average results deviate from the detailed history by almost 0.2% Δk for the AO isotope set and about half of that for the AFP set. In the both cases, the calculated k_{eff} result is a higher (conservative) value, but with only a single test, this cannot be considered a generic result. Instead, the results indicate that use of a cycle average moderator density value causes no loss in fidelity, but a lifetime average value may introduce a relatively small discrepancy. Without further investigation using real lifetime average data for an assembly, it is impossible to assert that the lifetime average value will always be conservative, and it is thus not recommended.

Table 4.1 Results of lifetime average moderator density study

Density model	AO		AFP	
	k_{eff}	σ	k_{eff}	σ
Detailed	0.80609	0.00010	0.72266	0.00010
Cycle average	0.80615	0.00010	0.72256	0.00010
Lifetime average	0.80794	0.00010	0.72368	0.00010

The results of this study demonstrate that despite the large variability of axial moderator profiles over a single cycle of operation and between cycles, cycle average moderator densities appear adequate to use in each axial node. This approach greatly simplifies depletion calculations. It should be emphasized that the averaging considered in this study is for each node over a single cycle of operation for the assembly, and that the axial moderator density profile is retained. A fuel assembly typically experiences several cycles of operation, with moderator density profiles varying within each cycle as shown in Figure 4.2. The first one or two cycles are high power cycles with a relatively high average void fraction but correspondingly lower variability, similar to the HA profile. The last cycle will see a larger change in moderator densities as the assembly average power decreases near EOL for the assembly, as seen in the MV profile. The depletion calculations performed to examine these profiles effectively assumed that each profile was experienced for three cycles of operation, which is not physically possible. Even so, the results show that even for the unrealistic case in which the maximum variability is experienced multiple times, only a small potential nonconservatism exists due to average void profile modeling. The largest difference resulting from the calculations performed in this study for cycle average values is just over 0.1% Δk_{eff}, so a penalty of 0.25% Δk_{eff} is judged to be sufficient to cover any potential nonconservatism resulting from using cycle average moderator density profiles for assemblies that have experienced typical use in a BWR core. This penalty should be applied to all assemblies, even those that are discharged after a single cycle of operation. The penalty need not be increased for assemblies reaching typical discharge burnups as long as the lowest density cycle average value is used. Although the data studied here are drawn from a single cycle, two different types of profiles are studied that cover the range of profile variations expected in BWR core operations.

4.5.2 Axial Moderator Density Study

The results of the temporal fidelity study indicate that cycle average moderator density profiles are adequate for making reactivity predictions for SNF casks containing discharged BWR assemblies. Based on this conclusion, STARBUCS can be used to study the effects of a range

of moderator profiles, since variable moderator densities as a function of burnup are not needed. The STARBUCS calculations are all performed with the same axial burnup profile and specific power to isolate the effect of the axial moderator profile. The specific power and burnup profile were taken from the assembly that generated the MV moderator profile used in the temporal fidelity study. They are therefore representative, but no attempt was made to identify a bounding set of parameters. Separate calculations are performed for the DOM and VAN lattices, and the depleted fuel compositions from the appropriate lattice are used in the KENO model.

Figure 4.5 demonstrates that the upper portion of a discharged BWR assembly dominates reactivity in a storage cask or transportation package. It has also been shown that low moderator densities lead to higher discharged assembly reactivity [9] owing to a combination of lower moderation leading to lower burnup and a harder neutron spectrum generating more ^{239}Pu per unit burnup in these regions. A set of cycle-averaged axial moderator profiles was selected to include those with low moderator density in the upper portions of the assembly, as well as all the profiles with at least one node with the minimum density for all profiles. Using engineering judgement, other profiles were added based on whether they were potentially limiting. The moderator density values and fuel design types for the 10 actual assembly profiles are shown in Table 4.2. Moderator density profiles from all 4 design types used in the core follow data set were considered, but only GNF2 and SVEA assemblies contained the high void profiles of interest for this study. Some increases in moderator density are noted as elevation increases in these data. These apparently anomalous values are due to changes in flow area or mixing causing slowing of the liquid phase and hence increased moderator density.

Two additional profiles were created to explore various aspects or approaches to axial moderator distribution modeling. First, a minimum density profile was created by using the minimum moderator density in each node from all profiles. This approach was considered because it represents a simple analysis technique which might be useful, especially for fixed assembly inventories, if the resulting profile conservatively bounds all actual profiles without introducing a large penalty. An average profile was created by averaging the moderator density in each node across all 624 profiles. This approach was expected to be nonlimiting, but the reactivity effect of this approach is quantified to assess its impact. The minimum density and average density profiles are provided in Table 4.3. In summary, a minimum density profile is constructed because it might prove simple and conservative; two additional approaches are included to determine the magnitude of the nonconservatism associated with them.

The use of a constant moderator density in all nodes was also investigated. The use of a single density will result in overpredictions of k_{eff} if nonphysical but conservative moderator densities are used in lower nodes within the fuel assembly. This condition would be met if the assembly outlet density were used for the entire assembly. However, if the associated penalty is small, then such a simplifying approach may prove useful in analysis. The minimum moderator density in any node in the data set (Table 4.2) is 0.1077 g/cm^3, so this value is used. A series of additional lower densities was also considered to examine the sensitivity of cask reactivity to this single moderator density. The other values considered were 0.107 g/cm^3, 0.105 g/cm^3, and 0.1 g/cm^3. A uniform profile equal to 0.4531 g/cm^3 (40% void) was also considered. This profile was also expected to be nonlimiting, but it is investigated because 40% void is frequently used as a core average value. It should be noted that the maximum moderator density profile (minimum void fraction) crosses the 40% void uniform profile three nodes from the top of the assembly in Figure 4.14.

Table 4.2 Axial moderator profiles from selected assemblies

Prof. 1 GNF2	Prof. 2 SVEA	Prof. 3 GNF2	Prof. 4 GNF2	Prof. 5 GNF2	Prof. 6 GNF2	Prof. 7 SVEA	Prof. 8 GNF2	Prof. 9 SVEA	Prof. 10 SVEA
0.1251	0.1208	0.1272	0.1270	0.1279	0.1282	0.1247	0.1312	0.1258	0.1259
0.1197	0.1077	0.1218	0.1216	0.1226	0.1229	0.1119	0.1258	0.1132	0.1133
0.1186	0.1312	0.1207	0.1207	0.1216	0.1219	0.1346	0.1245	0.1357	0.1358
0.1343	0.1298	0.1359	0.1363	0.1370	0.1373	0.1328	0.1392	0.1339	0.1340
0.1238	0.1258	0.1257	0.1262	0.1268	0.1272	0.1285	0.1287	0.1297	0.1299
0.1471	0.1483	0.1486	0.1496	0.1500	0.1503	0.1503	0.1509	0.1515	0.1517
0.1427	0.1461	0.1440	0.1456	0.1457	0.1460	0.1477	0.1460	0.1488	0.1490
0.1527	0.1497	0.1536	0.1559	0.1558	0.1562	0.1509	0.1554	0.1521	0.1523
0.1698	0.1740	0.1704	0.1734	0.1730	0.1733	0.1748	0.1716	0.1758	0.1761
0.1668	0.1750	0.1669	0.1710	0.1705	0.1707	0.1751	0.1679	0.1762	0.1765
0.1957	0.1876	0.1956	0.1999	0.1996	0.1998	0.1871	0.1960	0.1883	0.1887
0.2090	0.2115	0.2084	0.2129	0.2134	0.2134	0.2105	0.2083	0.2116	0.2121
0.2141	0.2189	0.2128	0.2179	0.2195	0.2193	0.2170	0.2120	0.2182	0.2187
0.2466	0.2415	0.2447	0.2496	0.2526	0.2522	0.2389	0.2433	0.2400	0.2405
0.2690	0.2693	0.2661	0.2715	0.2752	0.2746	0.2660	0.2640	0.2669	0.2675
0.2853	0.2883	0.2809	0.2870	0.2910	0.2905	0.2837	0.2778	0.2843	0.2848
0.3298	0.3264	0.3248	0.3309	0.3344	0.3339	0.3209	0.3209	0.3213	0.3218
0.3691	0.3684	0.3645	0.3707	0.3739	0.3736	0.3620	0.3591	0.3623	0.3627
0.4122	0.4139	0.4073	0.4148	0.4174	0.4173	0.4056	0.4007	0.4061	0.4065
0.4787	0.4766	0.4735	0.4819	0.4834	0.4835	0.4672	0.4657	0.4682	0.4685
0.5545	0.5507	0.5466	0.5563	0.5570	0.5587	0.5391	0.5398	0.5422	0.5430
0.6419	0.6394	0.6336	0.6405	0.6424	0.6446	0.6275	0.6318	0.6314	0.6329
0.7109	0.7107	0.7083	0.7107	0.7118	0.7121	0.7065	0.7077	0.7074	0.7079
0.7461	0.7456	0.7453	0.7461	0.7460	0.7463	0.7445	0.7451	0.7449	0.7450
0.7549	0.7549	0.7549	0.7549	0.7549	0.7549	0.7548	0.7549	0.7548	0.7548

(All densities in g/cm^3; Top of assembly at top of table)

Table 4.3 Constructed axial moderator profiles

Minimum moderator density	Average moderator density
0.1208	0.2020
0.1077	0.1961
0.1186	0.2095
0.1298	0.2164
0.1238	0.2159
0.1471	0.2380
0.1427	0.2398
0.1497	0.2506
0.1698	0.2717
0.1668	0.2764
0.1871	0.3002
0.2083	0.3225
0.2120	0.3357
0.2389	0.3670
0.2640	0.3958
0.2778	0.4194
0.3209	0.4598
0.3591	0.4993
0.4007	0.5395
0.4657	0.5903
0.5391	0.6433
0.6275	0.6956
0.7065	0.7309
0.7445	0.7500
0.7548	0.7552

(All densities in g/cm^3; Top of assembly at top of table)

All profiles considered in this analysis are shown in Figure 4.14. This figure is similar to Figure 4.1, except that it shows moderator density instead of void fraction, and it includes a limited number of profiles. Figure 4.15 is a detailed view of the profiles near the top end of the assembly, excluding the 40% void case. It is clear from the figure that more than one actual assembly profile contributes to the minimum moderator density profile.

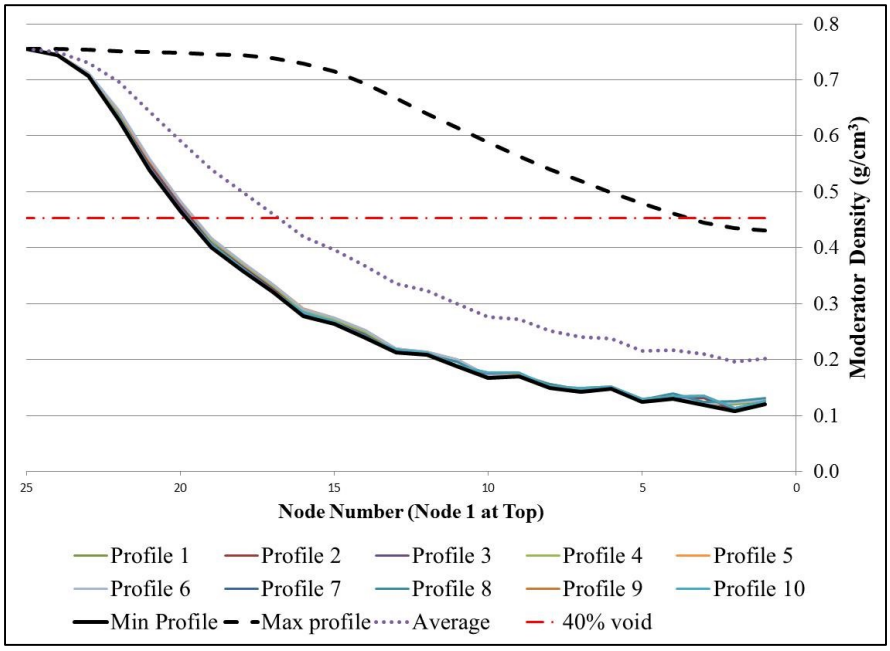

Figure 4.14 Moderator density profiles used in moderator density study

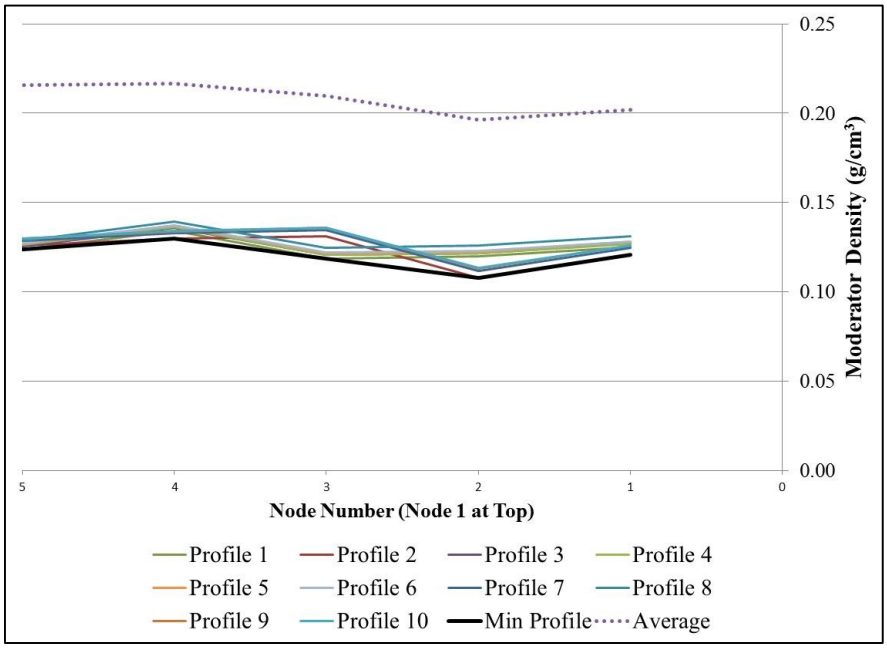

Figure 4.15 Detail of top five nodes of moderator density profiles

Results were generated at 30, 40, and 50 GWd/MTU with both the AO and AFP isotope sets using ORIGEN libraries generated for this study. The results for the 10 assembly moderator density profiles are provided in Table 4.4 for the AO isotope set and in Table 4.5 for the AFP isotope set. The reactivity rankings of the profiles are very similar, though not identical, across all burnups and with both sets of isotopes, indicating that the effect of the moderator profile is

consistent with respect to burnup and isotopes modeled. The k_{eff} differences are small, as are the differences in the moderator profiles used to generate them.

Table 4.4 GBC-68 cask k_{eff} values for 10 actual assembly moderator density profiles, AO isotope set

Profile	30 GWd/MTU		40 GWd/MTU		50 GWd/MTU	
	k_{eff}	σ	k_{eff}	σ	k_{eff}	σ
1	0.92150	0.00010	0.90669	0.00010	0.89406	0.00010
2	0.92095	0.00010	0.90594	0.00010	0.89348	0.00010
3	0.92083	0.00010	0.90560	0.00010	0.89301	0.00010
4	0.92072	0.00010	0.90540	0.00010	0.89277	0.00010
5	0.92037	0.00010	0.90514	0.00010	0.89249	0.00010
6	0.92018	0.00010	0.90500	0.00010	0.89200	0.00010
7	0.91970	0.00010	0.90435	0.00010	0.89142	0.00010
8	0.91924	0.00010	0.90380	0.00010	0.89091	0.00010
9	0.91929	0.00010	0.90384	0.00010	0.89078	0.00010
10	0.91916	0.00010	0.90386	0.00010	0.89079	0.00010

Table 4.5 GBC-68 cask k_{eff} values for 10 actual assembly moderator density profiles, AFP isotope set

Profile	30 GWd/MTU		40 GWd/MTU		50 GWd/MTU	
	k_{eff}	σ	k_{eff}	σ	k_{eff}	σ
1	0.86367	0.00010	0.84389	0.00010	0.82709	0.00010
2	0.86335	0.00010	0.84344	0.00010	0.82645	0.00010
3	0.86336	0.00010	0.84304	0.00010	0.82614	0.00010
4	0.86329	0.00010	0.84299	0.00010	0.82639	0.00010
5	0.86304	0.00010	0.84285	0.00010	0.82614	0.00010
6	0.86293	0.00010	0.84260	0.00010	0.82583	0.00010
7	0.86230	0.00010	0.84211	0.00010	0.82528	0.00010
8	0.86207	0.00010	0.84178	0.00010	0.82485	0.00010
9	0.86196	0.00010	0.84157	0.00010	0.82476	0.00010
10	0.86206	0.00010	0.84158	0.00010	0.82473	0.00010

The k_{eff} results are used to identify trends with the moderator density profiles. Figure 4.16 shows the k_{eff} values at 50 GWd/MTU for the AFP isotope set versus the top node moderator density. It is clear that there is a trend of increasing reactivity with lower moderator density within a given fuel assembly type. It is further evident that the correlations depend on fuel design type or core position. The separation of these effects is not attempted in this study, but it is likely that the differences in the moderator profiles are caused by the unique axial characteristics of the different fuel assembly design types. BWR BUC applications will need to consider the potential for multiple correlations such as those manifested in this work. However, the general trend of increasing reactivity with decreasing moderator density is clear within both fuel assembly design types. Similar plots are created by summing the moderator density of the top two nodes (Figure 4.17) and the top three nodes (Figure 4.18). The trend of increasing reactivity with decreasing moderator density is still evident, as it is with AO isotope set results for the top node (Figure 4.19) and the top three nodes (Figure 4.20). This trend starts to break down if all the nodes in the VAN lattice are considered, as shown in Figure 4.21. The moderator profile summed over the entire axial extent of the assembly is a poor indicator of relative reactivity, as shown in Figure 4.22 for the AFP isotope set and Figure 4.23 for the AO isotope set. These results confirm indications from earlier work, as shown in Figure 4.5, that (1) the upper portion of

the assembly determines reactivity and (2) that low moderator densities lead to higher discharged reactivities.

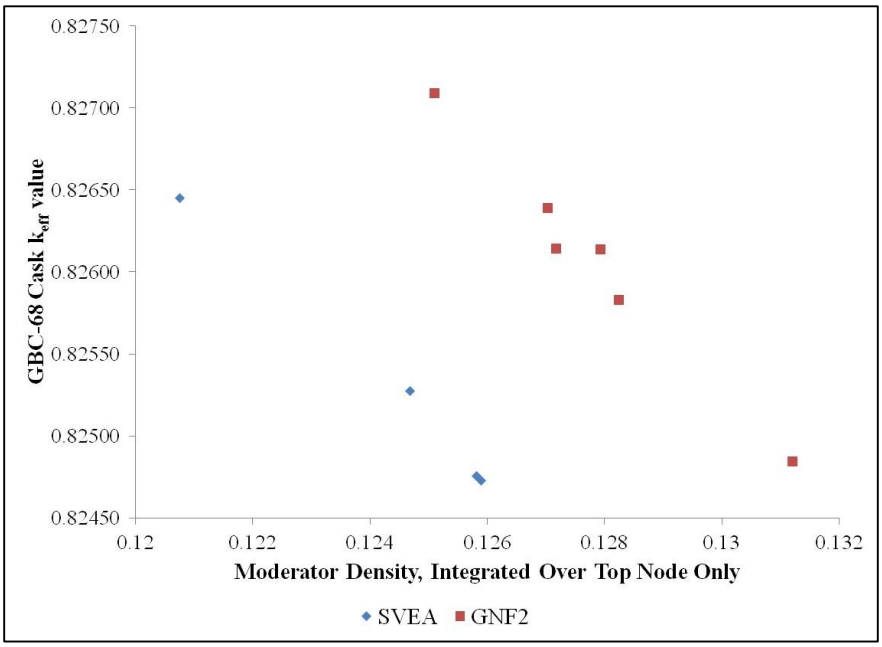

Figure 4.16 GBC-68 cask k_{eff} values (AFP isotope set) as a function of moderator density in top node

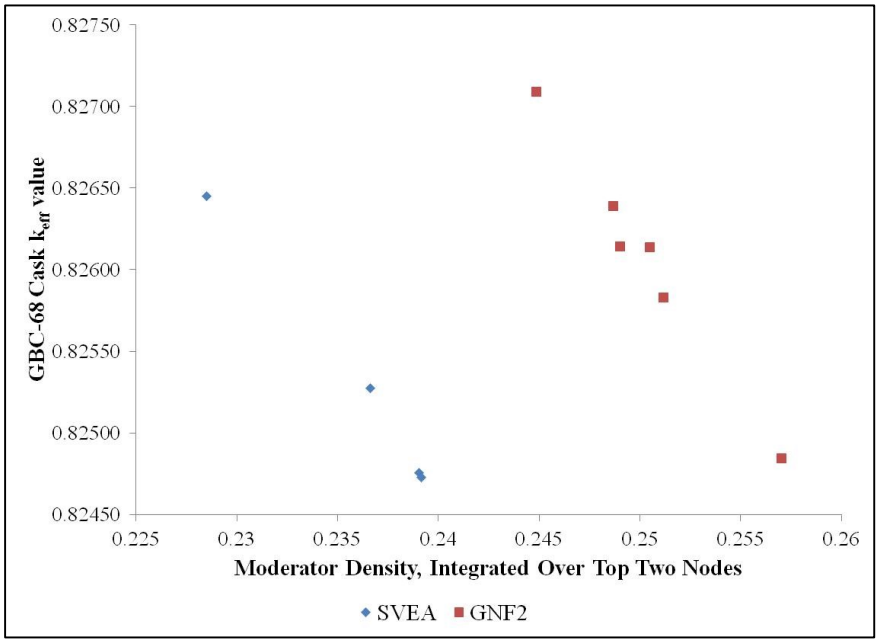

Figure 4.17 GBC-68 cask k_{eff} values (AFP isotope set) as a function of moderator density in top two nodes

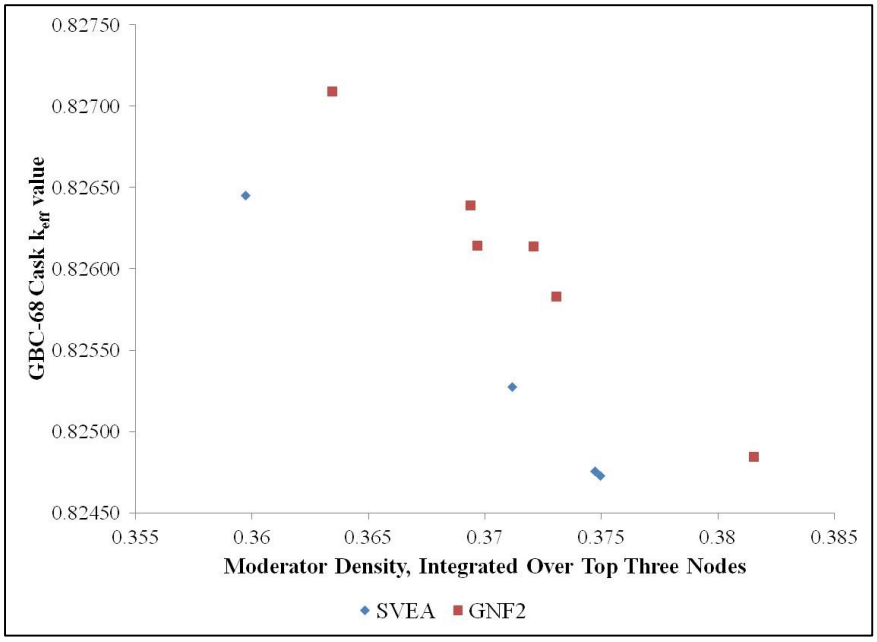

Figure 4.18 GBC-68 cask k_{eff} values (AFP isotope set) as a function of moderator density in top three nodes

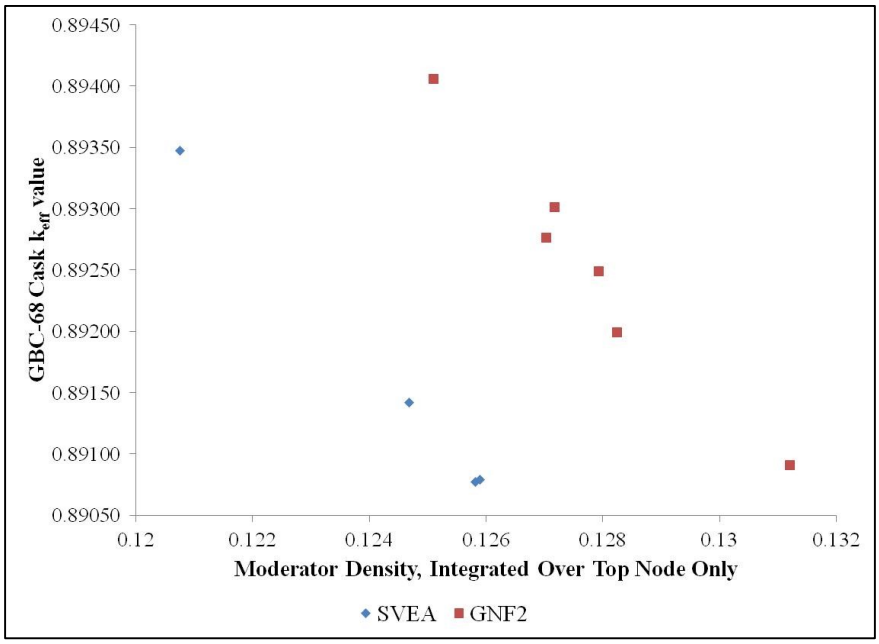

Figure 4.19 GBC-68 cask k_{eff} values (AO isotope set) as a function of moderator density in top node

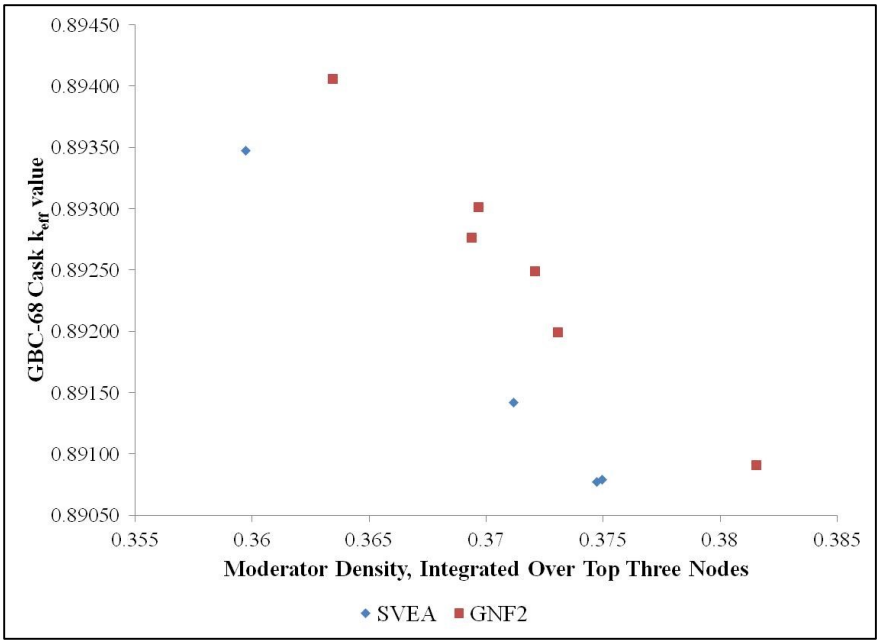

Figure 4.20 GBC-68 cask k_{eff} values (AO isotope set) as a function of moderator density in top three nodes

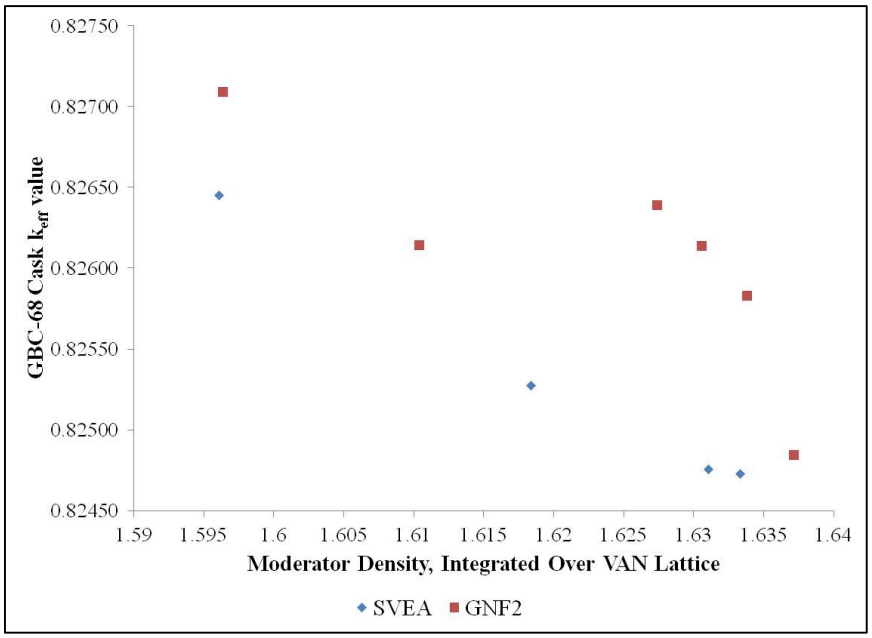

Figure 4.21 GBC-68 cask k_{eff} values (AFP isotope set) as a function of moderator density in VAN lattice

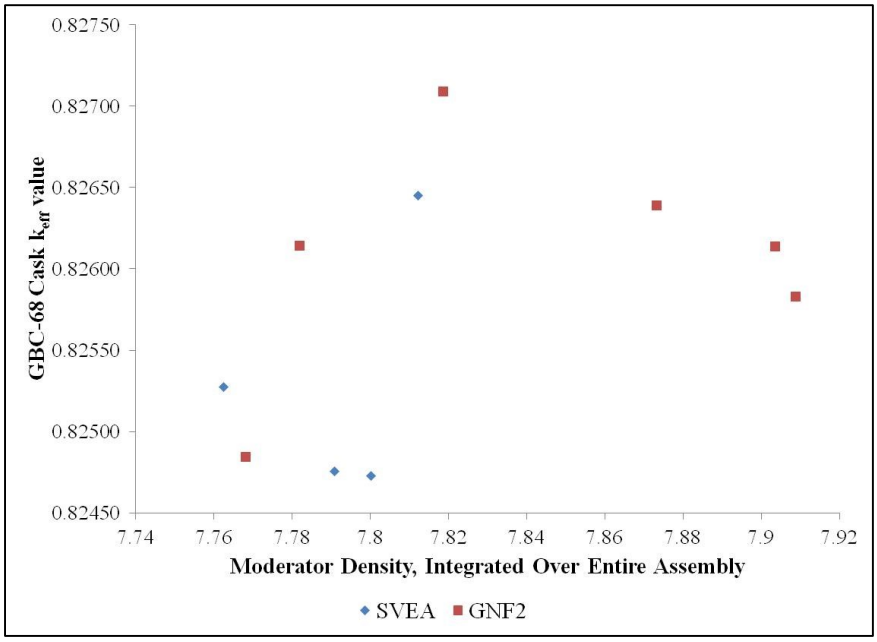

Figure 4.22 GBC-68 cask k_{eff} values (AFP isotope set) as a function of moderator density in entire assembly

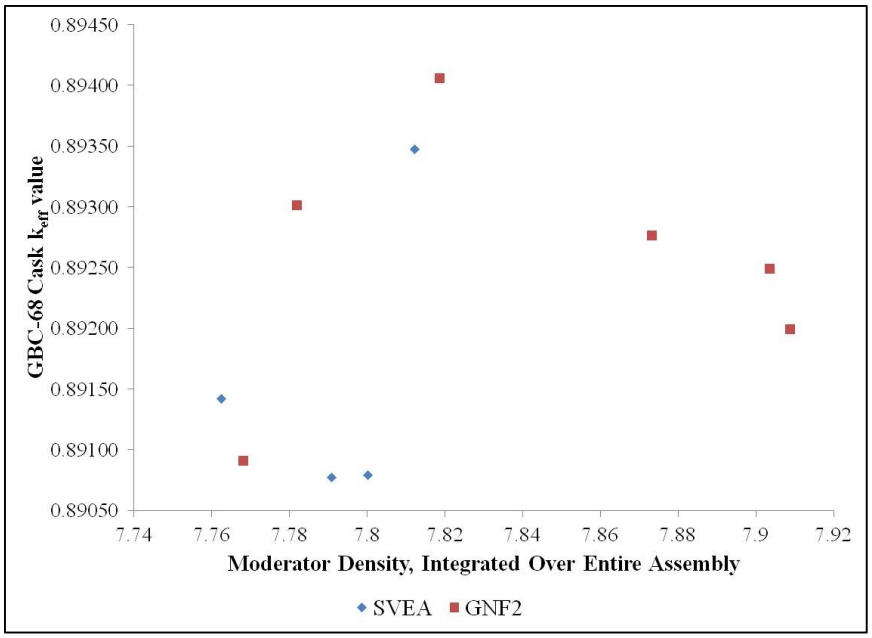

Figure 4.23 GBC-68 cask k_{eff} values (AO isotope set) as a function of moderator density in entire assembly

The results for the two constructed profiles are provided in Table 4.6 for the AO isotope set and Table 4.7 for the AFP isotope set. The difference between the k_{eff} calculated for each constructed profile is compared with the limiting actual assembly profile, and the results are also included in the appropriate table.

The results indicate that the minimum density profile can be used to conservatively bound the reactivity of the actual assemblies at all burnups and with both isotope sets. The margin provided by the minimum density profile is small for this set of assemblies. For the AO isotope set it ranges from 0.12% Δk_{eff} at 30 GWd/MTU to 0.19% Δk_{eff} at 50 GWd/MTU. The difference from the actual profiles is smaller for the AFP isotope set: 0.07% Δk_{eff} at 30 GWd/MTU, increasing to 0.14% Δk_{eff} at 50 GWd/MTU. The minimum density profile yielding a more reactive assembly is expected and is a potential approach to simplifying the treatment of axial moderator profiles in BWR BUC, especially considering the small penalty associated with the approach. However, the small margin provided would not provide a significant margin against more limiting profiles or a large margin to offset potential uncertainties in predicted moderator density distributions. Nevertheless, the minimum density profile approach is viable. The primary challenge for its application by a cask vendor is likely to be the collection of a significant and appropriate database of moderator density profiles.

The average void profile is clearly nonconservative, as expected. The average moderator density profile is from 3.0% to 4.2% Δk_{eff} less reactive than the limiting profile for the AO isotope set and from 2.0% to 2.9% Δk_{eff} less reactive for the AFP isotope set. This is evidence that the discharged assembly reactivity is highly sensitive to moderator density profile and that lower densities lead to higher reactivities. In the top node, the average profile has approximately 67% higher moderator density than the minimum case and nearly 62% higher moderator density than the limiting profile. The absolute differences are on the order of 0.08 g/cm^3, but at the high exit void fractions, this represents a significant relative change. Averaging of moderator densities from different profiles is clearly not an acceptable approach to treating the axial moderator density in BWR BUC.

Table 4.6 GBC-68 cask k_{eff} values for constructed profiles, AO isotope set

Profile	30 GWd/MTU			40 GWd/MTU			50 GWd/MTU		
	k_{eff}	σ	Δ*	k_{eff}	σ	Δ*	k_{eff}	σ	Δ*
Minimum	0.92268	0.00010	0.00118	0.90821	0.00010	0.00152	0.89599	0.00010	0.00193
Average	0.89143	0.00010	-0.03007	0.87037	0.00010	-0.03632	0.85179	0.00010	-0.04227

*Difference from limiting profile; positive value indicates constructed profile is more reactive

Table 4.7 GBC-68 cask k_{eff} values for constructed profiles, AFP isotope set

Profile	30 GWd/MTU			40 GWd/MTU			50 GWd/MTU		
	k_{eff}	σ	Δ*	k_{eff}	σ	Δ*	k_{eff}	σ	Δ*
Minimum	0.86438	0.00010	0.00072	0.84478	0.00010	0.00090	0.82848	0.00010	0.00139
Average	0.84364	0.00010	-0.02003	0.81910	0.00010	-0.02479	0.79799	0.00010	-0.02910

*Difference from limiting profile; positive value indicates constructed profile is more reactive

The results for the constant moderator density cases are provided in Table 4.8 for the AO isotope set and Table 4.9 for the AFP isotope set. The difference between the k_{eff} calculated for each moderator density is compared to the limiting actual assembly profile, and the results are also included in the appropriate table.

A constant density representing a 40% void fraction leads to large underpredictions of cask reactivity. For the AO isotope set, the difference from the limiting actual profile is approximately 6.9% Δk_{eff} at 30 GWd/MTU, and increases to almost 10% Δk_{eff} at 50 GWd/MTU. The differences are smaller in the AFP case, ranging from 4.8% to 7.4% Δk_{eff}. As noted previously, this core

average of 40% void fraction yields a higher moderator density in the top three nodes of the core than any actual assembly profile. This case provides additional proof that any averaging approach that increases moderator density in the upper portion of the assembly is likely to yield nonconservative k_{eff} calculations for discharged fuel assemblies.

As expected, the results show that a uniform low moderator density can be used conservatively to bound actual assembly profiles. The penalty associated with this approach varies significantly between the AO and AFP isotope sets, and it also increases with burnup. Using the minimum actual moderator density (0.1077 g/cm^3 from Profile 2 in Table 4.2) leads to k_{eff} values that are 1.6% to 2.0% Δk_{eff} more reactive than the limiting profile for the AO isotopes set and 0.6% to 0.7% more reactive for the AFP set. The increase in this penalty is linear, with decreasing moderator density over the range considered. Currently operating BWR plants may have exit void fractions of 90% or more, which would lead to moderator densities on the order of 0.07 g/cm^3. The reactivity effect of these lower moderator densities can be extrapolated from the results shown in Tables 4.8 and 4.9, but the limiting actual profile would also become more reactive at these higher void fractions because of the lower outlet moderator densities.

The results generated clearly show that a uniform moderator density value could be used conservatively. As with other aspects of analysis, however, any applicant that chooses this approach would have to provide justification for the specific moderator density used.

Table 4.8 GBC-68 cask k_{eff} values for uniform moderator densities, AO isotope set

Density	30 GWd/MTU			40 GWd/MTU			50 GWd/MTU		
(g/cm^3)	k_{eff}	σ	Δ*	k_{eff}	σ	Δ*	k_{eff}	σ	Δ*
40% void	0.85278	0.00009	-0.06872	0.82235	0.00010	-0.08434	0.79467	0.00010	-0.09940
0.1	0.94073	0.00010	0.01922	0.92878	0.00010	0.02197	0.91891	0.00010	0.02485
0.105	0.93843	0.00010	0.01692	0.92581	0.00010	0.01900	0.91568	0.00010	0.02161
0.107	0.93742	0.00010	0.01591	0.92462	0.00010	0.01780	0.91452	0.00010	0.02046
0.1077	0.93711	0.00010	0.01560	0.92432	0.00010	0.01751	0.91403	0.00010	0.01997

*Difference from limiting profile; positive value indicates constructed profile is more reactive

Table 4.9 GBC-68 cask k_{eff} values for uniform moderator densities, AFP isotope set

Density	30 GWd/MTU			40 GWd/MTU			50 GWd/MTU		
(g/cm^3)	k_{eff}	σ	Δ*	k_{eff}	σ	Δ*	k_{eff}	σ	Δ*
40% void	0.81541	0.00010	-0.04826	0.78298	0.00010	-0.06091	0.75351	0.00010	-0.07358
0.1	0.87235	0.00010	0.00845	0.85341	0.00010	0.00966	0.83766	0.00010	0.01076
0.105	0.87066	0.00010	0.00676	0.85155	0.00010	0.00780	0.83549	0.00010	0.00859
0.107	0.86998	0.00010	0.00608	0.85067	0.00010	0.00692	0.83451	0.00010	0.00762
0.1077	0.86993	0.00009	0.00603	0.85040	0.00010	0.00666	0.83412	0.00010	0.00723

*Difference from limiting profile; positive value indicates constructed profile is more reactive

4.6 Summary and Recommendations

The purpose of this section was to document studies examining the effects of axial moderator density profiles on extended BWR BUC. Further studies examining other phenomena related to extended BWR BUC are provided in Sections 5 and 6 as part of a technical basis for extended BUC. These studies are intended apply to fuel beyond peak reactivity; studies examining peak reactivity methods were documented in Marshall, Ade, et al. [3]. Two separate studies were

performed in this section: a temporal fidelity study and an axial moderator density study. The temporal fidelity study was required to examine the modeling approaches necessary for capturing the reactivity impacts of temporal variations in the axial moderator density profile, and the axial moderator density study was performed to determine the effect of these axial profiles once they were established. The results of the temporal fidelity study, presented in Section 4.5.1, indicate that cycle average moderator density profiles can be used in depletion calculations with the addition of a modest reactivity penalty. The axial moderator density profile study results, presented in Section 4.5.2, show that low moderator densities in the top few nodes of the profile lead to conservative reactivity determinations. Averaging the moderator densities across assemblies or nodes is not appropriate and will lead to nonconservative reactivity determinations.

The following are recommendations of these studies.

- A cycle-averaged moderator density can be used in each node of an axial moderator density profile for depletion calculations for simplicity, with an appropriate penalty for conservatism.

- A reactivity penalty of 0.25% Δk_{eff} is recommended to cover potential differences between detailed and cycle average moderator density treatments in depletion calculations. This penalty is nearly twice the magnitude of the largest discrepancy between detailed and average moderator density modeling observed in this study.

- A limiting axial moderator density profile will have low moderator densities in the top nodes of the assembly. Each applicant should present and defend the method used to identify limiting profiles.

- A limiting axial moderator density profile can be constructed by selecting the minimum density in each axial node from a collection of applicable actual profiles.

- Use of average moderator densities determined from consideration of multiple assemblies or multiple axial nodes will result in reactivity underprediction.

- A single moderator density value can be used conservatively in all nodes if it bounds the moderator densities in all nodes of the assembly.

5 CONTROL BLADE USAGE

5.1 Control Blade Histories

This section summarizes the analyses performed for the effects of control blade history on cask reactivity. To understand these effects, a number of different control blade histories need to be generated for testing. In the context of this study, *control blade history* refers to the position (height of insertion) of a control blade as a function of an adjacent fuel assembly's time in the reactor core.

In general, use of a control blade in a BWR hardens the neutron spectrum, resulting in increased ^{239}Pu production and decreased gadolinium consumption. Cask reactivity is expected to increase with control blade usage in extended BWR BUC because the increased ^{239}Pu production will add more positive reactivity than the small negative reactivity resulting from increased residual gadolinium. In addition, owing to the top-peaked axial fission distribution in typical fuel storage and transportation casks, the operating conditions experienced in the top portion of the fuel assembly have a disproportionate effect on cask reactivity. As a result, it is expected that especially deeper control blade insertion will be more limiting than shallower control blade insertion. From previous and ongoing work [23], it is also expected that control blade insertion near the end of assembly life will result in higher k_{eff} values than control blade insertion near BOL. For early control blade insertion, ^{239}Pu builds up and then has time to deplete after the control blade is removed. For late control blade insertion, there is less time for the ^{239}Pu to deplete before the fuel is discharged, leading to higher cask reactivity.

Gross reactivity control in BWRs is achieved primarily through the use of control blades inserted in the core during operation. This is a significant deviation from PWR operation that uses a soluble boron shim as a primary means of reactivity control during operation. The highly variable use of control blades to maintain power level and operational margins during operation makes BWR modeling significantly more complex.

This analysis used many control blade histories from the single cycle of core follow data described in Section 3.1. Because the data contain sufficient detail to model control blade histories and use modern fuel assemblies in a modern BWR cycle, this data set was used for the studies documented in this section. For illustration, actual control blade insertion histories for three selected locations are plotted in Figure 5.1. These three locations are selected to show the variety of control blade use in BWR operations. Each of these histories is extracted from the core follow data discussed in Section 3.1 and will be explicitly considered in this study along with seven other histories. A core map for the cycle of data used is shown in Figure 5.2, with the control blade layout and numbering scheme indicated. Each box in Figure 5.2 represents four fuel assemblies, and each "+" represents a cruciform control blade that can be inserted in the center channels between the four assemblies. The position indices provided in Figure 5.1 are (x,y) coordinates. For example, Position (4,6) is four positions to the right and six positions down in Figure 5.2. Symmetric locations showed a high degree of similarity in control blade use in the core follow data set.

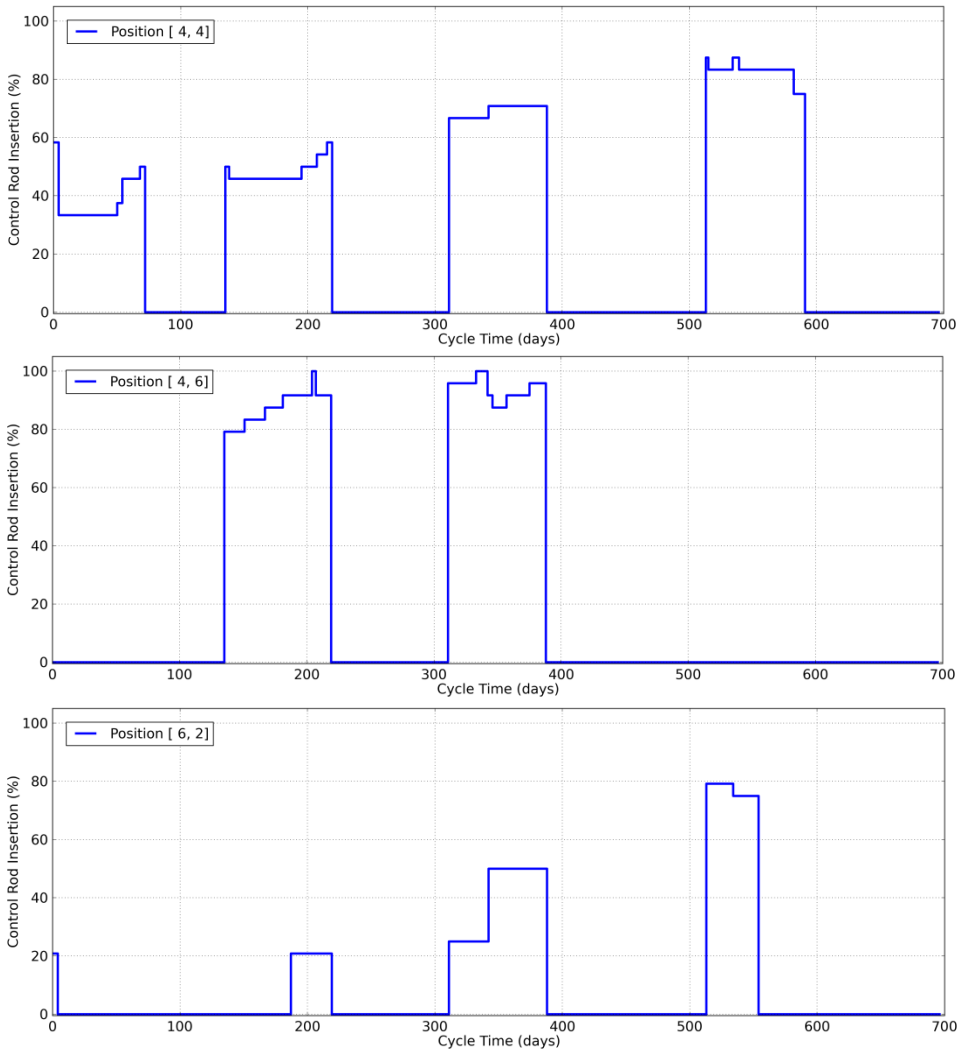

Figure 5.1 Selected control blade histories from the available operating data

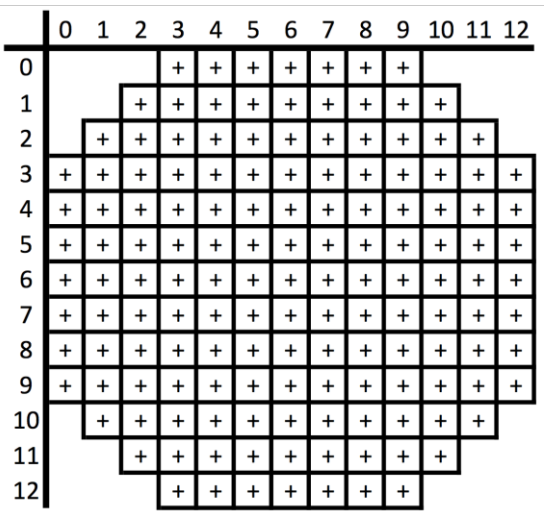

Figure 5.2 Core map showing control blade numbering scheme

Results from Section 4 indicate that the end effect (top-peaked axial fission distribution) has a significant impact on cask reactivity results. Axial peaking at the top of the fuel assembly is primarily due to relatively low burnup and increased plutonium production caused by reduced moderation in the top portion of the fuel assembly. The axial fission distribution in a fuel cask filled with depleted BWR fuel is shown in Figure 4.5. Most BWR fuel cask axial fission distributions will follow the same basic shape shown in Figure 4.5. The shape of the fission data indicates that the upper portion of the fuel assembly will have a significant impact on the reactivity of the fuel cask. With the axial fission distribution shape in mind, the burnup-integrated nodal control blade history (insertion fraction) was extracted and plotted (see Figure 5.3) for each of the 624 fuel assemblies in the core.

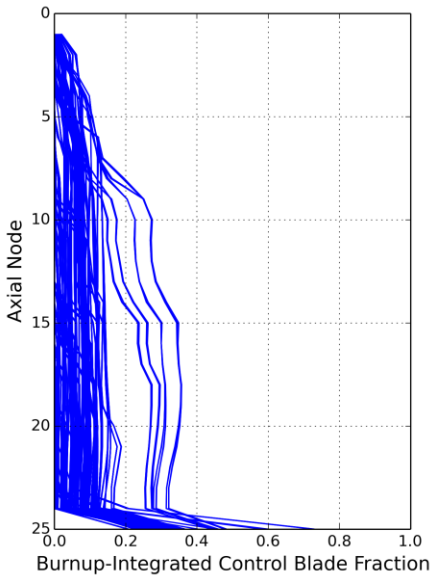

Figure 5.3 Burnup-integrated control blade fraction

The burnup-integrated control blade fraction for each node is defined as the fraction of the node total burnup for which a control blade was inserted adjacent to the fuel assembly in that particular axial node. Note that the burnup-integrated control blade history for an assembly would be summed over the entire assembly life. Therefore, the integrated control blade history inherently would include the operating history of all cycles for an assembly; however, only one cycle of data is available for this study. The data in Figure 5.3 indicate that certain fuel assemblies experience much higher control blade insertion fractions than others. These assemblies are likely to be more limiting with respect to cask criticality than fuel assemblies with lower control blade insertion fractions.

Because of the varied control blade usage in BWRs, as illustrated in Figures 5.1 and 5.3, similar fuel assemblies can experience significantly varied control blade histories. To study the effect of control blade usage on BWR fuel cask reactivity, a number of hypothetical control blade histories have been used, along with some histories from actual operating data. The total irradiation time for each of these histories is 2070 days, which is intended to represent three 2-year cycles with a capacity factor of approximately 95%. The hypothetical control blade histories are used to investigate the important effects of varied control blade usage, whereas the realistic control blade histories are used to determine the magnitude of reactivity penalties compared with hypothetical control blade histories. All control blade histories considered in this study have been evaluated using the same axial power distribution, the same axial moderator density distribution, and the same burnup, thus isolating the effect of the control blade history. This isolation of the control blade effect is nonphysical because control blade insertion will impact the axial moderator density distribution, assembly power, and fuel temperatures; but this isolation approach is used to examine each effect separately. The combined effect of these correlated parameter changes will be studied in future work.

A description of the hypothetical control blade histories is as follows:

1. Control blades are removed for the entire irradiation.

2. Control blades are inserted 100% for the entire irradiation.

3. Control blades are inserted 24% (6 nodes) for the entire irradiation.

4. Control blades are inserted 52% (13 nodes) for the entire irradiation.

5. Control blades are inserted 76% (19 nodes) for the entire irradiation.

6. Control blades are inserted 24% for the first half and then are removed for the remaining irradiation.

7. Control blades are removed for the first half then are inserted 24% for the remaining irradiation.

8. Control blades are inserted 52% for the first half then are removed for remaining irradiation.

9. Control blades are removed for the first half and then are inserted 52% for the remaining irradiation.

10. Control blades are inserted 76% first half and then are removed for remaining irradiation.

11. Control blades are removed for the first half and then are inserted 76% for remaining irradiation.

12. Control blades are inserted 100% the first half and then are removed for remaining irradiation.

13. Control blades are removed for the first half and then are inserted 100% for remaining irradiation.

14. Control blades are inserted 100% for the first third and then are removed for remaining irradiation.

15. Control blades are inserted 100% for the second third and then are removed for remaining irradiation.

16. Control blades are inserted 100% for the last third of the irradiation.

17. Control blades are fully removed for 360 days and then are inserted 100% for 360 days, alternating through the end of the irradiation.

18. Control blades are fully removed for 240 days and then are inserted 100% for 240 days, alternating through the end of the irradiation.

19. Control blades are fully removed for 120 days and then are inserted 100% for 120 days, alternating through the end of the irradiation.

20. Control blades are fully removed for 360 days and then are inserted 48% for 360 days, alternating through the end of the irradiation.

21. Control blades are fully removed for 240 days and then are inserted 48% for 240 days, alternating through the end of the irradiation.

22. Control blades are fully removed for 120 days and then are inserted 48% for 120 days, alternating through the end of the irradiation.

23. Control blade is inserted 56% (14 nodes) for the entire irradiation.

24. Control blade is inserted 60% (15 nodes) for the entire irradiation.

25. Control blade is inserted 64% (16 nodes) for the entire irradiation.

26. Control blade is inserted 68% (17 nodes) for the entire irradiation.

27. Control blade is inserted 72% (18 nodes) for the entire irradiation.

28. Control blade is inserted 80% (20 nodes) for the entire irradiation.

29. Control blade is inserted 84% (21 nodes) for the entire irradiation.

30. Control blade is inserted 88% (22 nodes) for the entire irradiation.

31. Control blade is inserted 92% (23 nodes) for the entire irradiation.

32. Control blade is inserted 96% (24 nodes) for the entire irradiation.

The hypothetical histories (HHs) are designated according to the history numbers in the list above. For example, *HH2* is hypothetical history 2, which represents the control blades inserted 100% in depth for the entire irradiation. Because the fuel assembly and cask models are constructed using 25 axial nodes, exact insertion percentages of 25%, 50%, and 75% are impossible to model directly. Therefore, 24%, 52%, and 76% are used.

HH1–HH16 were designed to test the sensitivity of three major aspects of control blade usage for BWR fuel cask criticality: (1) the length of time (burnup) for which a control blade is inserted, (2) the depth (or elevation) to which the control blade is inserted, and (3) the time at which the control blade is inserted (early in irradiation vs. late in irradiation). As discussed earlier in this section, control blades that are inserted deeper in the core for longer irradiation times and later in life are expected to result in higher cask reactivity than the converse. HH17–HH22 were designed to test the sensitivity of frequent, short control blade insertions vs. longer, less-frequent control blade insertions. HH23–HH32 were designed to allow determination of the sensitivity to control blade insertion depth in a more detailed manner.

In addition to the HHs, ten realistic control blade histories have been extracted from the operating data discussed in Section 3.1. Because only one cycle of operating data exists, the realistic control blade histories have been constructed so that the history for a single 690-day cycle is repeated for three consecutive cycles. Many control blades in BWRs, such as those near the core periphery, are used sparingly. Therefore, these control blade histories have been excluded from analysis. There are situations in which peripheral control blades would be used extensively, such as to suppress power in an assembly with a leaking fuel rod or in a fresh assembly located near the periphery in an uprated plant. These exceptions should be noted in reviewing control blade use assumptions. Control blades are typically inserted in a similar fashion in four symmetric locations in the core, so only one symmetric location is simulated rather than four nearly identical histories for different control blade locations. The ten chosen realistic histories (RHs) are chosen because these control blades are used frequently and/or are inserted deeply into the core. Plots depicting the control blade insertion depth as a function of time for these ten realistic histories are provided in Appendix A.

The ten realistic histories and their core locations are summarized as follows:

1. Location [3,4]: two short insertions during the cycle, one above 60% inserted.

2. Location [4,4]: four long insertions in the cycle, two of which are above 60% inserted; highest integral control blade history of the realistic histories.

3. Location [7,4]: two relatively long insertions, both greater than 70% inserted.

4. Location [2,5]: one insertion up to 40% inserted.

5. Location [3,5]: one relatively short insertion, up to 90% inserted.

6. Location [4,5]: one long insertion, up to 100% inserted.

7. Location [2,6]: three short insertions, one late in the cycle, up to 80% inserted.

8. Location [3,6]: one short insertion up to 35% inserted and one long insertion up to 100% inserted.

9. Location [4,6]: two long insertions, both to a maximum of 100% inserted.

10. Location [6,6]: one long insertion up to 85% inserted, and one short insertion near the end of the cycle, up to 100% inserted.

RHs are designated according to the history numbers in the list above.

5.2 Results

This section provides isotopic and criticality results for the hypothetical and realistic control blade histories.

5.2.1 Effect of Control Blade Insertion on ^{239}Pu

As discussed in Section 5.1, insertion of control blades in BWRs increases plutonium production relative to identical conditions without control blades inserted. This increase is due to the hardening of the neutron spectrum, which increases the parasitic absorption of neutrons in ^{238}U. To illustrate this effect, the ^{239}Pu atom density has been extracted from the TRITON simulation results and compared for various hypothetical control blade histories. Figure 5.4 plots the ^{239}Pu atom density as a function of burnup for the top axial node in the simulations using four hypothetical histories: HH1, HH2, HH12, and HH13. The top axial node has a low moderator density and a low burnup due to the axial moderator density profile and the axial power profile applied for the simulations. HH1 has the control blade withdrawn for the entire irradiation, HH2 has the control blade inserted for the entire irradiation, HH12 has the control blade inserted for the first half of irradiation, and HH13 has the control blade inserted for the last half of irradiation.

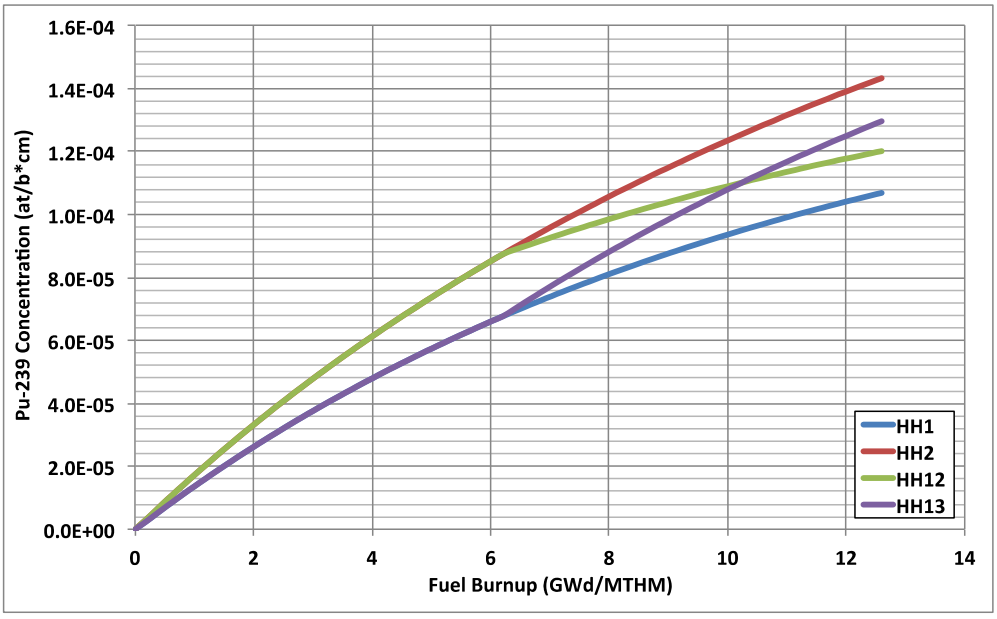

Figure 5.4 ^{239}Pu concentration as a function of burnup for HH1, HH2, HH12, and HH13 control blade histories

Figure 5.4 shows that the control-blade-out and control-blade-in cases bracket the cases in which control blades were inserted for either the first or last half of irradiation. Figure 5.4 also shows that the end-of-life (EOL) plutonium concentration for HH13 (inserted second half) is higher than that of HH12 (inserted first half), indicating that later control blade insertion is likely to result in higher cask reactivity than early control blade insertion. This is primarily due to the rates at which plutonium is produced and consumed in reactors. For the HH12 case, plutonium concentration increases quickly through the first half of irradiation because of the presence of the control blade; when the control blade is removed, ^{239}Pu is preferentially depleted because the fission cross section of ^{239}Pu is larger than that of ^{235}U. In the HH13 case, plutonium increases more slowly; and when the blade is inserted, ^{239}Pu is produced more rapidly, and then the fuel is immediately discharged. This leaves no opportunity for the ^{239}Pu to deplete toward the lower concentration resulting from unrodded operation before being discharged.

The same effect can be found in Figure 5.5, which plots the plutonium concentration as a function of burnup for HH14 (control blade fully inserted for the first third of operation), HH15 (control blade fully inserted for the second third of operation), and HH16 (control blade fully inserted for the last third of operation), as well as for HH1 and HH2. Again, the ^{239}Pu concentrations for HH14, HH15, and HH16 are bracketed by the 100% inserted (HH2) and 100% withdrawn (HH1) cases. As expected when comparing HH14, HH15, and HH16, the case with the latest control blade insertion produces the highest discharge ^{239}Pu concentration, whereas the case with the earliest control blade insertion produces the lowest discharge ^{239}Pu concentration, indicating that later control blade insertion has a greater impact on discharge ^{239}Pu than earlier control blade insertion.

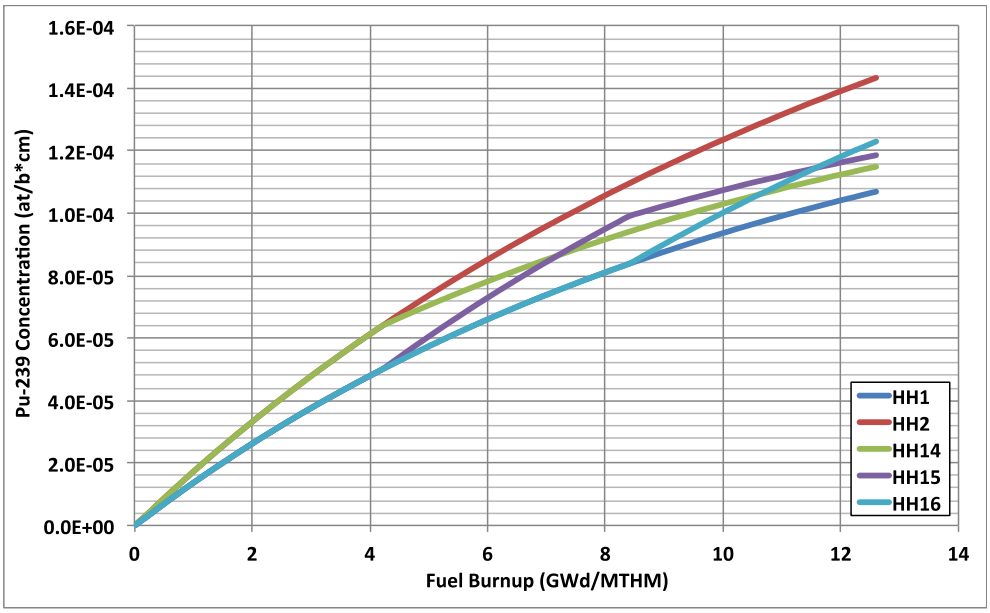

Figure 5.5 ^{239}Pu concentration as a function of burnup for HH1, HH2, HH14, HH15, and HH16 control blade histories

5.2.2 Control Blade Study with Hypothetical Histories

The study of moderator density profiles specified in Section 4.5.2 used STARBUCS extensively for generating depleted fuel compositions that corresponded to a variety of specified moderator density profiles. In this study, however, TRITON was used to generate all depleted fuel compositions, as the use of varying control blade histories is not possible in STARBUCS. The need to use TRITON for all depletion calculations significantly increased the computational requirements, as lattice depletion calculations are needed for every axial node of every control blade history used. All TRITON calculations were performed using the same axial moderator density profile and the same axial burnup profile. The moderator density profile corresponds to the average moderator density profile developed in Section 4, indicated by the thick black line in Figure 4.1. The average profile was used in this study because the key output is not the absolute reactivity of the cask but the relative difference among the different control blade histories. The axial burnup profile and associated power density correspond to the assembly in the core associated with the MV moderator density profile used in the temporal fidelity study in Section 4. The axial burnup profile is shown in Figure 2.7b. Additional studies involving other assembly design types and fuel lattice designs may be needed to demonstrate the applicability of the conclusions of this work more broadly.

The *ft71f001* file (ORIGEN concentration file) generated during the TRITON calculations was post-processed using ORIGEN to extract the isotopics for all depletion materials, and then a 5-year decay was performed to simulate cooling in a spent fuel pool. The isotopic number densities from the ORIGEN decay calculations were extracted and then converted into a composition file for use with CSAS/KENO. This process was performed for each axial node of each control blade history simulated.

In the axial moderator profile studies presented in Section 4, a number of cumulative burnups were simulated (i.e., 30, 40, 50 GWd/MTU); however, in this study, a single burnup value (assembly-averaged burnup of 45.2 GWd/MTU) with node burnups that correspond to the selected axial burnup profile is used. Other burnup values are not simulated in this study, as the burnup of the top end of the assembly changes significantly less than the assembly average. The top end of the assembly generally controls reactivity, so this is the most relevant consideration. The effects of control blade exposure are expected to scale with burnup, so lower burnups should see smaller differences than higher burnups.

The KENO GBC-68 criticality results for HH1–HH32, for AO and AFP isotope sets can be found in Table 5.1. The data in Table 5.1 have been sorted from highest to lowest k_{eff} values. The top three histories (in different orders) for both the AO and AFP isotope sets are HH2 (control blades inserted 100% for the entire fuel assembly life), HH32 (96% inserted for entire assembly life), and HH31 (92% inserted for entire assembly life). The maximum difference between these cases is 0.93% Δk_{eff} for the AO isotope set and 0.14% Δk_{eff} for the AFP isotope set. These results confirm that the most limiting conditions are virtually fully inserted control blades, which harden the spectrum and produce more plutonium. The next most limiting cases are (in different orders): HH13 (control blade inserted fully for second half of assembly life), HH16–HH19, and HH30 (88% inserted for entire assembly life). In HH16, the control blade is inserted fully for the last third of irradiation. HH17–HH19 alternate the control blades fully in and fully out at regular time intervals, resulting in a similar integral control blade history for each case.

Based on the results in Table 5.1, it is clear that increased control blade insertion produces higher cask reactivity, as many of the highest reactivity cases have integral control blade histories of 50% or more (100% for HH2). Comparison of HH12 and HH13 shows the sensitivity

of k_{eff} to the time period in the assembly irradiation history when the control blade is inserted. In both HH12 and HH13, the control blade was inserted fully for 50% of the irradiation time; however, there is a significant difference in k_{eff} between the two cases. HH13 differs from HH12 by 1.30% and 1.54% Δk_{eff} for the AO and AFP isotope sets, respectively. As expected from ^{239}Pu results in Figure 5.4, late control blade insertion is much more limiting than early control blade insertion. This is further confirmed by comparing HH14, HH15, and HH16, which simulate a fully inserted control blade in either the first, second, or third cycle of operation, and withdrawn for the rest of the irradiation time. HH16, which has blades inserted in the last third of assembly life, produces higher reactivity than HH14 and HH15. These results are expected based on the ^{239}Pu results shown in Figure 5.5. The results in Table 5.1 clearly indicate that control blade insertion later in assembly life produces higher cask reactivity than similar control blade insertion earlier in life.

Table 5.1 Criticality results for HH1–HH32

AO isotope set		AFP isotope set	
History	k_{eff}*	**History**	k_{eff}*
HH2	0.87394	HH31	0.77464
HH32	0.87124	HH2	0.77336
HH31	0.86468	HH32	0.77323
HH13	0.85978	HH30	0.76146
HH17	0.85407	HH13	0.75865
HH16	0.85282	HH16	0.75158
HH18	0.85206	HH17	0.75111
HH19	0.85197	HH18	0.75041
HH30	0.85018	HH29	0.75039
HH12	0.84678	HH19	0.74981
HH15	0.84421	HH28	0.74524
HH14	0.84175	HH12	0.74326
HH29	0.84056	HH5	0.74284
HH28	0.83503	HH15	0.74217
HH5	0.83304	HH27	0.74178
HH11	0.83276	HH26	0.74037
HH1	0.83268	HH25	0.73878
HH4	0.83265	HH14	0.73843
HH26	0.83265	HH24	0.73587
HH21	0.83263	HH11	0.73246
HH3	0.83263	HH20	0.73222
HH9	0.83261	HH10	0.73221
HH25	0.83261	HH23	0.73219
HH22	0.83261	HH4	0.73214
HH10	0.83259	HH21	0.73205
HH6	0.83256	HH7	0.73205
HH20	0.83256	HH8	0.73204
HH7	0.83253	HH22	0.73201
HH8	0.83251	HH9	0.73200
HH23	0.83249	HH3	0.73197
HH24	0.83229	HH6	0.73193
HH27	0.83228	HH1	0.73192

*All k_{eff} calculations have estimated standard deviations $\leq$ 0.0001.

Note that many of the lower cases in Table 5.1 for both the AO and AFP isotope sets differ by very little. For the AO isotope set, the lower 17 cases vary by a total of 0.05%; and for the AFP isotope set, the lower 13 cases vary by the same amount. This indicates very little sensitivity to the variations in the control blade history represented by these cases. A closer look at the control blade history for these particular cases indicates that none includes full-depth control

blade insertion, although a number of them have control blade insertion depths of 76%, whereas all of the highest reactivity cases have virtually full-depth control blade insertion. This result suggests once again that there is a significant sensitivity associated with control blade insertion depth.

HH23–HH32 were used to ascertain a detailed understanding of the cask reactivity as a function of control blade insertion depth. HH23–HH32 are combined with HH1–HH5 to simulate the control blade remaining in one axial location for the entire irradiation over all axial levels. The AO and AFP criticality results from HH1–HH5 and HH23–HH32 are plotted in Figure 5.6 as a function of control blade insertion depth.

The k_{eff} results for the AO and AFP isotope sets show marked differences once the blade is inserted more than halfway into the assembly. The AO curve is flat in the lower three quarters of the assembly, indicating that control blade insertion in the bottom portion of the fuel assembly has little impact on cask reactivity. For the upper seven nodes in the fuel assembly, cask reactivity increases significantly, indicating that cask reactivity is extremely sensitive to control blade insertion in the uppermost portions of the fuel assembly. The high sensitivity in the upper portion of the fuel assembly is due to the highly top-peaked axial fission distribution (Figure 4.5) in SNF within transportation and storage casks. The profile for the AFP isotope set is generally similar, but it has some differences. Control blade insertion in the bottom half of the assembly does not impact cask reactivity, consistent with the results seen for the AO set. Cask reactivity starts to increase slowly once the blade is inserted more than halfway into the assembly and then increases quickly from about node 6 to node 3. Cask reactivity drops slightly when the blade is inserted in the either of the top two nodes. The discharge burnups in both of these nodes are below 20 GWd/MTU, so residual gadolinium burnable absorber remains at these elevations. The poisoning effect of this residual absorber overwhelms the reactivity increases associated with additional ^{239}Pu production in these nodes and causes significant perturbation of the axial fission distribution in the cask.

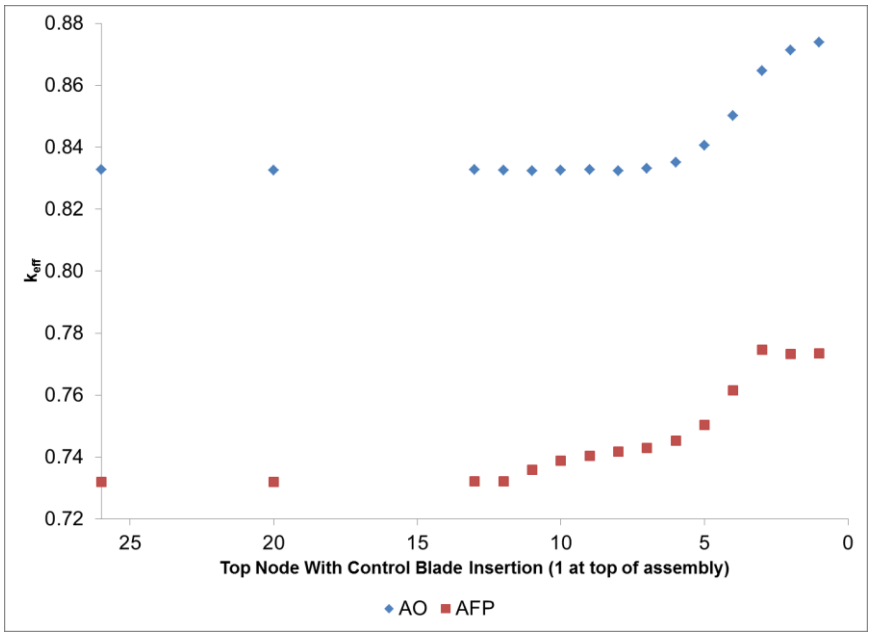

Figure 5.6 AO and AFP criticality results as a function of blade insertion depth

The AFP axial fission distributions for a range of hypothetical histories (insertions of 100%, 84%, 76% and 0%) are shown in Figure 5.7. Hypothetical histories with the control blade inserted more than halfway into the assembly show at least some shift in the fission distribution to the middle elevations of the cask.

The axial distribution of ^{239}Pu is shown for HH05 in Figure 5.8, and that of ^{155}Gd is shown in Figure 5.9. HH05 inserts the control blade into the bottom 19 nodes (76%), while HH29 inserts the control blade into the bottom 21 nodes (84%). In this range, as shown in Figure 5.8, the ^{239}Pu generation in the upper regions of the full lattice results in a higher ^{239}Pu concentration than at the top of the assembly. The ^{239}Pu concentration increases moving up the assembly as the moderator density decreases and the neutron spectrum shifts to higher energies. Node 11 is the first node of the vanished lattice, and the spectrum softens significantly at this elevation because of the additional water coolant in the lattice occupying the vanished rod locations. The ^{239}Pu concentration increases again until node 6, which is the first unrodded node. Figure 5.8 clearly illustrates the impact of the control blade on the neutron spectrum and thus ^{239}Pu generation. The ^{239}Pu concentration decreases in the top few nodes as the burnup decreases. The lower burnups result in a significant amount of residual gadolinium. The axial profile of the ^{155}Gd concentration is considerably simpler and is driven nearly entirely by burnup. The large concentration in the top two nodes is a direct result of the low burnup of these nodes. The overall cask k_{eff} drops for rod insertions into the uppermost two nodes (as illustrated in Figure 5.6) because the axial fission distribution shifts more strongly into these nodes, which contain significant residual gadolinium. Shifting the fission distribution more strongly into these nodes results in greater parasitic neutron absorption in the residual gadolinium, thus reducing reactivity. The additional ^{239}Pu produced when these nodes are rodded has a small effect on reactivity due to a shift in the fission distribution into these nodes with high concentrations of residual gadolinium.

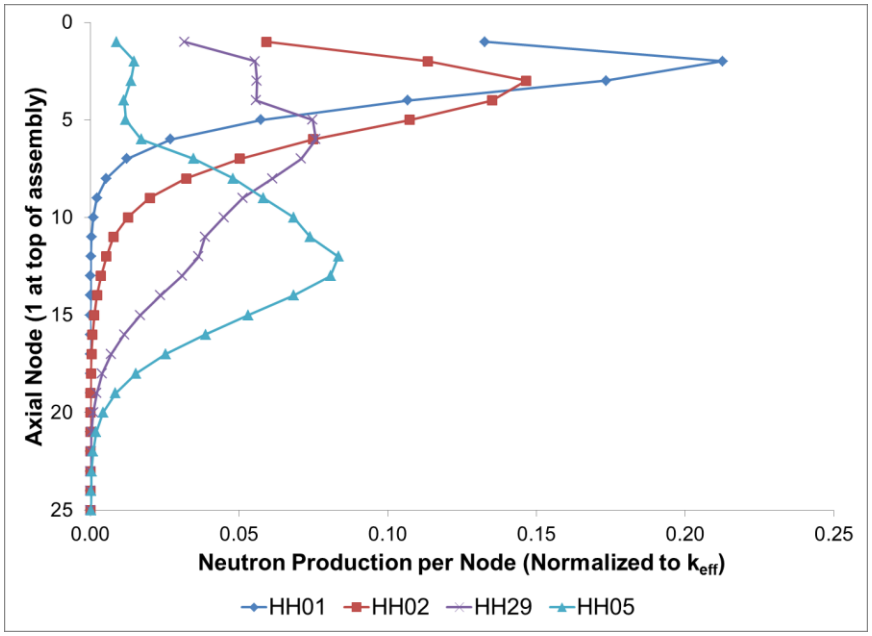

Figure 5.7 Axial fission distribution for several hypothetical histories

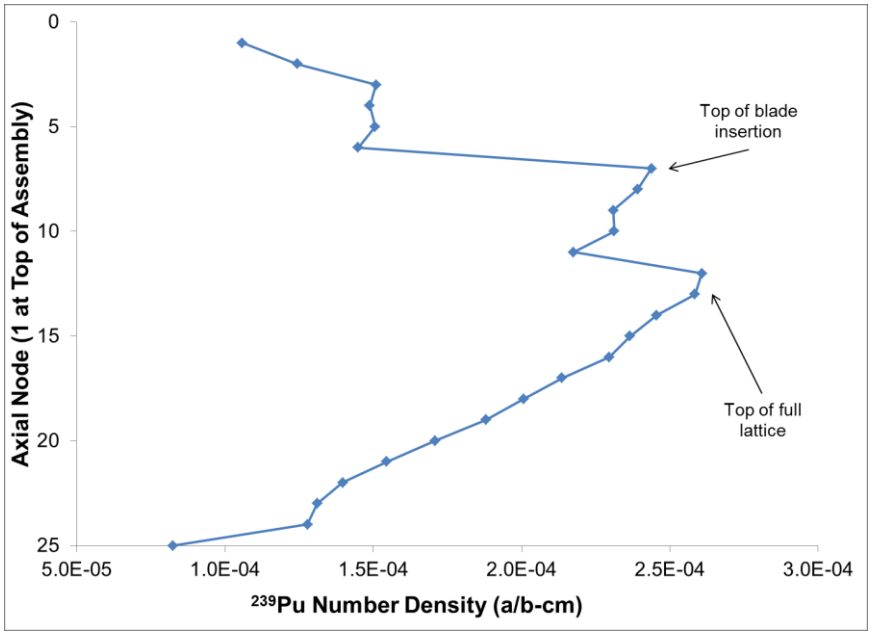

Figure 5.8 Axial distribution of ^{239}Pu

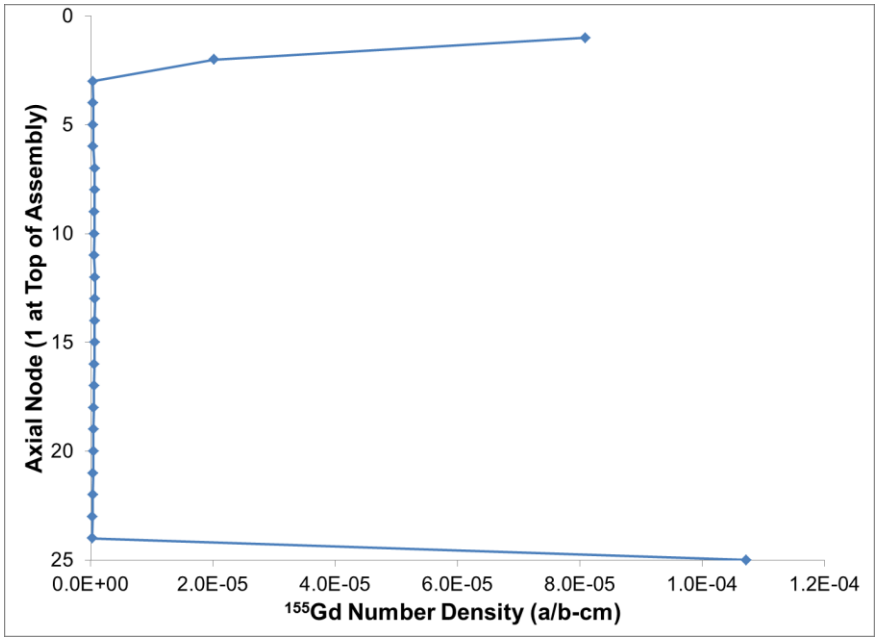

Figure 5.9 Axial distribution of ^{155}Gd

The axial fission profiles shown in Figure 5.7 demonstrate that significant departures from the expected top-peaked fission profile shown in Figure 4.5 are possible with these hypothetical histories. The interaction among assemblies within the cask can be strongly influenced by the alignment of the fission distributions; so cask reactivity can be affected not only by differences in discharged isotopic number densities caused by rodded operations, but also by shifts in the fission distributions. Although not shown in this report, fission profiles resulting from histories with the control blades inserted approximately halfway into the assembly for the entire

irradiation can generate double peaked (top and middle) fission distributions. These profiles are potentially susceptible to source convergence difficulties in Monte Carlo simulations, and results must be examined for indications of source convergence problems.

5.2.3 Control Blade Study with Realistic Histories

To compare the hypothetical histories with realistic histories, control blade insertion data were extracted from the available operating data. The control blade insertion depths were then plotted, and certain histories were selected for analysis. Because only one cycle of data exists for the operating data, the full-length control blade histories were constructed by simulating a selected single-cycle control blade history repeatedly for three consecutive cycles. Fuel assemblies are unlikely to experience significant operational periods with control blades inserted for three consecutive cycles because of fuel assembly shuffling and decreased fuel reactivity with burnup. In general, fresh fuel assemblies are placed relatively close to the center of the core and then moved to the radial periphery of the core. The control blades relatively close to the center of the core are typically used frequently, as they have the greatest effect on core reactivity, while the control blades near the periphery are not frequently used during operation. In addition, control blades are not typically used significantly at EOC owing to the reduction of total core reactivity as a result of fuel depletion. This cycle-by-cycle movement of fuel assemblies, preferential use of certain control blade locations, and limited use of control blades at EOC are likely to lead to fuel assemblies that experience more control blade insertion near BOL and less control blade insertion near EOL. Therefore the simulation of three cycles with large integral control blade histories should produce conservative criticality results when compared with typical operation.

The cask criticality results for RH1–RH10 can be found in Table 5.2, and plots depicting the control blade insertion depth as a function of time can be found in Appendix A. The data in Table 5.2 have been sorted from highest to lowest reactivity. The total spread (highest minus lowest) of realistic profile cask criticality data for the AO and AFP isotope is 0.49% and 0.59% Δk_{eff}, respectively. Initially, one might expect that RH2, which includes the highest integral control blade history, would also produce the highest cask reactivity. However, RH2 has the seventh-highest cask reactivity for both the AO and AFP isotope sets. This is the case because, although RH2 has the most frequent control blade usage, it contains only one instance per cycle when the control blade is inserted to a depth greater than 80% into the core. By contrast, RH9, which produces the highest cask reactivity for both the AO and AFP isotope sets, has two relatively lengthy control blade insertions, both at depths of greater than 90% into the core. Two clear conclusions can be drawn from these results, along with those shown in Figure 5.6. Because of the high sensitivity to very deep control blade insertion, realistic histories that have control blade insertions of greater than ~80% of the length of the fuel result in a noticeable impact on cask reactivity. By contrast, cases with control blade insertions of less than ~50% of the fuel length are virtually indiscernible (within the statistical deviation) from the base case with control blades withdrawn (HH1).

Table 5.2 Criticality results for RH1-RH10

AO isotope set		AFP isotope set	
History	**k_{eff}***	**History**	**k_{eff}***
RH9	0.83733	RH9	0.73781
RH8	0.83627	RH6	0.73583
RH3	0.83610	RH8	0.73533
RH6	0.83569	RH3	0.73532
RH10	0.83440	RH10	0.73397
RH5	0.83304	RH5	0.73300
RH2	0.83278	RH2	0.73281
RH1	0.83258	RH7	0.73248
RH4	0.83253	RH4	0.73210
RH7	0.83247	RH1	0.73188

*All k_{eff} calculations have estimated standard deviations ≤ 0.0001.

The most limiting realistic history (RH9) differs from the most limiting hypothetical history (HH2 for the AO isotope set and HH31 for the AFP isotope set) by −3.66% and −3.68% Δk_{eff} for the AO and AFP isotope sets, respectively. The differences between RH9 and HH2 indicate that the assumption of fully inserted rods for the entire irradiation is an overly conservative assumption. Comparing RH9 with HH1 (control blades withdrawn) shows differences of 0.49% and 0.59% Δk_{eff} for the AO and AFP isotope sets, respectively. This difference indicates that neglecting control blade insertion during depletion could result in nonconservative cask criticality values of ~0.6% Δk_{eff}. The axial fission distribution for RH09, shown in Figure 5.10, agrees closely with that for the unrodded depletion (HH01). However, this difference should not be viewed as a bounding estimate of the effect, because the result is based on only a single cycle of control blade histories. Additional data from other plants and for an entire assembly life would be needed to generate a more generically applicable estimate of the cask reactivity impact of realistic control blade usage.

In addition to Figure 5.10, the axial fission distributions from the rest of the realistic histories were plotted and analyzed. However, plots of these fission distributions have been omitted from the document, as they do not deviate significantly from the fission profiles shown in Figure 5.10. None of the simulated realistic histories result in middle- or double-peaked fission distributions, so it is very unlikely that a fission distribution other than top-peaked would be observed in an actual fuel assembly or cask. This analysis shows that the significant shifts in the fission shape are only an effect of modeling inserted blades at specific depths for very prolonged periods of irradiation. These extreme conditions are unlikely to occur in actual reactor operation.

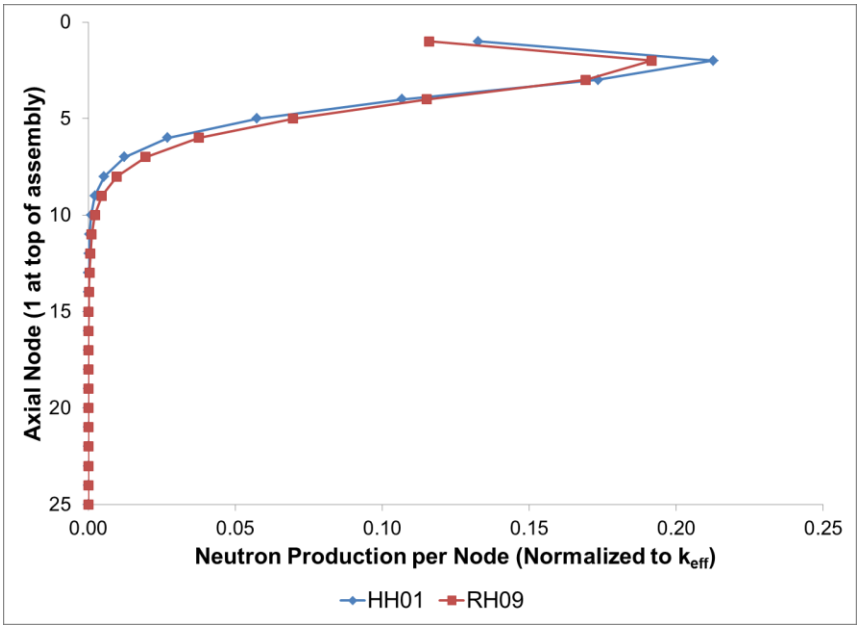

Figure 5.10 Axial fission distribution for the limiting realistic history and the unrodded hypothetical history

5.3 Summary and Recommendations

This section documents studies examining the effects of control blade insertion on extended BWR BUC. Two sets of control blade histories were analyzed as part of this study: (1) hypothetical histories to examine key effects of control blade insertion depth, length, and time in cycle and (2) realistic histories constructed from available operating data. The important effects ascertained using the HHs are compared with the results based on RHs to determine approximate differences associated with simulations of fuel assemblies over the entire irradiation. The results of the hypothetical control blade histories indicate three effects that result in increased cask reactivity: (1) control blades inserted deeply into the core, (2) control blades inserted near EOL, and (3) control blades inserted for longer periods of time (or burnup). In particular, cask reactivity is especially sensitive to control blade insertion deeply into the core due to the axially top-peaked fission distribution (end effect) typical in BWR storage and transportation casks. It has also been demonstrated that, under some hypothetical analysis conditions, it is possible to change this axial fission distribution in ways that probably are not representative of actual discharged fuel assemblies and have minimal effect on cask reactivity.

The results of this study indicate that neglecting control blade insertion during depletion could result in nonconservative cask criticality values of approximately 0.6% Δk_{eff}. Additional operating data from other plants would be needed to generate a more generically applicable estimate of the cask reactivity impact of realistic control blade usage.

Key observations of this study are summarized as follows.

- Control blade insertions of 50% or less for the entire depletion have virtually no impact on cask reactivity.

- Although unrealistic, the most limiting case for the AFP isotope set is 92% blade insertion for the entire irradiation, which increases cask reactivity by 4.3% Δk_{eff} (compared with unrodded irradiation). The limiting case for the AO isotope set, full control blade insertion for the entire irradiation, is also unrealistic and results in a cask reactivity increase of 4.1% Δk_{eff} (compared with unrodded irradiation).

- Deeper control blade insertions (80% of the active fuel length or higher) have a considerably greater impact than frequent shallower insertions.

- Deep control blade insertions in the last third of life have greater impact (~1%) on reactivity than similar insertions earlier in life.

- Control blades inserted more than half way into the core for significant periods can cause significant shifts in axial fission distribution. Insertions in the range of 75% to 85% for the entire depletion appear to maximize the observed shift in the cask. Analysis assumptions or simplifications regarding control blade use which introduce these shifts, such as partial control blade insertion for an extended period, are unnecessary and should be avoided because such shifts do not result from the realistic histories.

- Fuel assemblies are unlikely to experience significant operational periods with control blade insertion late in life because of lower reactivity and placement near the core periphery; therefore the limiting cases examined here are considered conservative.

- Some fuel assemblies may experience exceptional control blade use. This would be the result of suppressing assembly power because of leaking fuel rods or high assembly reactivity early in life.

- Based on the limiting realistic histories examined, a penalty of ~0.6% to 1.2% Δk_{eff} may be sufficient to account for control blade insertion effects. Applicants should provide a justification that any reactivity penalty taken is sufficient to account for rodded operations and should identify a process for handling assemblies that violate the underlying assumptions used in generating the penalty.

6 AXIAL BURNUP PROFILES

This section focuses on the effects of axial burnup profiles on cask reactivity and makes recommendations for identifying and using potentially limiting burnup profiles. Initially, a set of profiles had to be generated, as no BWR database analogous to the PWR database used in Wagner, DeHart, and Parks [21] currently exists. The set of profiles generated for this work are the normalized EOC axial burnup profiles for all 624 assemblies in the core follow data set. The BWR profile set generated is more limited than the PWR database but was sufficient for use in this study. The axial burnup profiles were used to generate a range of cask k_{eff} values at multiple burnups for each of the profiles considered, including both the AO and AFP isotope sets. Analysis of the calculation results is presented, including the range of k_{eff} values that result from the profiles considered, the magnitude of the end effect associated with the profiles, potential indicators of relative reactivity of axial burnup profiles, and a brief examination of the effect of the discharge burnup of the assembly from which each profile is taken on cask k_{eff}. This analysis is performed both for models that neglect the presence of natural enrichment blankets and for models that include these blanket regions. Finally, a summary of the findings on axial burnup profiles is presented.

Most of the BWR SNF in the domestic inventory has reduced-enrichment (typically natural) blankets. A routine modeling simplification made in PWR BUC is that no blankets are present, and this assumption is conservative because it significantly increases the quantity of fissile material in the relatively high-reactivity ends of the assembly. The assembly ends have high reactivity because they have low burnup; this effect was studied extensively for PWR SNF in Wagner, DeHart, and Parks [21]. The examination of the effects of BWR axial burnup profiles thus starts with the same modeling simplification: that the axial blankets are not present in the discharged fuel assemblies. This also provides a basis for comparison of the results of this study with those generally established for PWR axial burnup profile effects in [21]. The profiles used in this study were generated by a 3D core simulator model that appropriately represented the fuel as manufactured, (i.e., with blankets), but the GBC-68 cask model introduces a modeling simplification of full-enrichment fuel over the entire length of the assembly. The examination of axial burnup profile effects is extended in Section 6.3 to include explicit modeling of the blankets with the as-built natural enrichment. This further study allows for a quantification of the margin introduced by neglecting blankets and a comparison of limiting profiles in both blanketed and unblanketed models.

All depletion calculations used for analyses documented in this section were performed using the STARBUCS sequence within SCALE 6.1.3 [4]. Separate calculations were required for the full and vanished lattices, as only one ORIGEN library can be used in a STARBUCS calculation. Scenarios modeling axial blankets required four STARBUCS calculations, because the initial enrichment for natural enrichment blankets is different from that for the enriched nonblanket sections of the assembly. The difference in initial enrichments requires different ORIGEN libraries and thus separate STARBUCS calculations. The relevant SCALE composition inputs generated by STARBUCS were collected and inserted into a KENO model of the GBC-68 cask [8] loaded with GE14 fuel. All depletion parameters aside from the axial burnup profile—including specific power, axial moderator density, and operating history—were kept constant so that the only parameter that changed was the axial burnup profile. This single-variable approach is consistent with the treatments for axial moderator density (Section 4) and control blade usage (Section 5) in isolating each effect for study.

The ORIGEN libraries used in the STARBUCS depletions were all generated without control blade insertion. The effects of rodded operation are discussed in Section 5; and any impact of exposure to control rods on the burnup profile itself will be included in the axial burnup profiles considered in this study, because they were extracted from actual plant data. The impact of correlated parameters will be studied in future work.

6.1 Characteristics of Profiles Used

The EOC burnup profiles were generated for all 624 assemblies in the core follow data set used in Sections 4 and 5 and described in Section 3.1. These profiles were normalized to enable comparisons among profiles independent of burnup of the assembly from which the profile was taken. Representative profiles from low-burnup assemblies are shown in Figure 6.1, intermediate-burnup in Figure 6.2, and relatively high-burnup in Figure 6.3. The top of the assembly corresponds to low node numbers, i.e., node 1 is at the top of the assembly and node 25 is at the bottom.

Figure 6.1 shows normalized burnup profiles from assemblies that have experienced one cycle of irradiation. All of these assemblies have EOC burnups of less than 25 GWd/MTU. It is clear that there are two general profile shapes. The flatter profiles show evidence of control blade insertion, as the burnup in the lower portions of these assemblies is suppressed relative to the unrodded profiles, which manifest a much more bottom-skewed profile. The profiles resulting from rodded assemblies are shown with a dashed line, and the others with a solid line. The variation among profiles is significant; the difference between the maximum and minimum relative burnup at node 5 (relative to the top of the assembly) in the profiles shown is on the order of 30%. This variation is expected to lead to a large range of calculated cask k_{eff} values for these profiles.

Figure 6.2 shows normalized burnup profiles for assemblies that have experienced multiple cycles of irradiation and have EOC burnups between 25 and 40 GWd/MTU. In general, the burnup profiles are more similar in this burnup range than the first-cycle profiles shown in Figure 6.1. There is one profile that shows a more bottom-skewed burnup profile than the others, shown with a dashed line. Another profile has a unique profile at the top end of the assembly (low node number). This feature, hereafter referred to as the *hockey stick*, is present for many more profiles in the high-burnup profiles shown in Figure 6.3 and is related to a longer top axial blanket. Most fuel assemblies, 568 of the 624, have 6 in. top and bottom natural enrichment blankets. The remaining 56 profiles have a 12 in. long natural blanket, which results in the lower relative burnup in node 2 compared with the other profiles. Even considering the hockey stick feature, the variability among profiles is less for the intermediate-burnup profiles than for the low-burnup profiles. The range of relative burnups at node 5 is approximately 0.18; this is about 60% of the variation seen in the low-burnup profiles.

Figure 6.3 shows normalized burnup profiles for assemblies that have experienced multiple cycles of irradiation and have EOC burnups of greater than 40 GWd/MTU. Several profiles with the hockey stick feature are evident, shown with dotted lines, as are two profiles with a noticeably bottom-skewed profile. There is slightly less variability in the high-burnup profiles than in the intermediate-burnup profiles. The range of relative burnups at node 5 for profiles shown in Figure 6.3 is approximately 0.15, representing 83% of the variation seen in the intermediate-range profiles and a 50% reduction relative to the low-burnup profiles at the same elevation.

Each of the profiles shown in Figures 6.1–6.3 has a minimum relative burnup for the selected burnup range in at least one node. Each profile in each figure is shown in a unique color, but colors are reused from one figure to another.

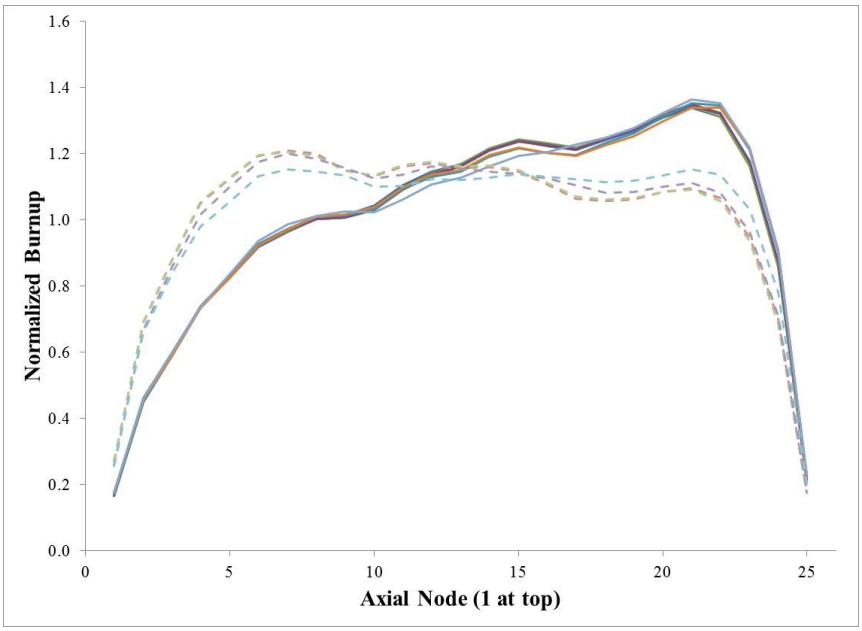

Figure 6.1 Selected normalized burnup profiles from assemblies with EOC burnups less than 25 GWd/MTU

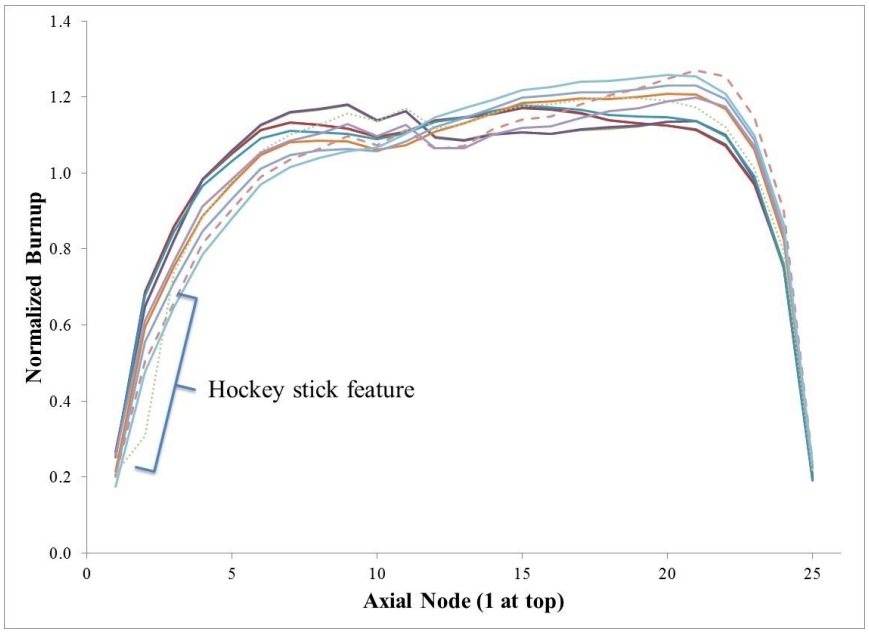

Figure 6.2 Selected normalized burnup profiles from assemblies with EOC burnups between 25 and 40 GWd/MTU

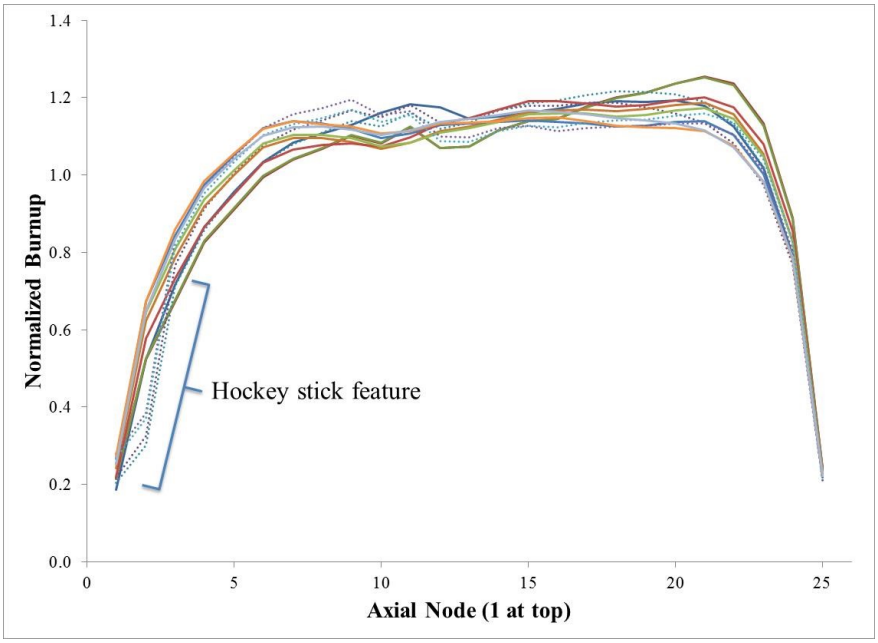

Figure 6.3 Selected normalized burnup profiles from assemblies with EOC burnups greater than 40 GWd/MTU

6.2 Results for Models Without Blankets

Results are presented in this section for all 624 normalized axial burnup profiles from the core follow data at assembly average burnup values of 30, 40, and 50 GWd/MTU. Cask k_{eff} values are determined for all three assembly average burnup values for each of the 624 profiles, regardless of the EOC burnup of the assembly from which the profile was taken. These models include the modeling simplification of full-length enriched fuel and are performed for both the AO and AFP isotope sets. A uniform axial burnup profile that is depleted with the same depletion conditions and axial moderator distribution as the nonuniform profiles is included for comparison.

The depletion calculations for the blanket nodes are performed in STARBUCS; the ORIGEN libraries are generated with the appropriate moderator density and number of rods for each axial location in the core, but with higher fuel enrichment. The GE14 assembly model includes the full and vanished lattices, but not a reduced enrichment section for the axial blankets.

6.2.1 Cask k_{eff} Results

The analysis of the reactivity effects of axial burnup profiles starts with a presentation of the cask k_{eff} values. These data are presented here and analyzed further in Sections 6.2.2, 6.2.3, and 6.2.4. Table 6.1 shows the minimum, average, and maximum k_{eff} values for each burnup for the AO and AFP isotope sets, as well as the standard deviation of the k_{eff} values for each distribution. The values presented in the table show that a wide range of cask k_{eff} values result from the 624 normalized axial burnup profiles analyzed at each of the three considered burnups and that the range increases with burnup. For the AO isotope set, the range is about 3.3% Δk at 30 GWD/MTU and increases to almost 5% Δk at 50 GWd/MTU. For the AFP isotope set, the range is 4% Δk at 30 GWd/MTU and increases to 6.1% Δk at 50 GWd/MTU. The range of cask

k_{eff} values is relatively constant in terms of standard deviations, with all six distributions (two isotope sets at each of three burnups) having a width between 3.35 and 3.77 standard deviations.

Table 6.1 Cask k_{eff} distribution data for the unblanketed fuel models

	AO isotope set			AFP isotope set		
Burnup (GWd/MTU)	**30**	**40**	**50**	**30**	**40**	**50**
Minimum	0.85722	0.82286	0.79255	0.81010	0.77259	0.73988
Maximum	0.89052	0.86527	0.84241	0.85027	0.82220	0.80089
Average	0.87505	0.84535	0.81854	0.83154	0.79842	0.76911
Standard deviation (Δk)	0.00883	0.01201	0.01477	0.01132	0.01481	0.01763

The ten most reactive profiles are identified and their associated cask k_{eff} values are provided for the AO isotope set in Table 6.2 for each of the three burnup values considered. For the 50 GWd/MTU burnup values, the ten most reactive profiles that result from assemblies with 6-in. blankets are also identified. None of the profiles with 12-in. axial blankets (profile numbers over 400 listed in Table 6.2) is in the ten most reactive profiles at 30 or 40 GWd/MTU. Aside from the 12-in. blanket (hockey stick) profiles appearing in the list, the top few profiles are generally consistent among the three burnups considered. Several of the profiles result in cask k_{eff} values that are statistically equivalent, but the range from the most reactive to the tenth most reactive profiles is large enough that there is high confidence that the most reactive profile is captured in the list presented.

The ten most reactive profiles are identified and their associated cask k_{eff} values are provided for the AFP isotope set in Table 6.3 for each of the three burnup values considered. For the 40 and 50 GWd/MTU burnup values, the ten most reactive profiles that result from assemblies with 6-in. blankets are also identified. None of the profiles from assemblies with 12-in. blankets (profile numbers over 400 listed in Table 6.3) is in the ten most reactive profiles at 30 GWd/MTU. The 50 GWd/MTU burnup point is dominated by 12-in. blanket profiles; the 29 most reactive profiles result from these hockey stick profiles. These profiles become limiting at high burnup as the relative reactivity difference between the low-burnup top end of the assembly and the high-burnup middle portion of the assembly becomes greater. The low relative burnup in the top nodes causes the reactivity of that portion of the assembly to drop more slowly with burnup, and this difference increases with burnup. The limiting 6-in. blanket profiles are fairly consistent at each burnup, as with the AO isotope set. Several profiles yield statistically equivalent cask k_{eff} values, which is also consistent with the AO isotope set results. The limiting profiles are largely the same, although in a slightly different order, for the AFP and AO isotope sets.

Table 6.2 Top ten most reactive axial burnup profiles, AO isotope set

30 GWd/MTU		40 GWd/MTU		50 GWd/MTU		50 GWd/MTU, only 6-in. blanket profiles	
Profile	**Cask k_{eff}**	**Profile**	**Cask k_{eff}**	**Profile**	**Cask k_{eff}**	**Profile**	**Cask k_{eff}**
31	0.89052	40	0.86527	443	0.84241	40	0.84190
52	0.89028	31	0.86505	442	0.84210	52	0.84167
22	0.89028	22	0.86488	452	0.84206	31	0.84166
77	0.89018	52	0.86487	447	0.84192	22	0.84166
11	0.89016	37	0.86483	444	0.84192	37	0.84138
40	0.89016	36	0.86468	40	0.84190	36	0.84137
81	0.89014	54	0.86466	52	0.84167	39	0.84135
36	0.89011	35	0.86463	31	0.84166	35	0.84133
67	0.89003	39	0.86456	22	0.84166	16	0.84124
39	0.89000	81	0.86450	441	0.84151	54	0.84123

(Monte Carlo uncertainty in all calculated k_{eff} values is approximately 0.00010 Δk_{eff}.)

Table 6.3 Top ten most reactive axial burnup profiles, AFP isotope set

30 GWd/MTU		40 GWd/MTU		50 GWd/MTU	
Profile	**Cask k_{eff}**	**Profile**	**Cask k_{eff}**	**Profile**	**Cask k_{eff}**
40	0.85027	443	0.82220	443	0.80089
52	0.85022	452	0.82196	452	0.80078
31	0.85018	31	0.82193	447	0.80036
35	0.85005	40	0.82190	442	0.80020
22	0.85000	444	0.82168	444	0.80007
54	0.84999	52	0.82166	441	0.79975
36	0.84999	442	0.82153	445	0.79962
77	0.84997	441	0.82148	446	0.79949
39	0.84991	447	0.82144	422	0.79876
81	0.84991	22	0.82143	424	0.79873
Only 6-in. blanket profiles					
No profiles with 12-in. blankets in the 10 most reactive		31	0.82193	40	0.79591
		40	0.82190	52	0.79567
		52	0.82166	22	0.79559
		22	0.82143	31	0.79553
		35	0.82124	36	0.79553
		36	0.82122	37	0.79541
		54	0.82121	11	0.79529
		39	0.82121	35	0.79519
		11	0.82120	39	0.79517
		16	0.82111	54	0.79516

(Monte Carlo uncertainty in all calculated k_{eff} values is approximately 0.00010 Δk_{eff}.)

Table 6.4 lists eight axial burnup profiles that occur in the top ten most reactive profiles, from assemblies with 6-in. blankets for multiple burnups with both the AO and AFP isotope sets. The profiles are plotted in Figure 6.4, showing clearly similar traits in the limiting profiles. The top end of the fuel assembly drives reactivity because of its low burnup but relatively high plutonium content relative to the low burnup in the last node of the assembly. Nodes adjacent to the lowest

node also have higher burnup, and thus lower reactivity, than the nodes adjacent to the top node. The profiles also come from assemblies that have experienced a single cycle of operation that has been at least primarily unrodded.

Table 6.4 Eight highly reactive normalized axial burnup profiles

Prof. 31	Prof. 52	Prof. 22	Prof. 40	Prof. 36	Prof. 39	Prof. 54	Prof. 35
0.169	0.172	0.168	0.168	0.169	0.170	0.172	0.170
0.455	0.455	0.456	0.454	0.456	0.457	0.456	0.457
0.596	0.594	0.598	0.596	0.598	0.599	0.596	0.598
0.743	0.744	0.744	0.743	0.744	0.745	0.747	0.745
0.837	0.838	0.837	0.837	0.838	0.840	0.841	0.838
0.933	0.937	0.933	0.934	0.934	0.936	0.940	0.934
0.979	0.983	0.977	0.978	0.979	0.981	0.985	0.979
1.013	1.019	1.013	1.013	1.013	1.015	1.020	1.014
1.018	1.024	1.018	1.018	1.017	1.019	1.023	1.018
1.041	1.044	1.045	1.042	1.041	1.042	1.042	1.041
1.101	1.104	1.108	1.104	1.101	1.102	1.102	1.102
1.146	1.141	1.154	1.150	1.146	1.147	1.138	1.148
1.171	1.158	1.180	1.175	1.171	1.171	1.155	1.173
1.218	1.204	1.228	1.223	1.219	1.219	1.201	1.220
1.247	1.229	1.257	1.253	1.248	1.248	1.226	1.249
1.234	1.215	1.244	1.239	1.235	1.235	1.212	1.236
1.219	1.209	1.230	1.226	1.222	1.222	1.206	1.223
1.249	1.245	1.259	1.256	1.252	1.252	1.243	1.253
1.278	1.275	1.287	1.283	1.281	1.280	1.274	1.281
1.324	1.325	1.330	1.327	1.326	1.325	1.324	1.326
1.361	1.367	1.359	1.359	1.361	1.359	1.367	1.360
1.345	1.359	1.325	1.333	1.340	1.338	1.361	1.338
1.206	1.224	1.175	1.190	1.199	1.196	1.229	1.196
0.896	0.912	0.865	0.881	0.889	0.886	0.917	0.886
0.222	0.223	0.213	0.218	0.220	0.219	0.225	0.219

(Top of assembly is at top of table)

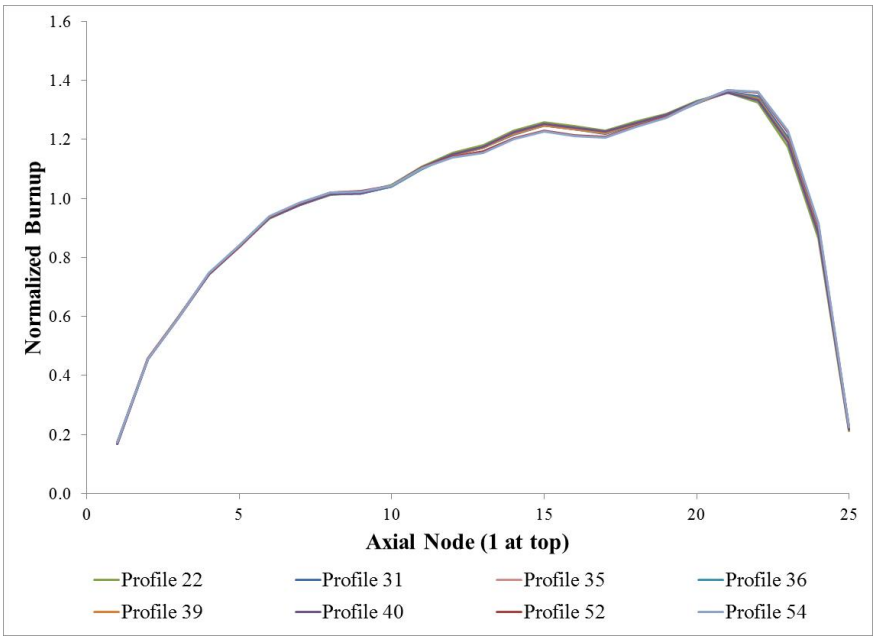

Figure 6.4 Eight limiting axial burnup profiles

6.2.2 End Effect

The difference between cask k_{eff} calculated using a distributed burnup profile and using a uniform profile is called the *end effect*. When the end effect is positive, modeling of the distributed burnup profile is more conservative. Figure 6.5 shows the distributed-burnup profile cask k_{eff} values and the uniform-burnup profile cask k_{eff} value for all three burnups for the AO isotope set. Figure 6.6 shows the same results for the AFP isotope set. The distributed profiles in both figures are sorted from least reactive to most reactive, so the horizontal axis represents the reactivity ranking of all 624 profiles. The end effect is calculated for each profile.

The end effect values for the AO isotope set increase with burnup as expected, although note that all 624 profiles have a positive end effect by 30 GWd/MTU. This result is influenced by the modeling simplification made by using fully enriched fuel in place of natural blankets. At 30 GWd/MTU, the end effect varies from 0.3% Δ*k* to 3.6% Δ*k*; at 50 GWd/MTU, the minimum end effect has increased to 3.7% Δ*k*, and the maximum value is 8.6% Δ*k*.

The end effect values for the AFP isotope set also increase with burnup, as expected. As with the AO isotope set, all profiles result in positive end effects by 30 GWd/MTU. The magnitude of the end effects is significantly greater for the AFP set than for the AO set. The end effect ranges from 1.6% Δ*k* to 5.7% Δ*k* at 30 GWd/MTU and from 6.6% Δ*k* to 12.7% Δ*k* at 50 GWd/MTU. These numbers are larger than the results presented in Wagner, DeHart, and Parks [21], but the burnup profiles considered in that work were exclusively unblanketed fuel.

These end effect values are quite large, and extrapolation to lower burnups would indicate that positive end effects could exist below 20 GWd/MTU. Positive end effects in this burnup range would potentially impact peak reactivity methods, such as those described in Marshall, Ade, et al. [3], since those methods typically assume a 2D planar representation of the fuel assembly. A positive end effect would indicate that this approach is potentially nonconservative without

considering distributed burnup profile effects. The burnup profiles that exist in the peak reactivity burnup range of 7–20 GWd/MTU might be significantly different from EOC profiles. The residual gadolinium burnable absorber would also potentially impact the results at these lower burnups. Residual burnable absorber concentrations are much lower by EOC and are therefore not a significant contribution to cask reactivity. Additional work is needed to examine this potential residual burnable absorber effect at lower burnups, because the burnup profiles used in this study are all EOC profiles.

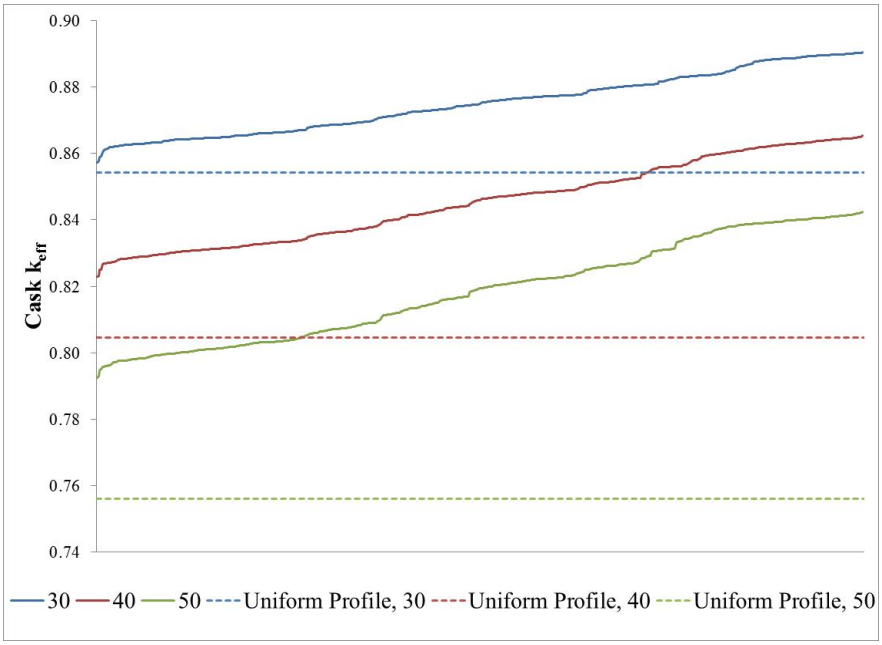

Figure 6.5 Cask k_{eff} values for distributed and uniform burnup profiles, AO isotope set

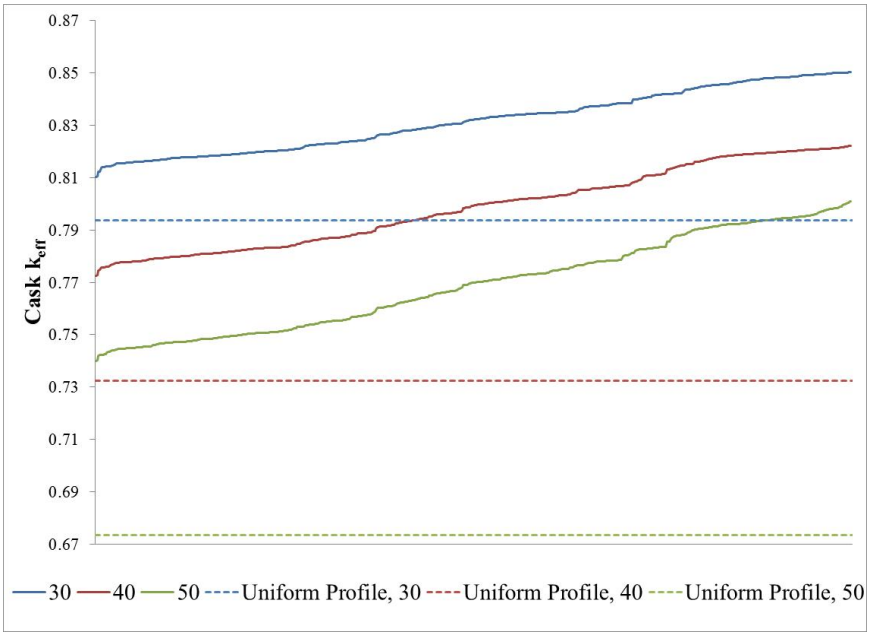

Figure 6.6 Cask k_{eff} values for distributed and uniform burnup profiles, AFP isotope set

6.2.3 Burnup Profile Selection

The work presented in this section includes 624 axial burnup profiles and calculates the GBC-68 cask k_{eff} resulting from all fuel assemblies loaded in the cask experiencing the same axial burnup profile. Many of these profiles are not close to limiting, as shown in Section 6.2.1, so a more efficient approach is desired. This section presents a method that may be used to assess the relative reactivity of different axial burnup profiles based on an examination of the relative burnup of the top end of the profile (assembly). This technique is suggested by the results of the studies performed for PWR BUC in Wagner, DeHart, and Parks [21].

An examination of the relative burnup at the top end of the profile generally indicates the relative reactivity for profiles taken from similar assemblies. The primary questions to be answered in detail are (1) how many nodes need to be considered and (2) how similar must the assemblies be. The cask k_{eff} values resulting from all 624 profiles are plotted versus the relative burnup summed over a given number of nodes at the top of the profile for all 3 burnup values. Separate data sets are plotted for the 568 profiles with 6-in. blankets and the 56 profiles with 12-in. blankets. Figure 6.7 shows the cask k_{eff} results for the AO isotope set and just the top node relative burnup. A general trend is clearly evident: lower relative burnups lead to higher cask k_{eff} values. However, several different bands are visible in the data. Figure 6.8 presents the cask k_{eff} values versus the sum of the top three node relative burnups. The data are much more closely clustered along a single trend for each blanket length, especially at 40 and 50 GWd/MTU. Considering too many nodes can also decrease the quality of the fit. This phenomenon is shown in Figures 6.9 and 6.10, which consider the top 6 node and top 11 node relative burnups, respectively. Note that the top 11 nodes constitute the entire vanished lattice, and significant spread in the data is evident in Figure 6.10, as it is in Figure 6.7. Similar results are observed for the AFP isotope set, as shown in Figures 6.11 through 6.14.

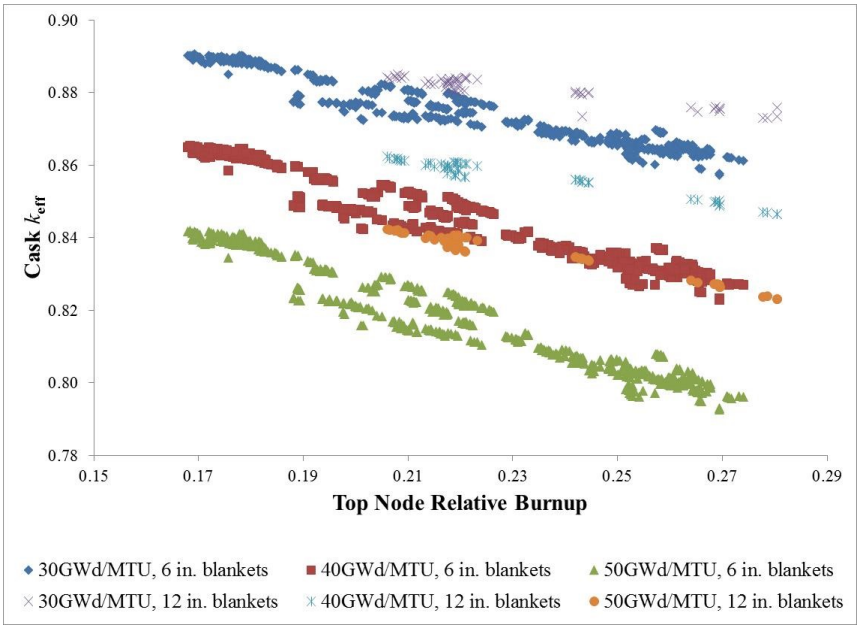

Figure 6.7 Cask k_{eff} versus top node relative burnup, AO isotope set

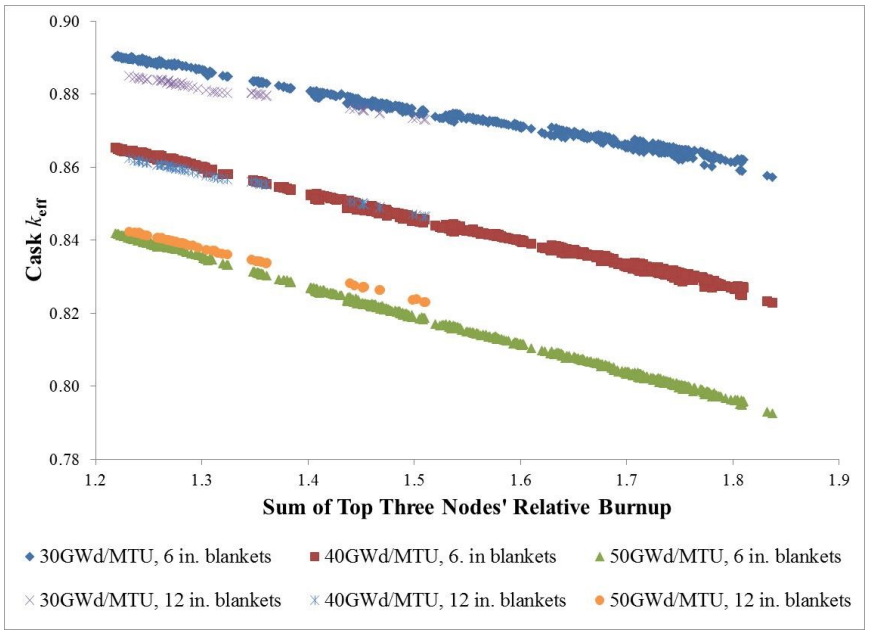

Figure 6.8 Cask k_{eff} versus sum of top three nodes' relative burnup, AO isotope set

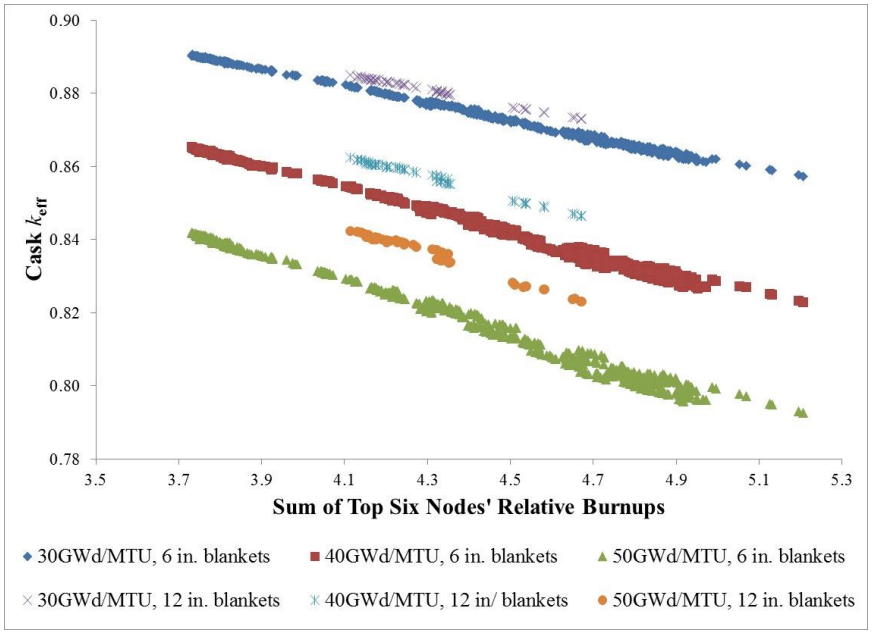

Figure 6.9 Cask k_{eff} versus sum of top six nodes' relative burnup, AO isotope set

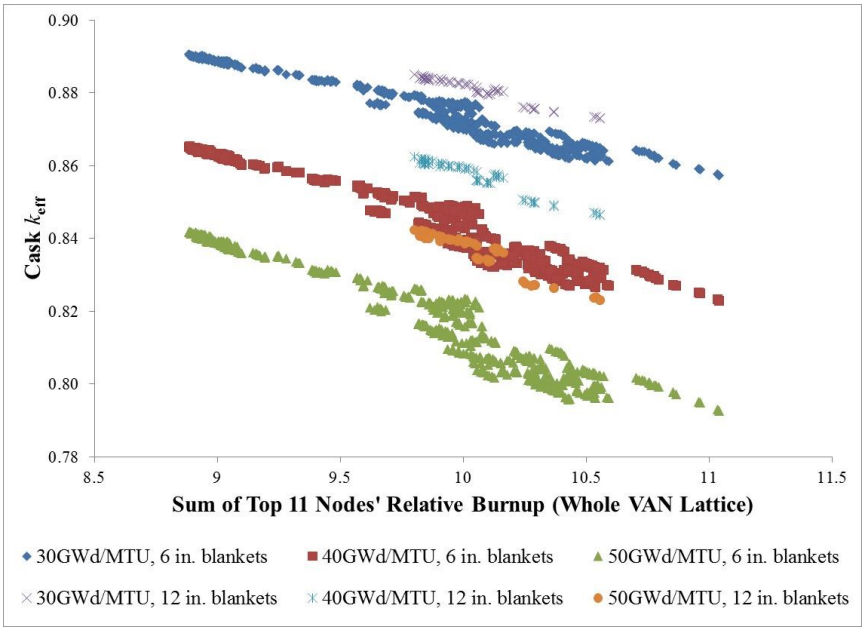

Figure 6.10 Cask k_{eff} versus sum of top 11 nodes' relative burnup, AO isotope set

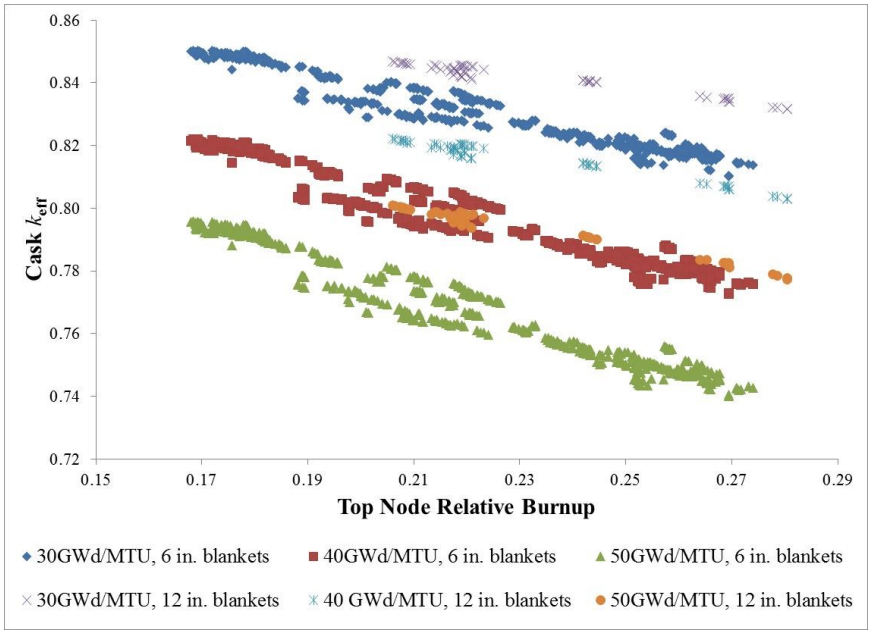

Figure 6.11 Cask k_{eff} versus top node relative burnup, AFP isotope set

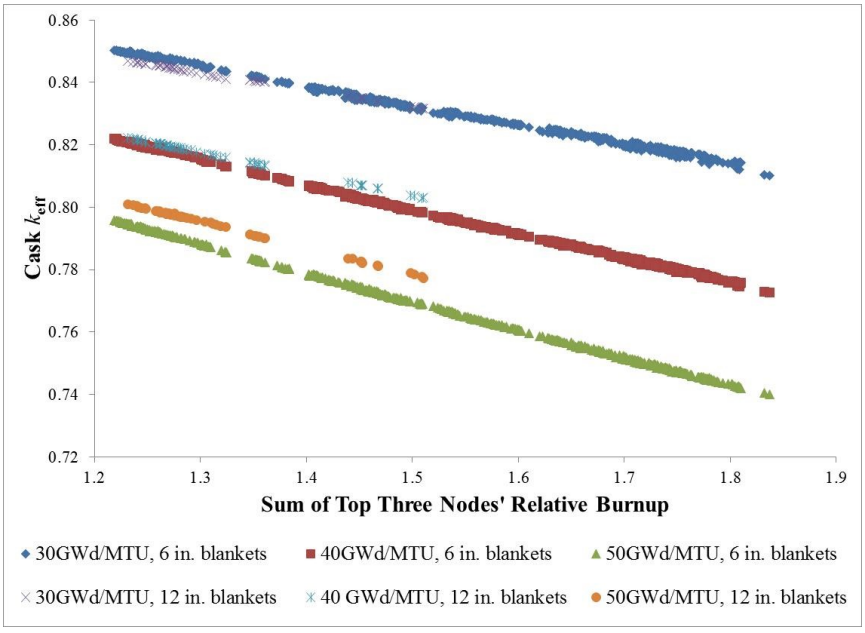

Figure 6.12 Cask k_{eff} versus sum of top three nodes' relative burnup, AFP isotope set

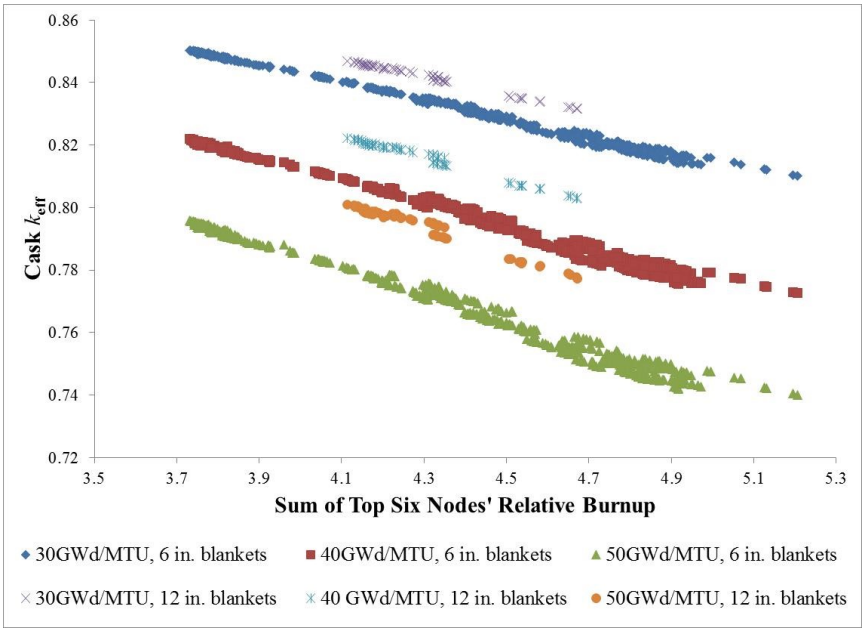

Figure 6.13 Cask k_{eff} versus sum of top six nodes' relative burnup, AFP isotope set

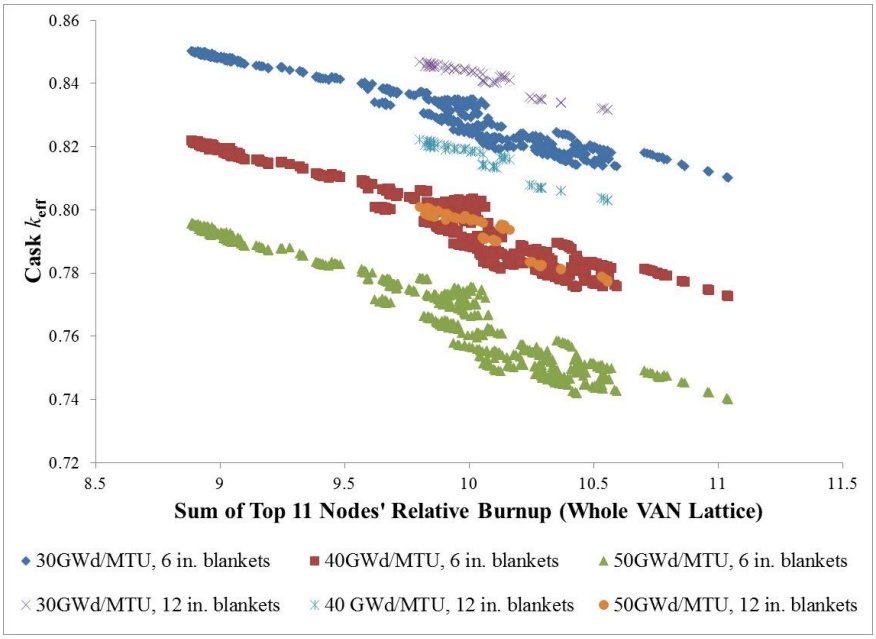

Figure 6.14 Cask k_{eff} versus sum of top 11 nodes' relative burnup, AFP isotope set

The profiles with 6-in. blankets come from four different assembly design types that have different numbers of part-length rods of differing lengths. Clearly, not all axial features must be identical for the relative burnup to be a strong indicator of relative reactivity for the profiles. The part-length rods end, in all cases, several feet from the top of the assembly and thus are not in the region that dominates discharged assembly reactivity. However, the differing blanket lengths cause differences in the relevant region of the assembly and therefore do cause different trends. It appears that models without axial blankets require consideration of approximately the top

1.5 ft—in this case, three 6-in. nodes—to generate reliable predictions of relative reactivity for the associated cask k_{eff} values. An applicant would need to justify the exact number of nodes or axial lengths used in any such profile selection scheme.

The relative positions of the trends for the profiles resulting from assemblies with 6-in. and 12-in. blankets also shift for different burnups and different numbers of nodes considered as the relative reactivity indicator. This clearly demonstrates that each population of profiles resulting from assemblies with significantly different features must be considered separately. In this case, a limited number of candidate 6-in. and 12-in. blanket profiles could be selected and depleted. The consideration of multiple burnup profiles is not eliminated, but the ability to identify a much more limited set of profiles is a significant improvement over including all 624 profiles.

6.2.4 Effect of Assembly Burnup

In this study, the normalized axial burnup profiles for all 624 assemblies from a single cycle of operation were generated and analyzed, assuming depletion to three fixed burnups of 30, 40, and 50 GWd/MTU. As documented in Wagner, DeHart, and Parks [21], burnup profiles in different burnup ranges may have different characteristics. The applicability of the profiles used in this study to low burnups was discussed in Section 6.2.2. It has been demonstrated for PWR fuel that burnup profiles tend to flatten as burnup increases, allowing the use of profiles taken from lower discharged burnups at higher burnups [21]. To examine the application of this conclusion to BWR fuel, a cursory examination of the reactivity resulting from profiles taken from assemblies in different burnup ranges is warranted.

The database of PWR axial burnup profiles used in Wagner, DeHart, and Parks [21], available in Cacciapouti and Volkinburg [24], contains more than 3000 profiles from a range of different plants and fuel designs. The set of profiles analyzed in this study contains 624 profiles from a single plant, although 4 different fuel design types are represented. The more limited nature of the data set used here precludes the type of detailed examination of narrow burnup bins, with a large number of profiles in each bin, presented in Wagner, DeHart, and Parks [21]. Instead, a more general examination is performed with the goal of determining the reactivity resulting from profiles taken from assemblies with high discharged burnups compared with profiles taken from assemblies with lower burnups.

Figure 6.15 shows the cask k_{eff} values resulting from the 568 profiles with 6-in. blankets at 50 GWd/MTU for the AO isotope set. Figure 6.16 shows these data for the AFP isotope set. All the k_{eff} values presented are calculated at a discharge burnup of 50 GWd/MTU. The horizontal axis shows the EOC burnup of the assembly from which the profile was taken. Three burnup bins are chosen, somewhat arbitrarily, as EOC assembly average burnup of (1) <25 GWd/MTU, (2) between 25 and 40 GWd/MTU, and (3) >40 GWd/MTU. These ranges are consistent with those considered in Section 6.1 (see Figures 6.1–6.3). A line added to each figure showing the highest k_{eff} value within each bin demonstrates that cask k_{eff} values decrease by 0.5% – 1% Δk from one axial profile burnup bin to the next higher bin. This is another aspect of burnup profile selection typical of PWR BUC that may also be advantageous in extended BWR BUC; excess margin may be removed from the analysis at high burnup by considering only normalized profiles from similarly high-burnup assemblies.

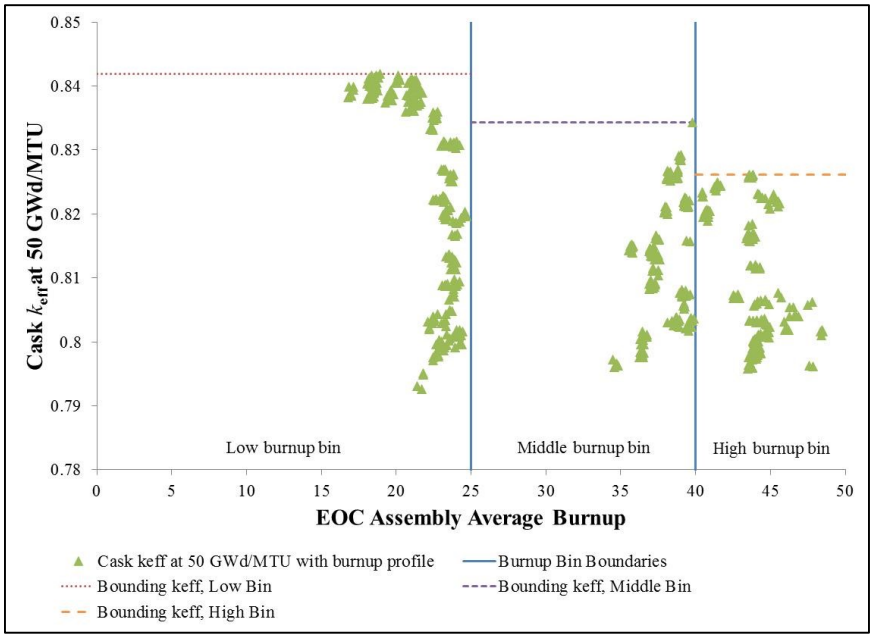

Figure 6.15 Cask k_{eff} value versus burnup of assembly generating profile, AO isotope set, no blankets modeled

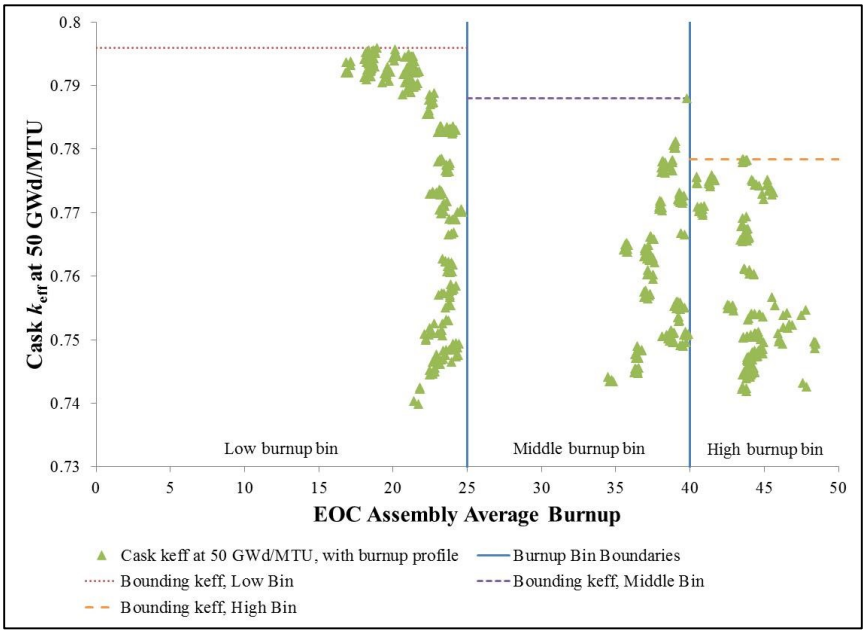

Figure 6.16 Cask keff value versus burnup of assembly generating profile, AFP isotope set, no blankets modeled

6.3 Results for Models with Blankets

This subsection presents results similar to those provided in Section 6.2. In this subsection, 6-in. natural blankets are modeled for all 624 profiles. A set of 10 of the 56 profiles with 12-in.

blankets is also modeled realistically, that is with the 12-in. blanket length modeled with natural enrichment fuel initially. The effect of modeling the blankets is examined with respect to the cask k_{eff} values, the end effect values, the prediction of the relative reactivity of the profiles, and the impact of the EOC assembly burnup that generated the profile on cask k_{eff}.

6.3.1 Cask k_{eff} Values

Table 6.5 shows the minimum, average, and maximum k_{eff} values for each burnup for the AO and AFP isotope sets, as well as the standard deviation of the k_{eff} values for each distribution. The values presented in the table show that a wide range of cask k_{eff} values result from the 624 axial burnup profiles analyzed and that the range increases with burnup. For the AO isotope set, the range is 3.8% Δk at 30 GWD/MTU and increases to 6.4% Δk at 50 GWd/MTU. For the AFP isotope set, the range is 4.9% Δk at 30 GWd/MTU and 7.6% Δk at 50 GWd/MTU. The range of cask k_{eff} values is relatively consistent in terms of standard deviations, with all six distributions (two isotope sets at each of three burnups) having widths between 3.6 and 4.1 standard deviations. These ranges are slightly larger than for the unblanketed fuel models and tend to be wider (in terms of standard deviations) at lower burnup values.

Table 6.5 Cask k_{eff} distribution data for the blanketed fuel models

	AO isotope set			AFP isotope set		
	30	40	50	30	40	50
Minimum	0.83747	0.78955	0.74592	0.77978	0.72556	0.67667
Maximum	0.87507	0.84162	0.80970	0.82842	0.78949	0.75287
Average	0.85778	0.81773	0.78011	0.80618	0.75993	0.71728
Standard deviation	0.00908	0.01306	0.01677	0.01216	0.01682	0.02104

The ten most reactive profiles and their associated cask k_{eff} values are provided for the AO isotope set in Table 6.6 for each of the three burnup values considered. None of the 12-in. blanket (hockey stick) profiles is in the ten most reactive profiles at any burnup. The top few profiles are generally consistent among the three burnups considered. Several of the profiles result in statistically equivalent cask k_{eff} values, but the range from the most reactive to the tenth most reactive profiles is large enough that there is high confidence that the most reactive profile is captured in the list presented.

The ten most reactive profiles and their associated cask k_{eff} values are provided for the AFP isotope set in Table 6.7 for each of the three burnup values considered. As was observed for the AO isotope set, none of the hockey stick profiles is in the ten most reactive profiles at any burnup. As with the AO isotope set, the limiting 6-in. blanket profiles are fairly consistent at each burnup. Also consistent with the AO isotope set results, several profiles yield statistically equivalent cask k_{eff} values. The same profiles are limiting, though in a slightly different order, for the AFP and AO isotopes sets. Generally, the limiting profiles are also the ones identified for unblanketed fuel, as discussed in Section 6.2.1. A selection of limiting profiles for models with no axial blankets is shown in Table 6.4 and Figure 6.6 in Section 6.2.1. Unlike the unblanketed results presented in Section 6.2.1, however, no hockey stick profiles are limiting for either isotope set for any burnup. This demonstrates that modeling these longer blankets with their actual enrichment makes them nonlimiting compared with the other profiles considered in this study.

Table 6.6 Top ten most reactive axial burnup profiles, AO isotope set, 6-in. blankets modeled

30 GWd/MTU		40 GWd/MTU		50 GWd/MTU	
Profile	**Cask k_{eff}**	**Profile**	**Cask k_{eff}**	**Profile**	**Cask k_{eff}**
63	0.87507	40	0.84162	63	0.80970
40	0.87500	81	0.84148	52	0.80961
69	0.87487	31	0.84147	31	0.80960
81	0.87483	52	0.84146	40	0.80954
52	0.87481	63	0.84143	77	0.80947
31	0.87479	77	0.84141	69	0.80938
36	0.87477	69	0.84140	81	0.80935
77	0.87476	22	0.84133	36	0.80928
22	0.87471	36	0.84124	35	0.80923
39	0.87463	37	0.84107	22	0.80907

(Monte Carlo uncertainty in all calculated k_{eff} values is approximately 0.00010 Δk_{eff}.)

Table 6.7 Top ten most reactive axial burnup profiles, AFP isotope set

30 GWd/MTU		40 GWd/MTU		50 GWd/MTU	
Profile	**Cask k_{eff}**	**Profile**	**Cask k_{eff}**	**Profile**	**Cask k_{eff}**
31	0.82842	40	0.78949	40	0.75287
77	0.82837	52	0.78942	52	0.75277
63	0.82833	63	0.78938	63	0.75253
40	0.82833	31	0.78936	31	0.75252
35	0.82831	77	0.78935	22	0.75250
36	0.82823	81	0.78925	77	0.75250
22	0.82823	36	0.78918	81	0.75245
69	0.82821	69	0.78916	69	0.75239
52	0.82820	35	0.78906	54	0.75223
81	0.82812	22	0.78900	36	0.75219

(Monte Carlo uncertainty in all calculated k_{eff} values is approximately 0.00010 Δk_{eff}.)

The reduction in cask k_{eff} caused by modeling the 6-in. blanket regions was calculated for each of the 624 profiles. The minimum, maximum, average, and standard deviations of the values for the k_{eff} reduction are presented in Table 6.8 for all three burnups for the AO and AFP isotope sets. The values in the table are all shown as positive values but should be understood to indicate a lowering of reactivity by including the blankets in the assembly model. Cask k_{eff} values are, on average, 3% Δk lower at 30 GWd/MTU because of the blankets for the AO isotope set. The average reactivity reduction increases in magnitude with burnup to 4.4% Δk at 40 GWd/MTU and 5.8% Δk at 50 GWd/MTU. The reactivity reduction caused by modeling the blankets is larger for the AFP isotope set. Credit for blankets is likely to be a fixture of extended BWR BUC, given the large reactivity margin associated with modeling them and the large number of assemblies in the inventory with blankets.

Table 6.8 Reactivity reduction introduced by modeling blankets

	AO Isotope Set			AFP Isotope Set		
Burnup (GWd/MTU)	**30**	**40**	**50**	**30**	**40**	**50**
Minimum	0.01295	0.02039	0.02856	0.01903	0.02888	0.03917
Maximum	0.05055	0.07246	0.09235	0.06767	0.09280	0.11537
Average	0.03024	0.04427	0.05815	0.04126	0.05843	0.07476
Standard deviation (Δk)	0.00908	0.01306	0.01677	0.01216	0.01682	0.02104

(Monte Carlo uncertainty in all calculated k_{eff} values is approximately 0.00010 Δk_{eff}.)

Including the natural blankets in the assembly models significantly reduces the reactivity of the hockey stick profiles. Results presented so far have modeled only 6-in. natural blankets, even for the hockey stick profile assemblies, which in reality contain 12-in. top blankets. Tables 6.9 and 6.10 provide the cask k_{eff} values for ten hockey stick profiles at 30 and 50 GWd/MTU considering the AO and AFP isotope sets, respectively. The results presented contain three different modeling assumptions: no blankets, 6-in. blankets, and the actual 12-in. top blanket with a 6-in. bottom blanket. At 30 GWd/MTU, the top node blanket causes the majority of the reactivity change from the unblanketed assumption. This reverses at 50 GWd/MTU so that the second blanket node is responsible for the majority of the reactivity change.

Table 6.9 Cask k_{eff} results for 10 selected 12-in. blanket profiles, AO isotope set

	30 GWd/MTU			50 GWd/MTU		
Profile number	**No blanket**	**6-in. blanket**	**12-in. blanket**	**No blanket**	**6-in. blanket**	**12-in. blanket**
349	0.88157	0.85846	0.84003	0.83791	0.79099	0.74476
352	0.88197	0.85849	0.84008	0.83849	0.79139	0.74497
424	0.88369	0.86077	0.84243	0.84048	0.79484	0.74938
426	0.88302	0.86020	0.84197	0.83974	0.79391	0.74867
427	0.88311	0.86016	0.84199	0.83966	0.79402	0.74845
437	0.88041	0.85636	0.83843	0.83621	0.78878	0.74176
439	0.88074	0.85696	0.83854	0.83707	0.78916	0.74227
441	0.88425	0.86142	0.84318	0.84151	0.79611	0.75071
583	0.88004	0.85682	0.83952	0.83388	0.78774	0.74281
584	0.87972	0.85688	0.83955	0.83399	0.78773	0.74314

(Monte Carlo uncertainty in all calculated k_{eff} values is approximately 0.00010 Δk_{eff}.)

Table 6.10 Cask k_{eff} results for 10 selected 12-in. blanket profiles, AFP isotope set

	30 GWd/MTU			50 GWd/MTU		
Profile number	**No blanket**	**6-in. blanket**	**12-in. blanket**	**No blanket**	**6-in. blanket**	**12-in. blanket**
349	0.84305	0.80999	0.78168	0.79588	0.73722	0.67229
352	0.84358	0.81002	0.78177	0.79635	0.73759	0.67275
424	0.84534	0.81289	0.78512	0.79873	0.74129	0.67791
426	0.84469	0.81235	0.78436	0.79747	0.74029	0.67671
427	0.84470	0.81222	0.78450	0.79759	0.74004	0.67652
437	0.84177	0.80806	0.77941	0.79382	0.73421	0.66865
439	0.84195	0.80801	0.77969	0.79467	0.73493	0.66894
441	0.84607	0.81395	0.78593	0.79975	0.74274	0.67916
583	0.84031	0.80759	0.78069	0.79015	0.73229	0.66956
584	0.84030	0.80788	0.78052	0.79059	0.73274	0.67022

(Monte Carlo uncertainty in all calculated k_{eff} values is approximately 0.00010 Δk_{eff}.)

6.3.2 End Effect

The uniform burnup profile used as the reference in this section also models 6-in. natural enrichment blankets to be consistent with the distributed burnup profile assembly model. Figure 6.17 shows the distributed burnup profile cask k_{eff} values and the uniform burnup profile cask k_{eff} value for all three burnups for the AO isotope set. Figure 6.18 shows the same results for the AFP isotope set. The distributed profiles in both figures are sorted from least reactive to most reactive, so the horizontal axis represents a reactivity ranking of the 624 burnup profiles.

The end effect values for the AO isotope set increase with burnup, as expected. Not all profiles generate positive end effects when the blankets are modeled, as opposed to the results presented in Section 6.2.2 when the blankets are neglected. As the end effect increases with burnup, fewer profiles generate a negative end effect. At 30 GWd/MTU, the end effect varies from −1.6% Δ*k* to 2.2% Δ*k*; at 50 GWd/MTU, the minimum end effect has increased to −1.0% Δ*k* and the maximum value is 5.4% Δ*k*.

The end effect values for the AFP isotopes set also increase with burnup, as expected. Some profiles result in negative end effects at 30 and 40 GWd/MTU, as with the AO isotope set. At 50 GWd/MTU, all profiles result in positive end effects. The magnitude of the end effects is significantly greater for the AFP set than for the AO set. The end effect ranges from −1.3% Δ*k* to 3.6% Δ*k* at 30 GWd/MTU and from 0.4% Δ*k* to 8.0% Δ*k* at 50 GWd/MTU. These numbers are larger than the results presented in Wagner, DeHart, and Parks [21], but the assemblies considered in that work were exclusively unblanketed fuel. These results, as well as those presented in Section 6.2.2, indicate that positive end effects are possible below 20 GWd/MTU. Such positive end effects could impact peak reactivity analyses and should be studied further.

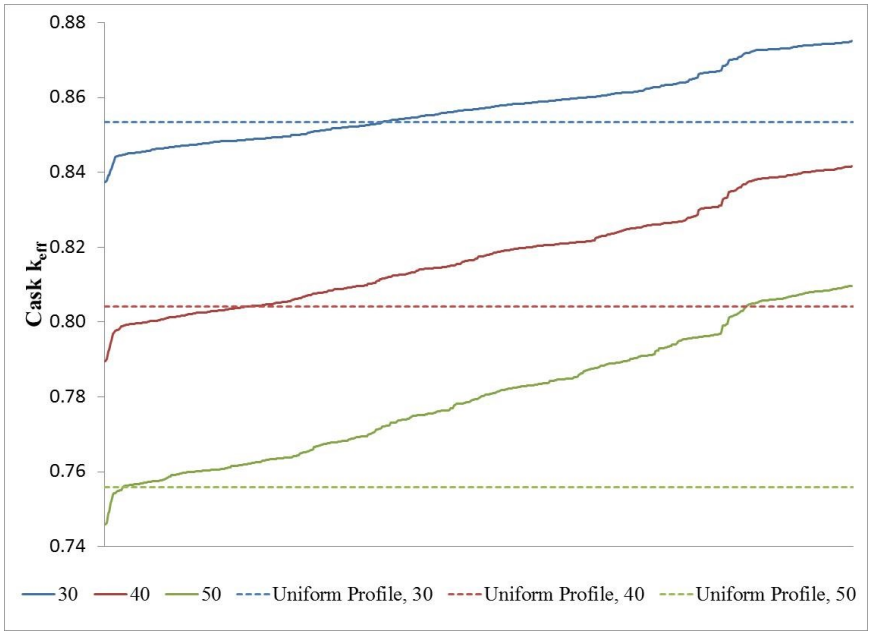

Figure 6.17 Cask k_{eff} values for distributed and uniform burnup profiles, AO isotope set, blanketed fuel

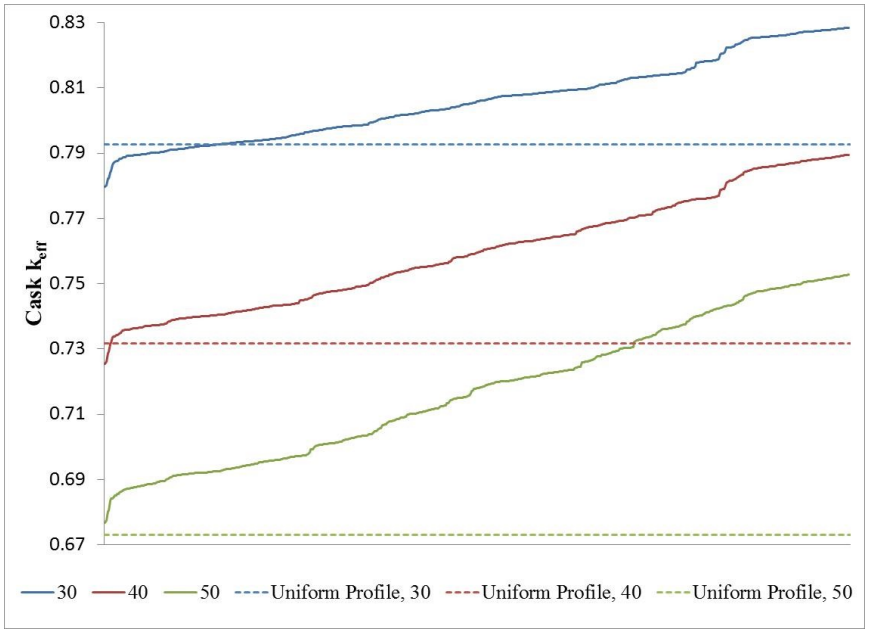

Figure 6.18 Cask k_{eff} values for distributed and uniform burnup profiles, AFP isotope set, blanketed fuel

6.3.3 Burnup Profile Selection

This section examines the method of assessing the relative reactivity of different axial burnup profiles based on an examination of the relative burnup of the top end of the profile, discussed for unblanketed fuel models in Section 6.2.3.

The following discussion is similar to the text describing the method and results in Section 6.2.3, but it is retained to maintain the clarity of the process. It is also important because the conclusion differs from that presented previously; the consideration of more nodes appears warranted for blanketed fuel assembly models.

The cask k_{eff} values resulting from all 624 profiles are plotted versus a given number of nodes for all three burnup values. Separate data sets are plotted for the 568 profiles with 6-in. blankets and the 56 profiles with 12-in. blankets. Figure 6.19 shows results for the AO isotope set and the top node only. A general trend is clearly evident: lower relative burnups lead to higher cask k_{eff} values. However, there are several different bands evident in the data. Figure 6.20 presents the cask k_{eff} values versus the sum of the top three node relative burnups. The data are more closely clustered along a single trend for each blanket length, especially at 40 and 50 GWd/MTU. The integrated relative burnup over six nodes is illustrated in Figure 6.21 and shows the desired linearity of results. As with the unblanketed fuel models, considering too many nodes can also decrease the quality of the fit. This phenomenon is shown in Figure 6.22, which shows the top 11 nodes, the entire vanished lattice, and significant spread in the data. It is also evident in Figure 6.19. Similar results are observed for the AFP isotope set, as shown in Figures 6.23 through 6.26.

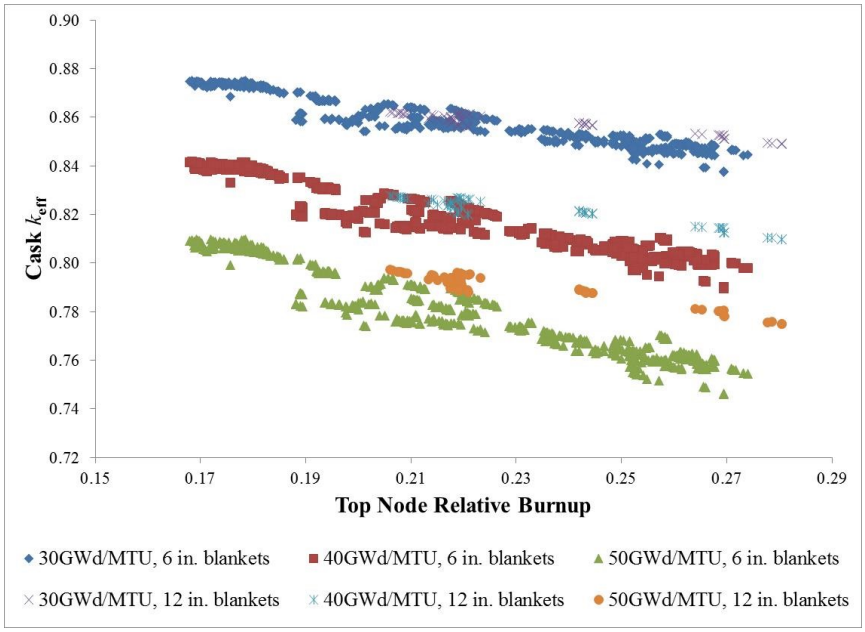

Figure 6.19 Cask k_{eff} versus top node relative burnup, AO isotope set, blankets modeled

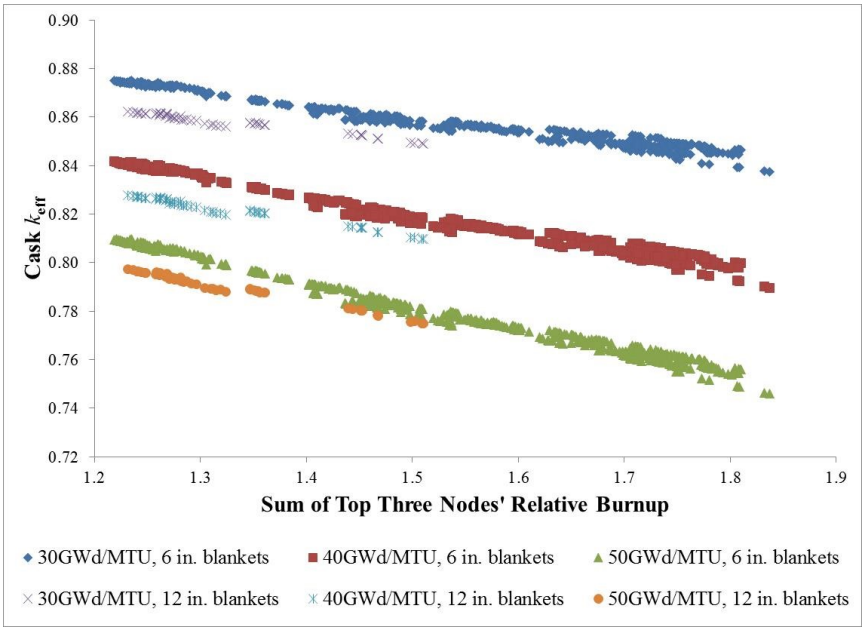

Figure 6.20 Cask k_{eff} versus sum of top three nodes' relative burnup, AO isotope set, blankets modeled

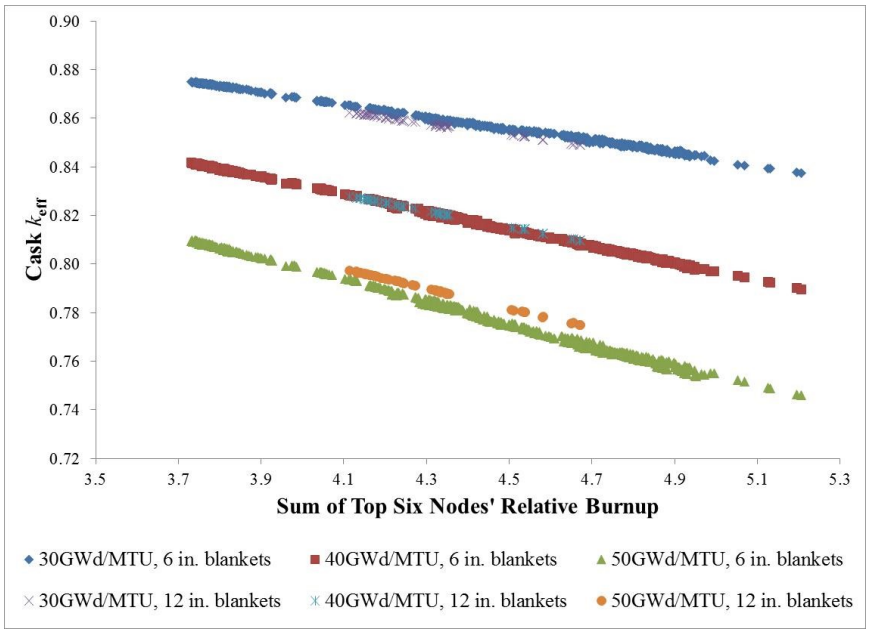

Figure 6.21 Cask k_{eff} versus sum of top six nodes' relative burnup, AO isotope set, blankets modeled

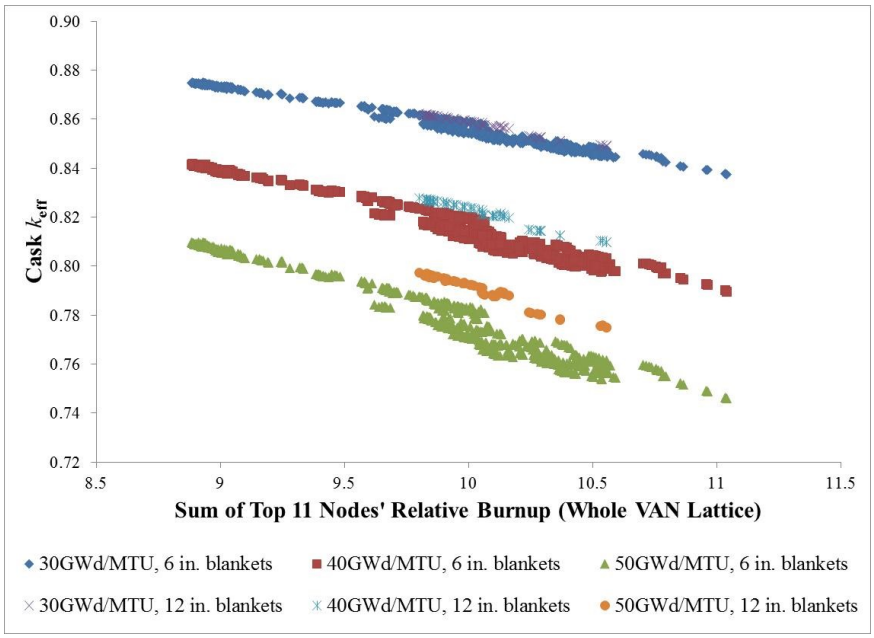

Figure 6.22 Cask k_{eff} versus sum of top 11 nodes' relative burnup, AO isotope set, blankets modeled

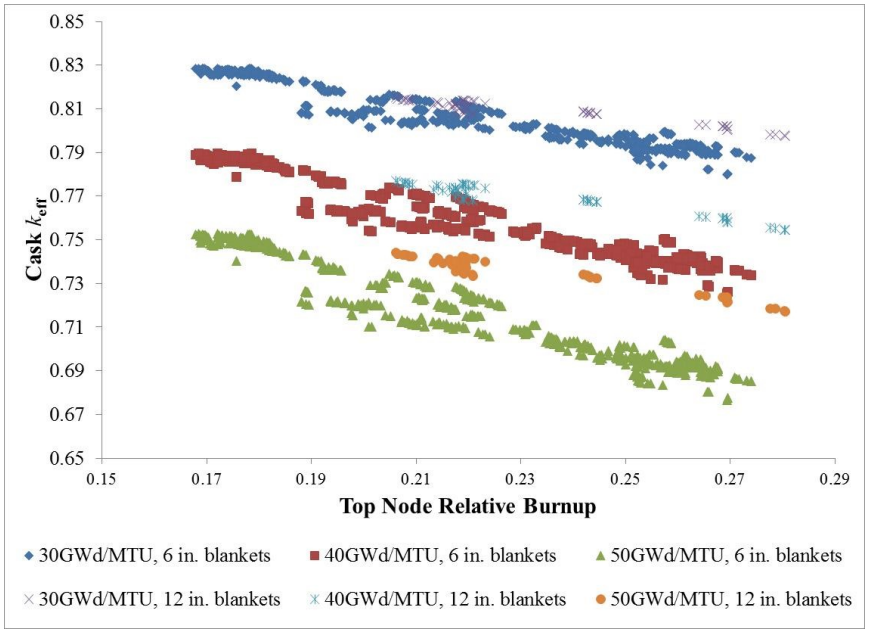

Figure 6.23 Cask k_{eff} versus top node relative burnup, AFP isotope set, blankets modeled

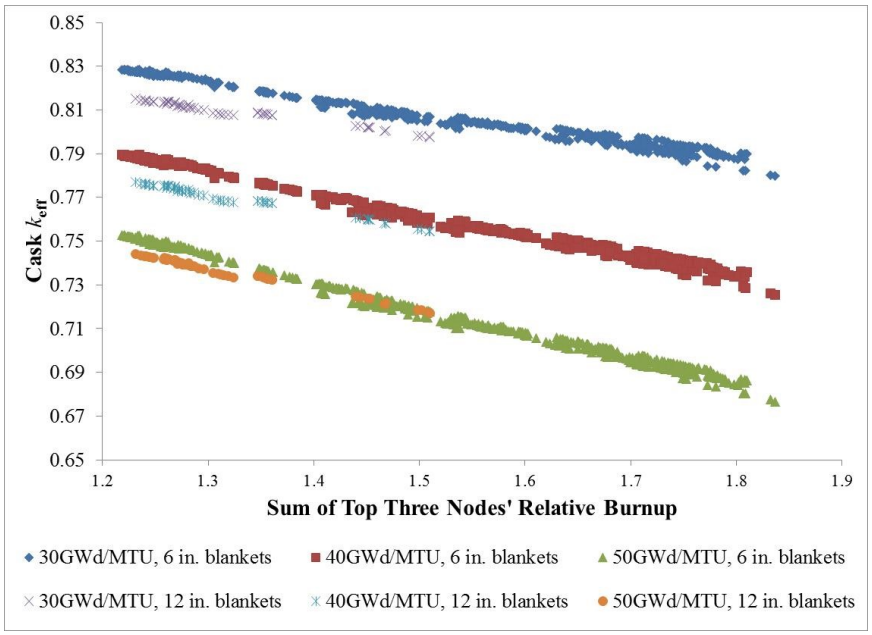

Figure 6.24 Cask k_{eff} versus sum of top three nodes' relative burnup, AFP isotope set, blankets modeled

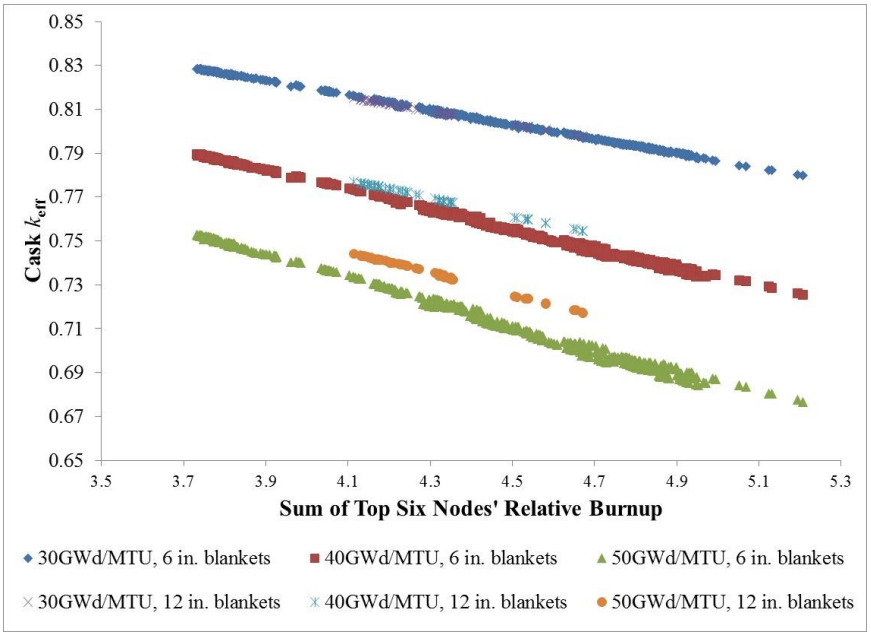

Figure 6.25 Cask k_{eff} versus sum of top six nodes' relative burnup, AFP isotope set, blankets modeled

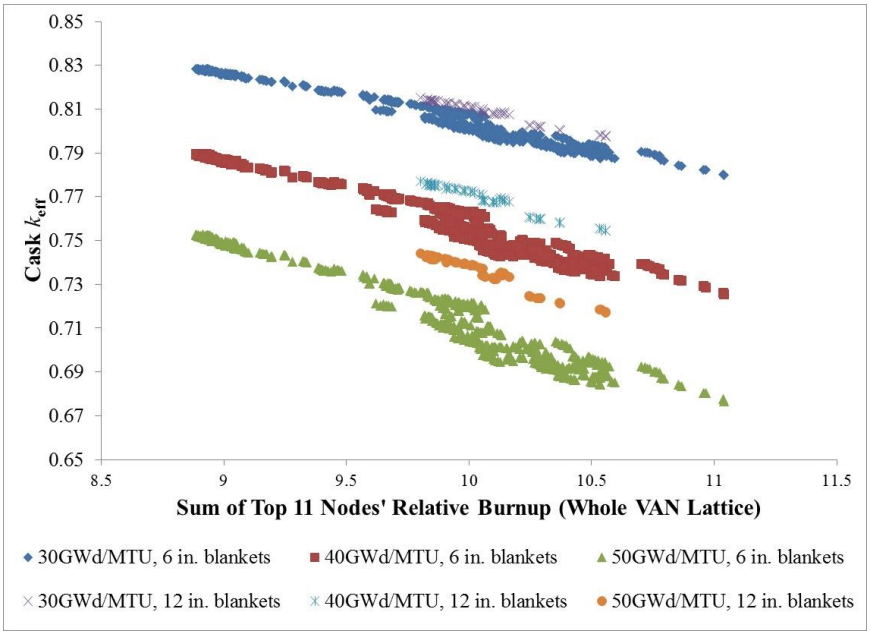

Figure 6.26 Cask k_{eff} versus sum of top 11 nodes' relative burnup, AFP isotope set, blankets modeled

As discussed in Section 6.2.3, not all axial features must be identical for the relative burnup to be a strong indicator of relative reactivity for the profiles. The part-length rods end several feet from the top of the assembly, so the changes do not significantly impact discharged assembly reactivity among different fuel assembly design types. However, the differing blanket lengths

cause differences in the relevant region of the assembly and therefore do cause different trends. It appears that models including axial blankets require consideration of approximately the top 3 ft—in this case, six 6-in. nodes—to generate reliable predictions of relative reactivity for the associated cask k_{eff} values. An applicant would need to justify the exact number of nodes or the axial length used in any such profile selection scheme. Note that a greater fraction of the fuel assembly must be considered in the models that include blankets as compared with the unblanketed case, as discussed in Section 6.2.3.

The relative positions of the trends for the 6-in. and 12-in. blankets also shift for different burnups and different numbers of nodes considered as the relative reactivity indicator. This clearly demonstrates that each population of profiles resulting from assemblies with significantly different features must be considered separately. In this case, for example, a limited number of candidate 6-in. blanket profiles and 12-in. blanket profiles could be selected and depleted. As discussed in Section 6.2.3, a range of burnup profiles will still need to be considered, but this case is nonetheless a significant improvement over performing calculations for all 624 profiles.

6.3.4 Effect of Assembly Burnup

A relevant discussion of the differences in analysis approach between this work and Wagner, DeHart, and Parks [21] is provided in Section 6.2.4 and should be reviewed before the following discussion.

Figure 6.27 shows the cask k_{eff} values resulting from the 568 profiles with 6-in. blankets at 50 GWd/MTU for the AO isotope set; Figure 6.28 provides these same data for the AFP set. All the k_{eff} values presented are calculated at a discharge burnup of 50 GWd/MTU. The horizontal axis shows the EOC burnup of the assembly from which the profile was taken. Three burnup bins are chosen somewhat arbitrarily as the EOC assembly average burnup: (1) below 25 GWd/MTU, (2) between 25 and 40 GWd/MTU, and (3) above 40 GWd/MTU. These ranges are consistent with those considered in Section 6.1(see Figures 6.1–6.3). A line added to each figure, showing the highest k_{eff} value within each bin, demonstrates that cask k_{eff} values decrease by about 1% Δk from one axial profile burnup bin to the next higher bin. This is another aspect of burnup profile selection typical of PWR BUC that may also be advantageous in extended BWR BUC.

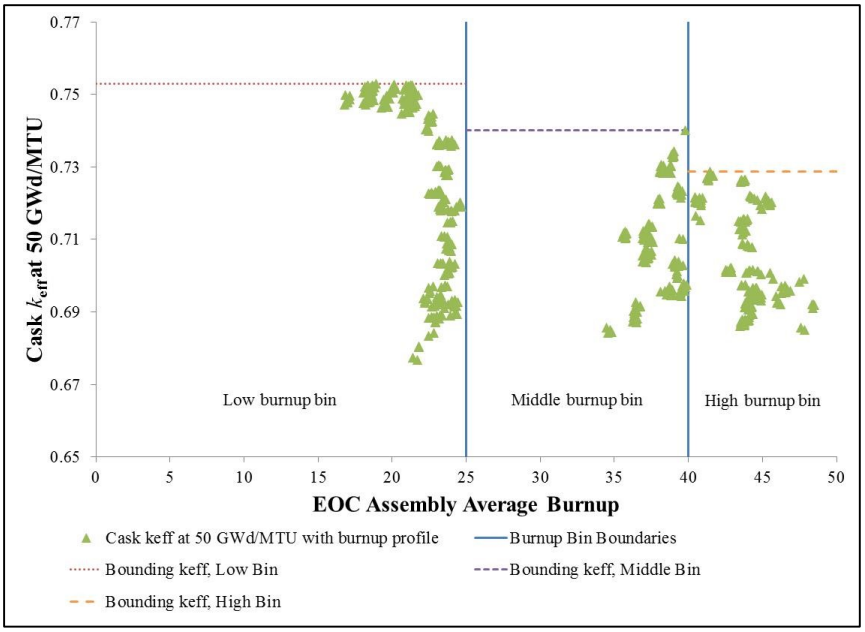

Figure 6.27 Cask k_{eff} value versus burnup of assembly-generating profile, AO isotope set, blankets modeled

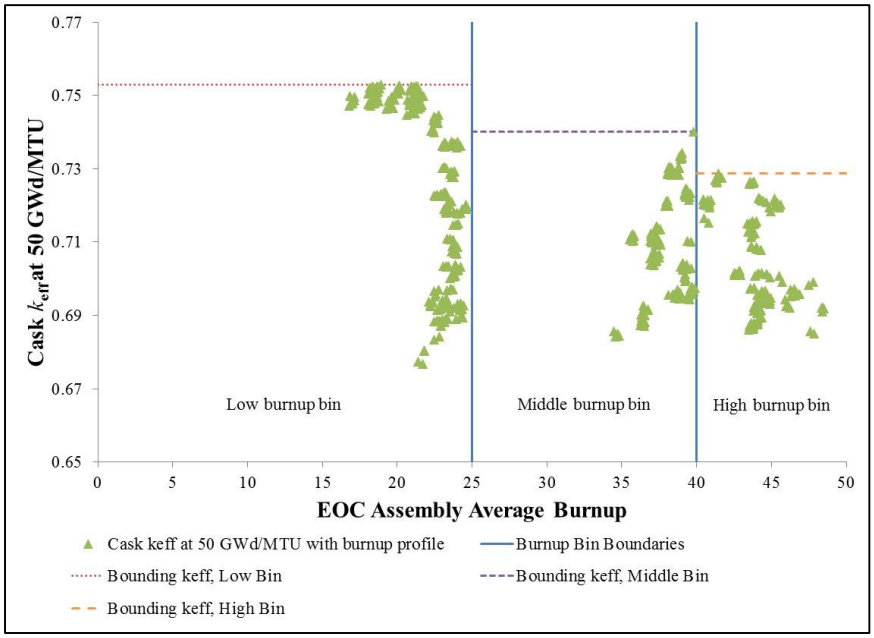

Figure 6.28 Cask k_{eff} value versus burnup of assembly-generating profile, AFP isotope set, blankets modeled

6.4 Summary and Recommendations

Section 6 documents studies performed to examine the effect of axial burnup distributions on extended BWR BUC. The burnup range examined was 30–50 GWd/MTU. The lower burnup

was selected to be higher than the burnups typical of peak reactivity for fuel lattices, whereas the upper bound is typical of discharge burnups for BWR assemblies. Detailed calculations were performed using 624 axial burnup profiles generated from the core follow data set discussed in Section 3.1.

All 624 assemblies considered had natural enrichment blankets at the top and bottom of the assembly; 568 had 6-in. blankets at both ends of the assembly. The remaining 56 assemblies had 6-in. blankets on the bottom end of the assembly but 12-in. blankets at the top end. The profiles resulting from these assemblies are discussed in detail in Section 6.1. Some PWR BUC analyses credit blankets while others do not, so both approaches are considered here. Section 6.2 presents results from models neglecting the blankets and assuming all fuel had the same initial enrichment. Section 6.3 presents the results from calculations modeling the 6-in. and in some cases the 12-in. blankets. The general trends in the results for both modeling approaches are similar.

The profiles used in this study lead to a wide range of cask k_{eff} values. The range of calculated k_{eff} values varies from 3.3% Δk at 30 GWd/MTU for the AO isotope set with no blankets modeled, to 7.6% Δk at 50 GWd/MTU for the AFP isotope set with blankets modeled. The range is larger with blankets modeled and for the AFP isotope set. The calculated k_{eff} values are not normally distributed, and the range corresponds to approximately 3–4 standard deviations. The most reactive profiles are generally the same with or without blankets for both isotope sets, as long as the profiles considered have the same axial features near the top end of the assembly. As an example of the effects that differences in axial features, such as blankets, can have, the 12-in. blanket profiles are significantly more reactive than 6-in. blanket profiles when no blanket is modeled.

The end effect was calculated for each profile at each burnup considered. A positive end effect indicates that the distributed burnup profile must be considered in the analysis, as it is more reactive than the uniform profile at the same burnup. Large positive end effects appear to be common for BWR fuel; all 624 profiles had positive end effects for the models neglecting blankets at all burnups, and at 50 GWd/MTU when blankets were modeled. The largest end effect for the profile with no blankets modeled ranges from 1.6% Δk at 30 GWd/MTU to 12.7% Δk at 50 GWd/MTU. The profiles with blankets modeled have end effects of 3.6% Δk to 8.0% Δk, also at 30 and 50 GWd/MTU, respectively. These end effects are larger than those typically seen in PWR BUC. As discussed in Sections 6.2.2 and 6.3.2, the magnitude of the end effects identified in this study also indicates that examination of the 2D approach to peak reactivity analyses may be appropriate. The core follow data set used in this study could be used to extract burnup profiles from the peak reactivity burnup range of 7–20 GWd/MTU to support such an investigation, although no such work has been performed to date.

A method to identify potentially limiting burnup profiles was investigated in Sections 6.2.3 and 6.3.3. It appears that for models both with and without blankets, such an approach can generate a reliable indication of the relative reactivity of profiles taken from assemblies with similar axial features near the top end of the assembly. For assemblies with no blankets modeled, it appears that around three 6-in. nodes, or a total of 18 in., near the top of the assembly is an optimum length for making these determinations. The fuel length that must be considered is longer when blankets are modeled, probably on the order of six 6-in. nodes, or a total fuel length of 36 in. The number of nodes that should be considered will depend on nodalization and fuel assembly characteristics; therefore, the method used by any applicant must be justified. It also appears that axial feature differences that are not near the top end—such as differences in the number and length of part-length rods or differences in the number and loading of gadolinium pins—do

not need to be tracked to determine limiting axial burnup profiles. The success of these basic methods in predicting relative reactivity can greatly simplify the work needed to determine the appropriate profile for use in a BWR BUC analysis.

The final aspect considered is the dependence of cask k_{eff} on the burnup of the assembly from which the profiles were taken. The results are presented in Section 6.2.4 for the models with no blankets and in Section 6.3.4 for the models with blankets. Three burnup bins were generated: 0–25 GWd/MTU, 25–40 GWd/MTU, and >40 GWd/MTU assembly average burnup at EOC. The lowest-burnup bin captures all fuel assemblies that were loaded fresh into the cycle for which the core follow data set was generated. The separation of high-burnup assemblies into two bins at 40 GWd/MTU was largely arbitrary. For the profiles considered in this study, cask k_{eff} decreases as burnup increases. The use of burnup bins to ensure appropriate profiles in each burnup range is common in PWR BUC and will likely be useful in BWR BUC, as well.

The following recommendations can be made based on the results of this study:

- The choice of axial burnup profiles can have significant impacts on cask reactivity. The range of cask k_{eff} values resulting from the profiles used in this study was as large as 7.6% Δk. Applicants must provide justification for the profiles used in an analysis, including the burnups over which uniform and distributed burnup profiles are used.

- The limiting profile resulting from a set of available profiles is largely independent of the isotope set used. Axial blanket modeling approaches also have only a small impact on identifying the limiting profile for assemblies with 6-in. natural blankets.

- Distributed burnup profiles must be considered for extended BWR BUC. End effects of up to 12.7% Δk were identified in this study.

- The relative reactivity of different axial burnup profiles can be predicted reliably by considering the relative burnup in the top few nodes. Lower relative burnups lead to higher cask k_{eff} values. More nodes must be considered if axial blankets are modeled, and the relative ranking prediction is reliable only within a population of assemblies with blankets of the same length. Other axial feature differences in the top 4 ft of the assembly might also require separate consideration. Any scheme used to identify potentially limiting axial burnup profiles should be justified.

- Grouping axial burnup profiles into bins based on the EOC burnup of the assembly from which the profile was taken is likely to lower calculated cask k_{eff} values at higher burnups.

7 CONCLUSIONS

Many important conclusions relating to BWR BUC beyond peak reactivity can be drawn from the studies documented in this report. Similar studies related to peak reactivity analyses are documented in Reference 3. These conclusions are drawn from a relatively limited range because the core follow data set used represents a single cycle from a single plant. Ideally, these studies would have included data from different plants and several cycles of operation to provide greater coverage of operating ranges. Unfortunately, the detailed data needed for most of the studies were readily available only from one source. Additional work should be performed to demonstrate wider applicability of the conclusions drawn here.

7.1 Axial Moderator Density Distributions

Details of the axial burnup profile analyses are presented in Section 4 and summarized in Section 4.6. It is clear that the axial moderator density profiles used in modeling fuel depletion can have a significant impact on calculated cask k_{eff} and must be treated appropriately to ensure conservative analysis results. Although the set of profiles analyzed is somewhat limited, being based on only one cycle of operation, important conclusions can still be drawn from these studies.

- A cycle-averaged moderator density can be used in each node of an axial moderator density profile for depletion calculations with an appropriate penalty for conservatism.

- A reactivity penalty of 0.25% Δk_{eff} is recommended to cover potential differences between detailed and cycle average moderator density treatments in depletion calculations.

- A limiting axial moderator density profile will have low moderator densities in the top nodes of the assembly. Each applicant should present and defend the method used to identify limiting profiles.

- A limiting axial moderator density profile can be constructed by selecting the minimum density in each axial node from a collection of applicable actual profiles.

- Use of average moderator densities determined from consideration of multiple assemblies or multiple axial nodes will result in reactivity underprediction.

- A single moderator density value can be used conservatively in all nodes if it is lower than the moderator densities in all nodes of the assemblies to be placed in the cask.

7.2 Control Blade Usage

The details of the control blade usage analyses are presented in Section 5 and summarized in Section 5.3. Control blade usage can have an impact on cask k_{eff} and must be treated appropriately to ensure conservative analysis results. The impact is less severe than original expectations, given that the control blades need to be inserted more than 50% into the core for an extended period before they have a noticeable effect. The set of realistic histories analyzed is somewhat limited, being based on only one cycle of operation; but important conclusions can be drawn from these studies, especially with consideration of the hypothetical histories used to investigate the sensitivity of cask k_{eff} to blade position, exposure duration, and time in irradiation.

- Control blade insertions of 50% or less for the entire depletion have virtually no impact on cask reactivity.

- Although unrealistic, the most limiting case for the AFP isotope set is 92% blade insertion for the entire depletion; it increases cask reactivity by 4.3% Δk_{eff}. The limiting case for the AO isotope set is also unrealistic, full control blade insertion for the entire depletion, and results in a cask reactivity increase of 4.1% Δk_{eff}.

- Deeper and longer-duration control blade insertions have a much greater impact than frequent, shallower, shorter-duration insertions.

- Deep control blade insertions in the last third of life have greater impact (~1%) on reactivity than similar insertions earlier in life.

- Control blades inserted more than halfway into the core for significant periods can cause significant shifts in axial fission distribution. These shifts appear not to occur in realistic histories. Analysis assumptions or simplifications regarding control blade use which introduce these shifts, such as partial control blade insertion for an extended period, are unnecessary and should be avoided.

- Fuel assemblies are unlikely to experience significant operational periods with control blade insertion late in life because of lower reactivity and placement near the core periphery; therefore the limiting cases considered here may be conservative.

- Some fuel assemblies may experience exceptional control blade use. This would be the result of suppressing assembly power owing to leaking fuel rods or high assembly reactivity early in life.

- Based on the limiting realistic histories examined, a penalty of ~0.6% to 1.2% Δk_{eff} may be sufficient to account for control blade insertion effects. Applicants should provide a justification that any reactivity penalty taken is sufficient to account for rodded operations and should identify a process for handling assemblies that violate the underlying assumptions used in generating the penalty.

7.3 Axial Burnup Profiles

The details of the axial burnup profile analyses are presented in Section 6 and summarized in Section 6.4. It is clear that the axial burnup profiles can have a significant impact on cask k_{eff} and must be treated appropriately to ensure conservative analysis results. Although the set of profiles analyzed is not as extensive as that used in Wagner, DeHart, and Parks [21] for PWR BUC, important conclusions can still be drawn from these studies.

- The choice of axial burnup profiles can have significant impacts on cask reactivity. The range of cask k_{eff} values resulting from the profiles used in this study was as large as 7.6% Δk. Applicants must provide justification for the profiles used in an analysis, including the burnups over which uniform and distributed burnup profiles are used.

- The limiting profile resulting from a set of available profiles is largely independent of the isotope set used. Axial blanket modeling approaches also have only a small impact on identifying the limiting profile for assemblies with 6-in. natural blankets. No axial enrichment zoning effects were studied other than the effects of modeling natural enrichment blankets at the top and bottom of the fuel assembly.

- Distributed burnup profiles must be considered for extended BWR BUC. End effects of up to 12.7% Δk were identified in this study.

- The relative reactivity of different axial burnup profiles can be predicted reliably by considering the relative burnup in the top few nodes. Lower relative burnups lead to higher cask k_{eff} values. More nodes must be considered if axial blankets are modeled, and the relative ranking prediction is reliable only within a population of assemblies with blankets of the same length. Other axial feature differences in the top 4 ft of the assembly might also require separate consideration. Any scheme used to identify potentially limiting axial burnup profiles should be justified.

- Grouping axial burnup profiles into bins based on the EOC burnup of the assembly from which the profile was taken is likely to lower calculated cask k_{eff} values at higher burnups, thereby lowering excess conservatism.

8 REFERENCES

1. US Code of Federal Regulations Title 10, “Energy,” US Nuclear Regulatory Commission, Washington, DC (2014).
2. Division of Spent Fuel Storage and Transportation, *Interim Staff Guidance—8, Revision 3, Burnup Credit in the Criticality Safety Analyses of PWR Spent Fuel in Transportation and Storage Casks*, US Nuclear Regulatory Commission (September 26, 2012).
3. W. J. Marshall, B. J. Ade, S. M. Bowman, I. C. Gauld, G. Ilas, U. Mertyurek, and G. Radulescu, *Technical Basis for Peak Reactivity Burnup Credit for BWR Spent Nuclear Fuel in Storage and Transportation Systems*, NUREG/CR-7194 (ORNL/TM-2014/240), prepared for the US Nuclear Regulatory Commission by Oak Ridge National Laboratory, Oak Ridge, Tenn. (April 2015).
4. *SCALE: A Comprehensive Modeling and Simulation Suite for Nuclear Safety Analysis and Design,* ORNL/TM-2005/39, Version 6.1, Oak Ridge National Laboratory, Oak Ridge, Tenn. (June 2011). Available from Radiation Safety Information Computational Center at Oak Ridge National Laboratory as CCC-785.
5. M. D. DeHart and S. M. Bowman, “Reactor Physics Methods and Analysis Capabilities in SCALE,” *Nuclear Technology*, 174(2) (May 2011): 196–213.
6. B. J. Ade, *SCALE/TRITON Primer: A Primer for Light Water Reactor Lattice Physics Calculations*, NUREG-7041 (ORNL/TM-2011/21), prepared for the US Nuclear Regulatory Commission by Oak Ridge National Laboratory, Oak Ridge, Tenn. (November 2012).
7. J. M. Scaglione, D. E. Mueller, J. C. Wagner, and W. J. Marshall, *An Approach for Validating Actinide and Fission Product Burnup Credit Criticality Safety Analyses – Criticality (k_{eff}) Predictions*, NUREG/CR-7109 (ORNL/TM-2011/514), prepared for the US Nuclear Regulatory Commission by Oak Ridge National Laboratory, Oak Ridge, Tenn. (April 2012).
8. D. E. Mueller, J. M. Scaglione, J. C. Wagner, and S. M. Bowman, *Computational Benchmark for Estimated Reactivity Margin from Fission Products and Minor Actinides in BWR Burnup Credit*, NUREG/CR-7157 (ORNL/TM-2012/96), prepared for the US Nuclear Regulatory Commission by Oak Ridge National Laboratory, Oak Ridge, Tenn. (February 2013).
9. D. E. Mueller, S. M. Bowman, W. J. Marshall, and J. M. Scaglione, *Review and Prioritization of Technical Issues Related to Burnup Credit for BWR Fuel*, NUREG/CR-7158 (ORNL/TM-2012/261), prepared for the US Nuclear Regulatory Commission by Oak Ridge National Laboratory, Oak Ridge, Tenn. (February 2013).
10. J. Rhodes, K. Smith, and D. Lee, “CASMO-5 Development and Applications,” *Proceedings of PHYSOR-2006*, Vancouver, BC, Canada (September 10–14, 2006).
11. N.H. Larsen, Core *Design and Operating Data for Cycles 1 and 2 of Peach Bottom 2*, NP-563, Electric Power Research Institute (June 1978).
12. N. H. Larsen and J. G. Goudey, *Core Design and Operating Data for Cycle 1 of Hatch 1*, NP-562, Electric Power Research Institute (January 1979).

13. G. L. Holloway, J. E. Fawks, and B. W. Crawford, *Core Design and Operating Data for Cycles 2 and 3 of Hatch 1*, NP-2106, Electric Power Research Institute (February 1984).
14. R. Chang, et al., *State-of-the-Art Reactor Consequence Analysis (SOARCA) Report*, NUREG-1935, US Nuclear Regulatory Commission (2012).
15. F. Sturek, L. Agrenius, and O. Osifo, *Measurements of Decay Heat in Spent Nuclear Fuel at the Swedish Interim Storage Facility, Clab*, Svensk Kärnbränslehanterig AB (SKB), R-05-62 (December 2006).
16. L. B. Wimmer, *Commercial Reactor Criticality Depletion for Grand Gulf, Unit 1*, 32-5028092-00, DOC.20040109.0004, Framatome ANP (September 22, 2003).
17. D. P. Henderson et al., *Summary Report of Commercial Reactor Criticality Data for LaSalle Unit 1*, B00000000-01717-5705-00138, Civilian Radioactive Waste Management System Management & Operating Contractor (September 1999).
18. D. P. Henderson et al., *Summary Report of Commercial Reactor Criticality Data for Quad Cities Unit 2*, B00000000-01717-5705-00096 Revision 01, Civilian Radioactive Waste Management System Management & Operating Contractor (September 1999).
19. F. Lindström, A. Fernandez, *Forsmark 3—Characteristic Data of Fuel Rod J8 in Bundle GN592*, Vattenfall Report VNF-1002152744/02 (February 8, 2011).
20. H. R. Radulescu, *Limerick Unit 1 Radiochemical Assay Comparisons to SAS2H Calculations*, CAL-DSU-NU-000002 Rev 00A, Office of Civilian Radioactive Waste Management (August 2003).
21. J. C. Wagner, M. D. DeHart, and C. V. Parks, *Recommendations for Addressing Axial Burnup in PWR Burnup Credit* Analyses, NUREG/CR-6801 (ORNL/TM-2001/273), prepared for the US Nuclear Regulatory Commission by Oak Ridge National Laboratory, Oak Ridge, Tenn. (March 2003).
22. J. M. Scaglione, G. Radulescu, W. J. Marshall, and K. R. Robb, *A Quantitative Impact Assessment of Hypothetical Spent Fuel Reconfiguration in Spent Fuel Storage Casks and Transportation Packages*, NUREG/CR-7203 (ORNL/TM-2013/92), prepared for the US Nuclear Regulatory Commission by Oak Ridge National Laboratory, Oak Ridge, Tenn. (September, 2015).
23. T. R. Younkin, *Piecewise Prediction of Nuclide Densities with Control Blade Use as a Function of Burnup in BWR Used Nuclear Fuel*, Master's thesis, Georgia Institute of Technology (December 2014).
24. R. J. Cacciapouti and S. Van Volkinburg, *Axial Burnup Profile Database for Pressurized Water Reactors*, YAEC-1937, Yankee Atomic Electric Company (May 1997).

9 GLOSSARY

1D	one dimensional
2D	two dimensional
3D	three dimensional
actinide only isotope set	a limited set of isotopes with only actinide elements and oxygen (Table 2.1 lists the isotopes in this set.)
actinide plus major fission products isotope set	a less limited set of isotopes that includes more actinide isotopes than the actinide only set, some major fission product isotopes, and oxygen. (Table 2.1 lists the isotopes in this set.)
AFP	actinides and major fission products (isotope set)
AO	actinide only
axial moderator density study	a series of calculations to determine the effect of various axial moderator density distributions during depletion on the k_{eff} value of the SNF loaded in a storage and/or transportation system
axial profile parameterization	determination of a single quantitative value to describe an axial moderator profile, typically for the purpose of identifying limiting moderator density profiles
BOC	beginning of cycle
BOL	beginning of life
BUC	burnup credit
burnup	a measure of the energy produced by a fuel assembly or reactor per unit mass of initial heavy metal (in this report, initial uranium)
BWR	boiling water reactor
Cask	generic term for a storage and/or transportation system
CFR	Code of Federal Regulations
CSAS	Criticality Safety Analysis Sequence (in SCALE)
distributed burnup profile	any nonuniform axial representation of accumulated burnup in a fuel assembly
DOM	dominant or full fuel assembly lattice

end effect	the difference in calculated k_{eff} for a spent fuel system based on modeling a distributed burnup profile instead of a uniform burnup profile. A positive end effect indicates that the use of a distributed burnup profile results in a higher calculated k_{eff} value.
EPRI	Electric Power Research Institute
EOC	end of cycle
EOL	end of life
extended BWR BUC	crediting reactivity reduction due to fuel depletion at higher burnups beyond peak reactivity
GE	General Electric
HA	high average (specific axial void fraction distribution in this study)
hockey stick profile	axial burnup profile unique to a subset of the burnup profiles in the set considered in this report, caused by a longer top blanket which causes the increase in normalized burnup to start farther from the top end of the assembly than for the majority of the profiles considered
HH	hypothetical history; refers to control blade usage histories
ISG	Interim Staff Guidance
limiting conditions/ assumptions	assumptions that lead to higher k_{eff} values for fuel contained in a storage or transportation system
minimum density profile	moderator density profile constructed by selecting the minimum moderator density in each node from the entire set of assembly profiles
MV	most variable (specific axial void fraction distribution in this study)
NRC	US Nuclear Regulatory Commission
ORNL	Oak Ridge National Laboratory
Peak reactivity	phenomenon in which the effective multiplication factor (k_{eff}) for an assembly or 2D slice is higher after some burnup than it is at BOL; a common feature of BWR assemblies caused by depletion of the burnable absorber at a more rapid rate than depletion of the fuel
peak reactivity analysis	a class of criticality safety methods used to demonstrate safe storage of fuel assemblies, discussed in some depth in NUREG/CR-7194

PWR	pressurized water reactor
RCA	radiochemical assay
reactivity	in this document, used interchangeably with k_{eff}; not meant in the strict technical sense of relative distance from the critical condition
RH	realistic history; refers to control blade usage histories
relative burnup	is the burnup of one assembly or region of an assembly in comparison to another assembly or assembly region.
relative reactivity	reactivity of one assembly, region of an assembly, or model in comparison to another.
SKB	Svensk Kärnbränslehantering AB (Swedish Nuclear Fuel and Waste Management Company)
SNF	spent nuclear fuel
T-H	thermal-hydraulic
temporal fidelity study	a series of calculations to determine the frequency with which the axial moderator density fraction must be updated to yield accurate k_{eff} values for SNF contained in a storage or transportation system
TIP	traveling in-core probe
VAN	vanished fuel assembly lattice

APPENDIX A: REALISTIC CONTROL BLADE HISTORIES

APPENDIX A: REALISTIC CONTROL BLADE HISTORIES

This section provides plots of the realistic control blade histories. Ten realistic control blade histories have been extracted from the operating data and used throughout the analysis. The ten realistic histories (RHs) used in this report and depicted in this section represent control blade histories believed to be particularly limiting. That is, control blade histories were selected by choosing those that contain especially high integral control blade history (those inserted for a long period of time) and those in which control blades are inserted deeply into the core. These ten RHs were chosen after the hypothetical history (HH) simulations were completed, so some engineering judgment was gained in the process. The realistic control blade histories are plotted in Figures A.1–A.10. The plots contain the control blade insertion depth (or elevation) in percentage of the active fuel length versus the irradiation time in days. Because only one cycle of operating data exists, the control blade history for the single cycle has been repeated three times. Each cycle is modeled as 690 days, so the control blade history is repeated on that interval to a total time of 2,070 days to correspond to three cycles.

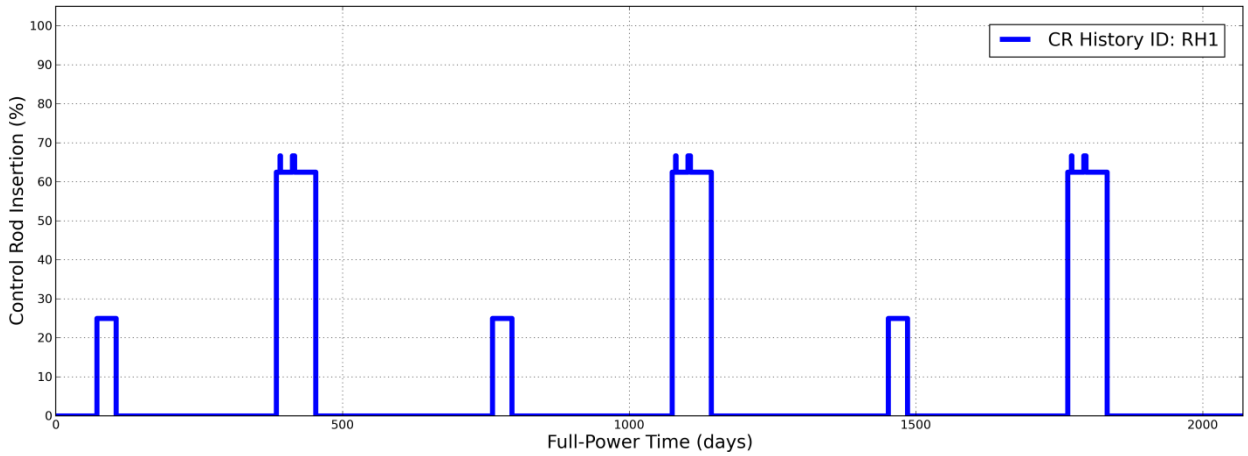

Figure A.1 Control blade history RH1 (blade location 3,4)

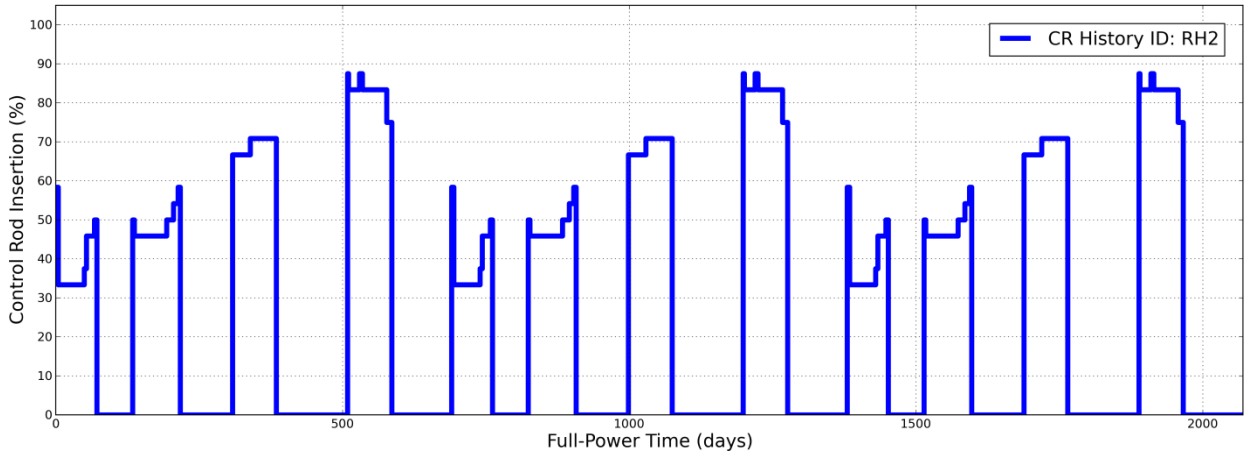

Figure A.2 Control blade history RH2 (blade location 4,4)

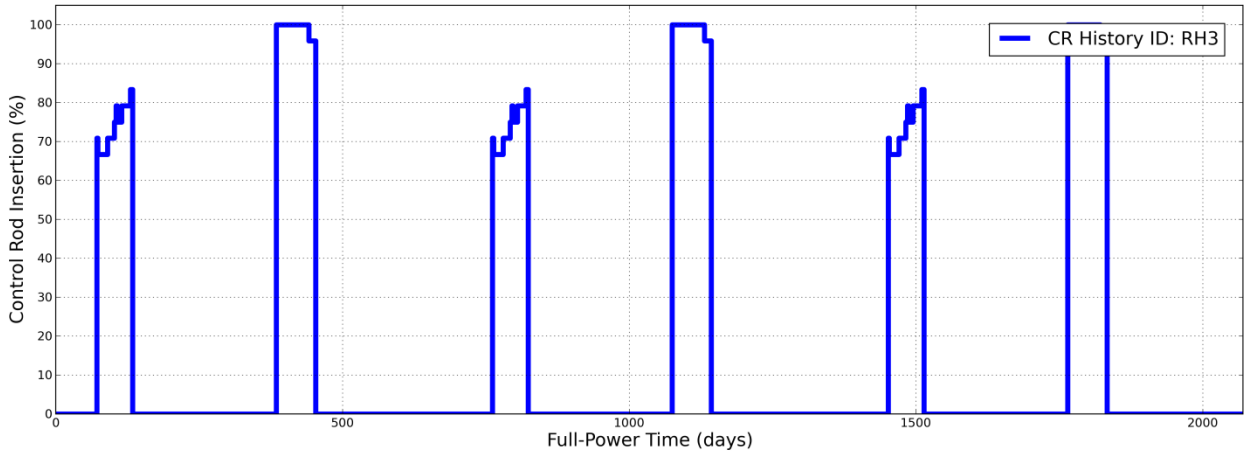

Figure A.3 Control blade history RH3 (blade location 7,4)

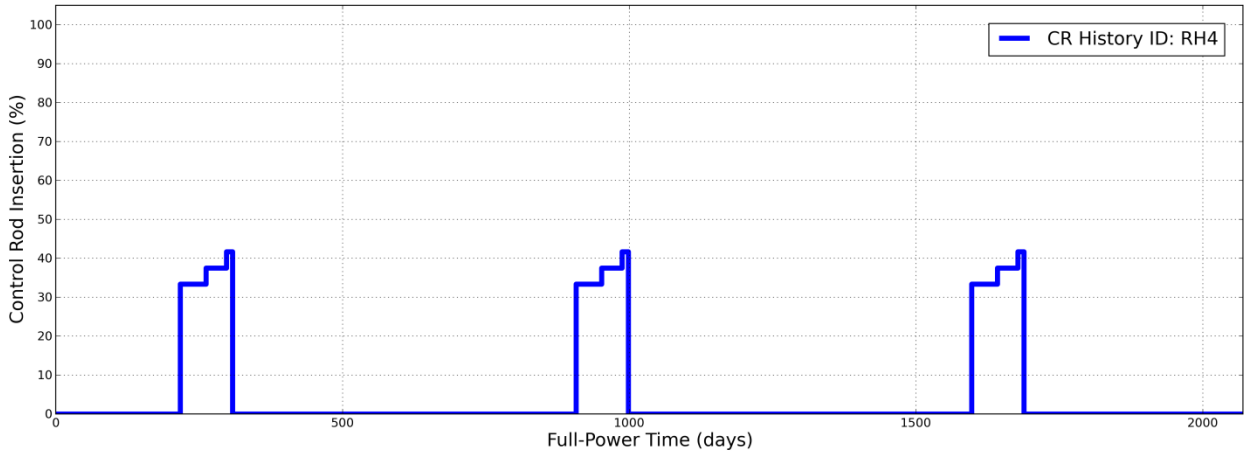

Figure A.4 Control blade history RH4 (blade location 2,5)

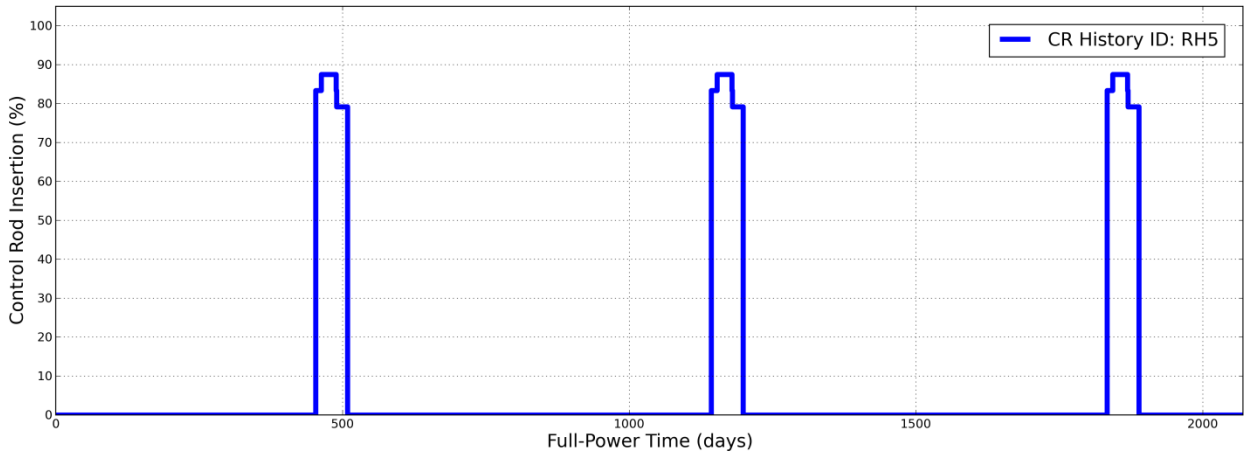

Figure A.5 Control blade history RH5 (blade location 3,5)

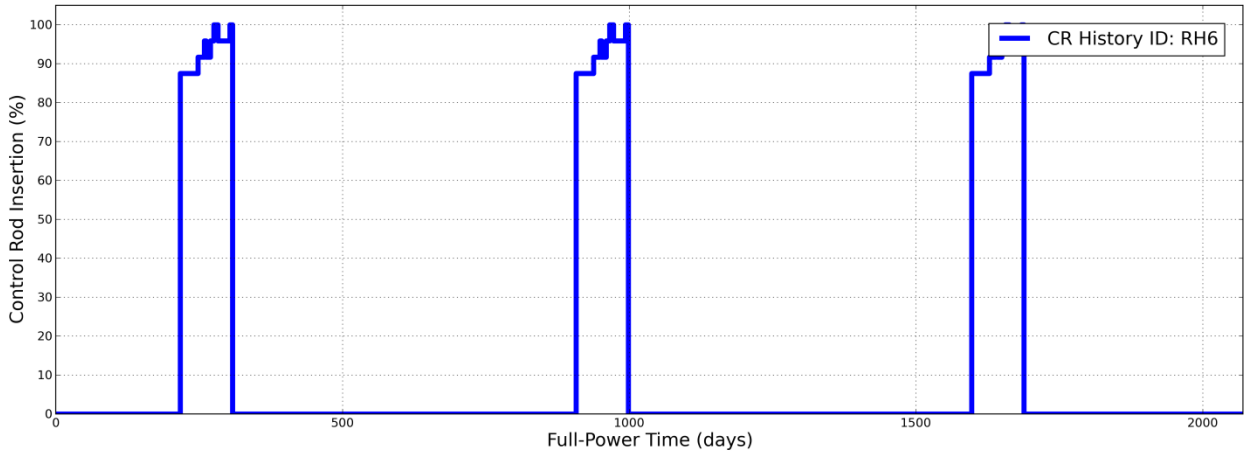

Figure A.6 Control blade history RH6 (blade location 4,5)

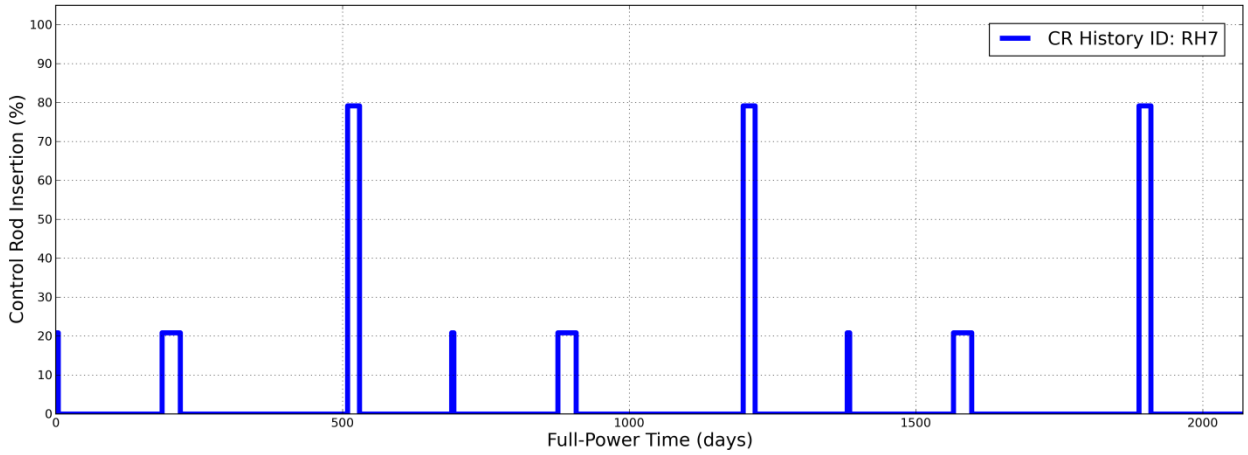

Figure A.7 Control blade history RH7 (blade location 2,6)

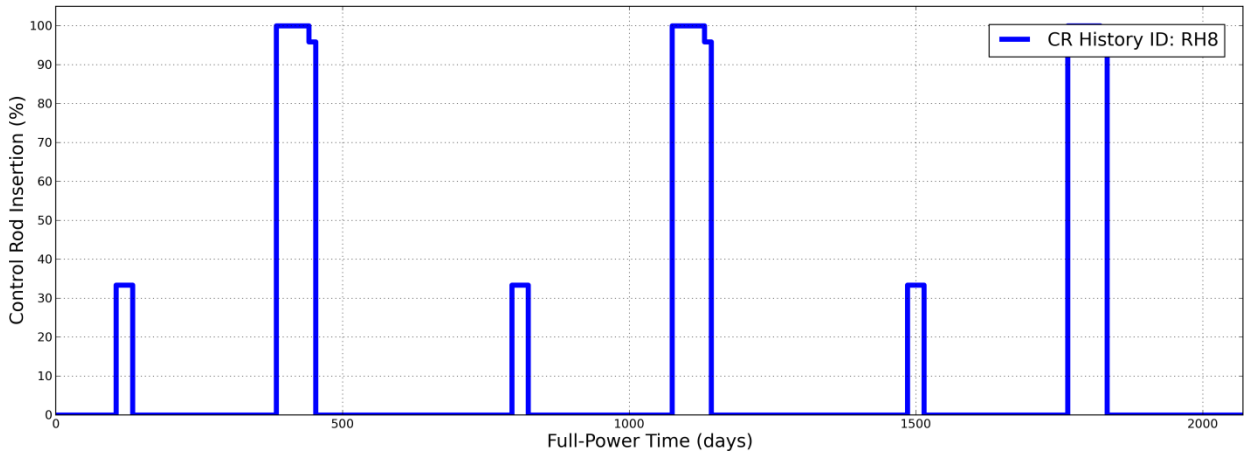

Figure A.8 Control blade history RH8 (blade location 3,6)

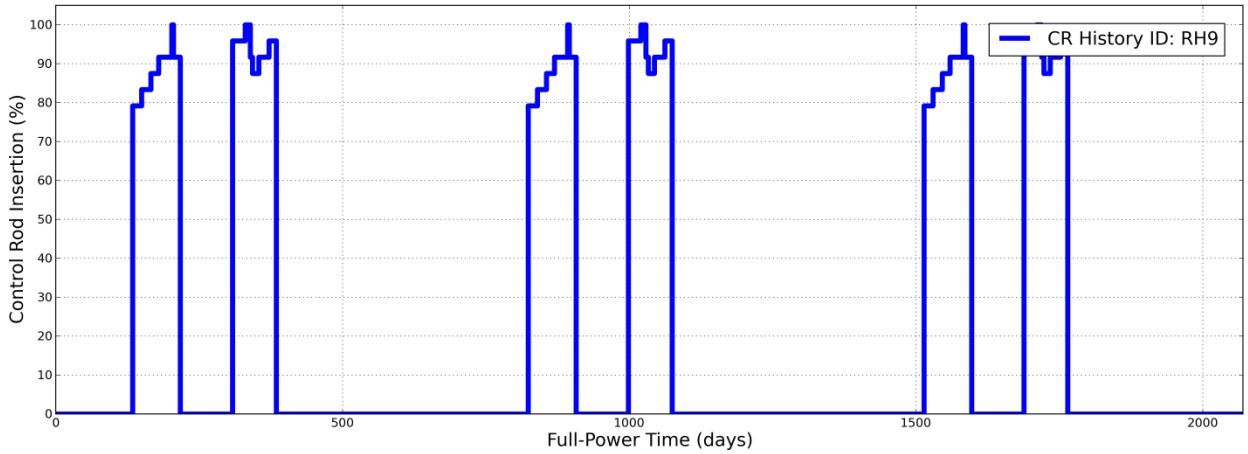

Figure A.9 Control blade history RH9 (blade location 4,6)

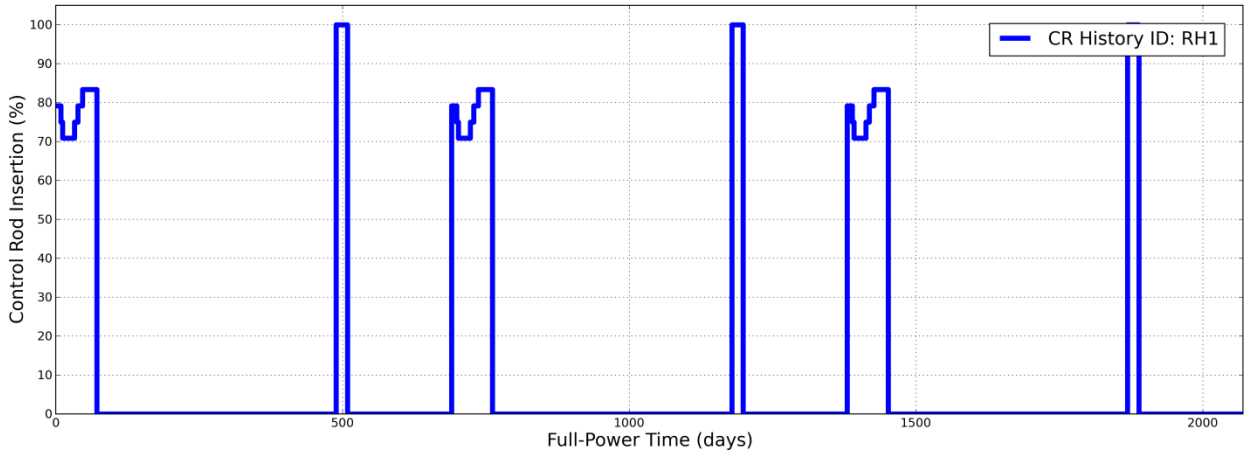

Figure A.10 Control blade history RH10 (blade location 6,6)

NRC FORM 335
(12-2010)
NRCMD 3.7

U.S. NUCLEAR REGULATORY COMMISSION

BIBLIOGRAPHIC DATA SHEET

(See instructions on the reverse)

1. REPORT NUMBER
(Assigned by NRC, Add Vol., Supp., Rev., and Addendum Numbers, if any.)
NUREG/CR-7224

2. TITLE AND SUBTITLE
Axial Moderator Density Distributions, Control Blade Usage, and Axial Burnup Distributions for Extended BWR Burnup Credit

3. DATE REPORT PUBLISHED
MONTH: August
YEAR: 2016

4. FIN OR GRANT NUMBER
NRC JCN V6452

5. AUTHOR(S)
William (B.J.) Marshall, Brian J. Ade, Stephen M. Bowman, and Jesus S. Martinez-Gonzalez

6. TYPE OF REPORT
Technical

7 PERIOD COVERED (Inclusive Dates)

8. PERFORMING ORGANIZATION NAME AND ADDRESS (If NRC, provide Division, Office or Region, U. S. Nuclear Regulatory Commission, and mailing address; if contractor, provide name and mailing address.)
Oak Ridge National Laboratory Managed by UT-Battelle, LLC
1 Bethel Valley Road
Oak Ridge, TN 37831-6170

9. SPONSORING ORGANIZATION NAME AND ADDRESS (If NRC, type "Same as above" if contractor, provide NRC Division, Office or Region, U. S. Nuclear Regulatory Commission, and mailing address.)
Division of Systems Analysis
Office of Nuclear Regulatory Research
U. S. Nuclear Regulatory Commission, Washington, DC 20555–0001

10. SUPPLEMENTARY NOTES

11. ABSTRACT (200 words or less)
This report documents the studies performed to extend BWR BUC beyond peak reactivity by assessing the impacts of (1) axial moderator density distributions, (2) control blade usage, and (3) axial burnup profiles on extended BWR BUC. The impact of each of these phenomena is evaluated, with the objective of identifying limiting conditions and assumptions in the analyses.

The data used in this report are typical BWR core follow data from a recent cycle of a BWR-6 core that contained four different modern BWR fuel assembly design types. The data from the core simulator model has 25 different axial nodes, and the cycle has been simulated using more than 240 time steps.

Specific recommendations based on the analyses performed in this report are provided to help identify limiting conditions for modeling the impact of axial moderator density distributions, control blade usage, and axial burnup profiles in storage and transportation casks. Because the detailed data used in these studies were only readily available from one source and only covered a single cycle of operations from a single plant, these recommendations should be regarded as instructive but preliminary in nature.

12. KEY WORDS/DESCRIPTORS (List words or phrases that will assist researchers in locating the report.)
burnup credit
BWR
fission products
actinides
spent fuel
control blades
burnup profiles
moderator density

13 AVAILABILITY STATEMENT
unlimited

14 SECURITY CLASSIFICATION
(This Page)
unclassified
(This Report)
unclassified

15. NUMBER OF PAGES

16. PRICE

Federal Recycling Program

UNITED STATES
NUCLEAR REGULATORY COMMISSION
WASHINGTON, DC 20555-0001

OFFICIAL BUSINESS

NUREG/CR-7224

Axial Moderator Density Distributions, Control Blade Usage, and Axial Burnup Distributions for Extended BWR Burnup Credit

August 2016